

MASTER

Validation and Enhancement of a Tractor Semi-trailer Multibody Simulation Model

Spijkers, T.L.

Award date:
2008

[Link to publication](#)

Disclaimer

This document contains a student thesis (bachelor's or master's), as authored by a student at Eindhoven University of Technology. Student theses are made available in the TU/e repository upon obtaining the required degree. The grade received is not published on the document as presented in the repository. The required complexity or quality of research of student theses may vary by program, and the required minimum study period may vary in duration.

General rights

Copyright and moral rights for the publications made accessible in the public portal are retained by the authors and/or other copyright owners and it is a condition of accessing publications that users recognise and abide by the legal requirements associated with these rights.

- Users may download and print one copy of any publication from the public portal for the purpose of private study or research.
- You may not further distribute the material or use it for any profit-making activity or commercial gain

Validation and Enhancement of a Tractor Semi-trailer Multibody Simulation Model

ing. T.L. Spijkers

DCT 2008.068

Master's thesis

Supervisor: Prof. Dr. H. Nijmeijer (Eindhoven University of Technology)

Coach(es): Ir. W.J.E Evers (Eindhoven University of Technology)
Ir. J. Vandenhoudt (TNO Automotive)
Dr. Ir. I.J.M. Besselink (Eindhoven University of Technology)

Committee: Dr. Ir. T. Hofman (Eindhoven University of Technology)

TNO Science & Industry
Business Unit Automotive
Department Integrated Safety

Eindhoven University of Technology
Department Mechanical Engineering
Dynamics and Control Group

Eindhoven, June, 2008

Preface

This Master thesis investigation was conducted from July 2006 till June 2008 at the section for Integrated Safety of the Netherlands Organisation for Applied Scientific Research (*TNO Automotive*) in Helmond.

For the supervision and guidance during the investigation I would like to thank Prof. Dr. H. Nijmeijer, Dr. Ir. I.J.M. Besselink and Ir. W.J.E Evers of the *Eindhoven University of Technology* and Ir. J. Vandenhoudt of *TNO Automotive*. Furthermore, I would like to thank my study colleagues, especially Ivo op het Veld, for the fruitful discussions and for their friendship.

Last but not least, I am thankful to my family and Simone for their non-technical support, patience and encouragements throughout my entire study career.

Abstract

Validation and Enhancement of a Tractor Semi-trailer Multibody Simulation Model - T.L. Spijkers

TNO Automotive in association with *Eindhoven University of Technology* and *DAF Trucks* initiated a project for the development of a three-dimensional tractor semi-trailer multibody simulation model. This simulation model is constructed in *MATLAB® SimMechanics* and in July 2006 the first version of this model has been completed. Using a specially prepared tractor semi-trailer, a wide variety of experiments are performed. These experiments have been performed on a proving ground and consist of acceleration, braking and different steering tests. Furthermore, experiments with regard to riding over different road surfaces and obstacles are also performed. In order to make a comparison between the test vehicle and the simulation model, each test is simulated. For the simulation of a test, measured experimental data is used in order to accurately simulate the performed tests.

In this study, the experimental and simulation data is compared for every type of experiment. The problem statement of this master's thesis project is defined as the validation and improvement of a three-dimensional tractor semi-trailer simulation model that is capable of accurately predicting dynamic vehicle behaviour. The objectives of this master's thesis are: (1) evaluation of the *baseline* model using test truck data; (2) analysis of the simulation results and improving the model and (3) validation of the modified model. Herein the *baseline* model is defined as the first version of the simulation model, dated July 2006. To achieve these objectives, an evaluation methodology and algorithm are developed for the evaluation and validation of the simulation model. Using this evaluation methodology in combination with time-domain graphs of the evaluated signals, a profound study of the *baseline* simulation results is performed to indicate the weakness and strength of the simulation model. Based on these results, some adjustments are made to improve the simulation model. Finally the modified model is validated.

After analysing the *baseline* model, some adjustments are made and implemented in an updated version of the *baseline* model called *reference* model. The implemented adjustments consist of updating the model parameters and removing some modelling errors. Furthermore, the *MF-Swift* tyre model is implemented for riding over discrete road obstacles, the acceleration sensor for measuring the longitudinal and lateral accelerations is modified and the driver model is adjusted. Evaluation of the *reference* model shows that considerable improvement is achieved with respect to vertical axle, chassis and cabin accelerations. Furthermore, the primary and cabin suspension deflections show also some improvement. However, additional adjustments are required for further improvement.

The first additional model adjustment is the implementation of a rear axle suspension geometry which is similar to the test vehicle suspension geometry. This introduces an *anti-rise* effect when braking and an *anti-squat* effect when accelerating and improve the rear axle suspension deflections. Further improvement of the rear axle suspension deflection when braking is achieved by adding a variable brake force distribution. For the steering experiments, the lateral accelerations and yaw velocities are improved by implementing a similar steering geometry as used for the test vehicle. In order to improve the cabin suspension, a physical anti-roll bar is added, the cabin levelling control is adjusted, aero dynamic drag force is added and measured spring/damper characteristics are implemented. Evaluation of the cabin suspension adjustments show improvement of deflections after the vehicle has come to a standstill but also shows that these adjustments are not sufficient for accurately predicting cabin suspension deflections when braking. Furthermore, the evaluation also shows peculiar cabin suspension deflections for the test vehicle.

Finally, every model adjustment is included in a final simulation model. After validation and comparing its simulation results with the *baseline* model, it is concluded that this final model represents the dynamic vehicle behaviour fairly accurately for the considered tractor-semi trailer combination. Considerable improvements are achieved concerning the primary suspension deflections; the vertical accelerations; and the lateral cabin and chassis accelerations with regard to the *baseline* model. However, there is still room for further improvement of the cabin suspension.

Samenvatting

Valideren en verbeteren van een driedimensionaal multibody simulatiemodel van een vrachtwagen met oplegger
- T.L. Spijkers

TNO Automotive in samenwerking met de Technische Universiteit Eindhoven en DAF Trucks zijn een project gestart voor de ontwikkeling van een driedimensionaal multibody simulatiemodel van een vrachtwagen met oplegger. Dit simulatiemodel is gemaakt met *MATLAB*[®] *SimMechanics* en in juli 2006 was de eerste versie van het model klaar. Met een speciaal geprepareerd testvoertuig zijn vervolgens diverse experimenten uitgevoerd op een testterrein. Deze experimenten bestaan uit acceleratie, stuur en remtesten. Verder zijn er ook experimenten uitgevoerd waarbij het testvoertuig over verschillende wegdekken en obstakels rijdt. Om vervolgens een vergelijking tussen testvoertuig en simulatiemodel te maken is iedere test ook uitgevoerd met het simulatiemodel. Hierbij is er gebruik gemaakt van gemeten testvoertuig signalen om zo nauwkeurig mogelijk de test te kunnen simuleren.

In dit onderzoek worden het testvoertuig en het simulatiemodel met elkaar vergeleken. De probleemstelling is gedefinieerd als het valideren en verbeteren van driedimensionaal vrachtwagen met oplegger model dat in staat is om nauwkeurig dynamisch voertuig gedrag te simuleren. Hierbij zijn de volgende doelstellingen gedefinieerd: (1) evalueren van het *baseline* simulatiemodel gebruikmakend van testvoertuig data; (2) analyse van de simulatie resultaten en verbeteren van het model en (3) valideren van het aangepaste model. Het *baseline* model is gedefinieerd als de eerste versie van het model uit juli 2006. Om deze doelstellingen te verwezenlijken zijn er een evaluatie methode en algoritme ontwikkeld voor het evalueren en valideren van het simulatiemodel. Gebruikmakend van deze evaluatie methode in aanvulling met grafieken in het tijdsdomein is er een diepgaand onderzoek uitgevoerd naar de sterke en zwakke kanten van het *baseline* model. Vervolgens zijn er enkele aanpassingen gedaan ter verbetering van het model. Tenslotte is het aangepaste model gevalideerd.

Na de uitgebreide analyse van het model zijn er enkele aanpassingen gedaan en samengevoegd in een geupdate versie van het *baseline* model genaamd *reference* model. Deze aanpassingen bestaan uit het updaten van de model parameters en het verwijderen van fouten in het model. Bovendien is het *MF-Swift* bandmodel toegevoegd voor het rijden over obstakels, de sensoren die de longitudinale en laterale versnellingen meten zijn aangepast en het driver model is aangepast. Evaluatie van het *reference* model heeft aangetoond dat aanzienlijke verbeteringen zijn bereikt voor de verticale versnellingen van assen, chassis en cabine. Verder zijn de primaire en cabine vering iets verbeterd. Echter, aanvullende aanpassingen zullen moeten worden gedaan om het model verder te verbeteren.

Voor verdere verbetering van het model is als eerste de achteras geometrie van het testvoertuig overgenomen in het model. Hierdoor treedt er een *anti-rise* effect op tijdens het remmen en een *anti-squand* effect tijdens het accelereren welke zorgen voor een verbetering van de achteras vering. De vering van de achteras tijdens het remmen is verder verbeterd door het toepassen van een variable remdrukverdeling. Voor het sturen zijn de laterale versnellingen en gier snelheden verbeterd door het implementeren van een stuurgeometrie die gelijk is aan die van het testvoertuig. Voor de verbetering van de cabine vering zijn een anti-roll stang constructie toegevoegd, de cabine hoogteregelaar is aangepast, de aerodynamische weerstandskracht op de cabine is toegevoegd en gemeten veer/demper karakteristieken zijn geïmplementeerd. Evaluatie van de aanpassingen met betrekking tot de cabine vering heeft aangetoond dat de vering is verbeterd nadat het voertuig tot stilstand is gekomen bij een remtest, maar laat tevens zien dat de gemaakte aanpassingen niet voldoende zijn voor het nauwkeurig simuleren van de cabine vering tijdens het remmen. Bovendien is er naar voren gekomen dat de cabine vering van het testvoertuig opmerkelijke gedrag vertoont tijdens het remmen.

Tenslotte zijn alle aanpassingen samengevoegd in een definitief model genaamd *final* model. Na het valideren van dit model en het vergelijken met het *baseline* model kan worden geconcludeerd dat het model redelijk nauwkeurig het dynamisch voertuig gedrag kan simuleren. Bovendien zijn aanzienlijke verbeteringen bereikt met betrekking tot de primaire vering, de verticale versnellingen en de laterale cabine en chassis versnellingen. Echter, de cabine vering kan nog verder worden verbeterd.

Contents

Preface	i
Abstract	iii
Samenvatting	v
1 Introduction	I
1.1 Motivation and background	1
1.2 Problem statement	3
1.3 Objective	3
1.4 Outline of the report	3
2 Vehicle simulation models and validation methods	5
2.1 Vehicle simulation models	5
2.1.1 Modelling approach	5
2.1.2 Comparison of approaches	6
2.2 Validation	7
2.2.1 What is verification and validation?	7
2.2.2 The difficulties of validation	8
2.2.3 Validation methods	9
2.2.4 Operational validity	9
2.2.5 Operational validation techniques	10
3 Test vehicle and experiments	II
3.1 Test vehicle	11
3.1.1 Tractor	12
3.1.2 Semi-trailer	12
3.1.3 Data acquisition system	12
3.2 Experiments	14
3.2.1 Road excitation	14
3.2.2 Driver controlled manoeuvres	16
3.2.3 Experimental data	16
4 Baseline simulation model	17
4.1 SimMechanics	17
4.2 Model construction	18
4.2.1 Chassis	18
4.2.2 Cabin	18
4.2.3 Drive line	18
4.2.4 Axles	18
4.2.5 Other model components	19
4.3 Coordinate systems	19
4.4 Excluded elements and phenomena	20

4.5	Simulation data	20
5	Model evaluation method	21
5.1	Methodology	21
5.1.1	Statistical measures	22
5.1.2	Score computation	24
5.1.3	Evaluation signals	25
5.2	Algorithm implementation	25
5.2.1	General evaluation details	25
5.2.2	Data preparation	25
5.2.3	Interval selection	27
5.2.4	Score calculation	27
5.2.5	Output	27
6	Baseline model analysis	29
6.1	Evaluation scores	29
6.2	Updating model parameters	31
6.3	Modelling errors	32
6.4	Tyre model	33
6.5	Sensor modification	34
6.6	Driver model	36
6.7	Evaluation <i>reference</i> model	38
6.7.1	Axles	38
6.7.2	Chassis	39
6.7.3	Cabin	40
6.8	Summarising this chapter	40
7	Model modifications	43
7.1	Rear axle suspension	43
7.1.1	Trucklab	43
7.1.2	Simulation model	43
7.1.3	Analysis	44
7.1.4	Model adjustments	45
7.1.5	Evaluation	47
7.2	Brake system	47
7.2.1	Trucklab	48
7.2.2	Simulation model	49
7.2.3	Model adjustments	50
7.3	Steering system	52
7.3.1	Trucklab	52
7.3.2	Simulation model	53
7.3.3	Model adjustments	54
7.3.4	Evaluation	58
7.4	Cabin suspension	58
7.4.1	Trucklab	58
7.4.2	Simulation model	58
7.4.3	Analysis	59
7.4.4	Model adjustments	61
7.4.5	Evaluation	62
7.5	Summarising this chapter	65

8	Model validation	67
8.1	Discrete obstacles	67
8.1.1	Vertical accelerations	67
8.1.2	Suspension deflections	69
8.1.3	Lateral accelerations	69
8.1.4	Angular velocities	71
8.1.5	Conclusion	71
8.2	Acceleration	73
8.2.1	Suspension deflections	73
8.2.2	Longitudinal accelerations	75
8.2.3	Angular velocities	75
8.2.4	Conclusion	76
8.3	Braking	77
8.3.1	Suspension deflections	77
8.3.2	Longitudinal accelerations	79
8.3.3	Angular velocities	79
8.3.4	Conclusion	80
8.4	Steering	81
8.4.1	Suspension deflections	81
8.4.2	Lateral accelerations	83
8.4.3	Angular velocities	83
8.4.4	Conclusion	83
9	Conclusions and recommendations	87
9.1	Conclusions	87
9.1.1	Model adjustments	88
9.1.2	Validation of the final simulation model	89
9.1.3	Evaluation methodology	89
9.1.4	Main conclusion	89
9.2	Recommendations	90
	bibliography	93
A	<i>Trucklab</i> and simulation model sensors and signals	95
A.1	<i>Trucklab</i> sensor position	95
A.2	Experimental test filename definition	96
A.3	Sensor signal names for <i>Trucklab</i> and simulation model	97
B	Evaluation data	99
B.1	Dominant vehicle modes	99
B.2	Evaluation signals	100
B.3	RMS value <i>Trucklab</i> sensor noise	101
B.4	Time-shift signals	102
C	Evaluation scores	103
C.1	<i>baseline</i> model vs. <i>reference</i> model evaluation scores	103
C.2	<i>baseline</i> model vs. <i>final</i> model evaluation scores	108
C.3	<i>reference</i> model vs. <i>final</i> model evaluation scores	113

Chapter 1

Introduction

1.1 Motivation and background

Thanks to its geographical position, the Netherlands serves as an important transit country for the rest of Europe. Trade goods arrive with huge container ships in the harbor of Rotterdam. After arrival, these goods are transferred to other types of transport being: inland shipping, railroad transport, road transport, air transport and pipeline transport. Figure 1.1 displays the contribution of each type of transport to the national and international goods transport.

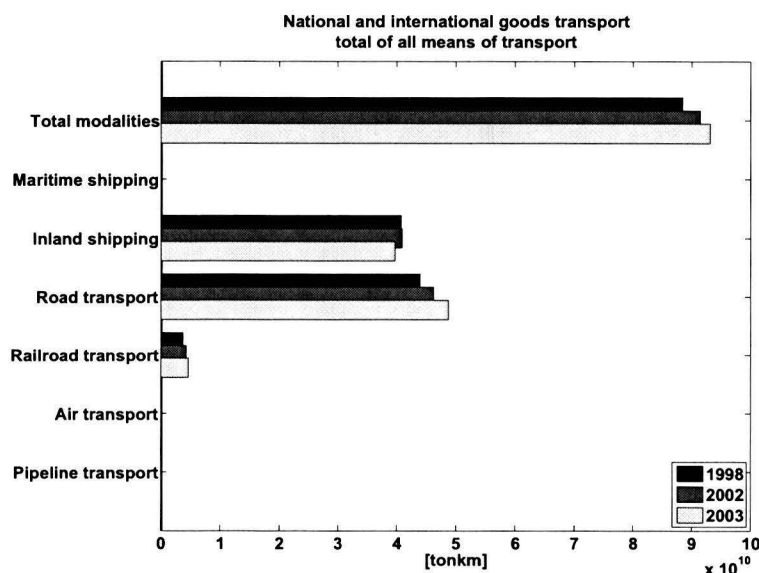


Figure 1.1: National and international goods transport, [29].

As can be seen in figure 1.1, road transportation by trucks is the most popular form of transportation. The trend, for the period of 1998 till 2003, is that road transportation is increasing its share with respect to the total of all means of transport. Note that the goods transport by maritime shipping, air transport and pipeline transport are not equal to zero but are very small compared to the other means of transport.

Haulage contractors often own huge truck fleets for transportation of a large range of goods. This large range of goods requires a large variety in truck configurations. These configurations can be subdivided into three groups: light trucks, medium trucks and heavy trucks. Light trucks are car sized and are used by individuals or small businesses. Their weight is limited to 3500 kg. Medium trucks are larger than light trucks, with respect to size and weight, but smaller than heavy trucks. They weigh

between 3.5 and 7.5 tonnes and are often used for short-haul purposes. Heavy trucks are the largest trucks allowed on the road. They are mostly used for long-haul purposes, often in tractor semi-trailer (Europe and US) or B-double configuration (Australia).

Most trucks share a common construction: they are made of a chassis, a cabin, an area for placing cargo or equipment, axles, suspension and wheels, an engine, fuel tank and a drive-train. The chassis or frame of a truck mainly consists of two parallel straight C-shaped beams held together by cross-members. The chassis is the main structure of the truck, and the other parts attach to it. The cabin is an enclosed space where the driver is seated and available in a few possible configurations:

- *Cabin over engine (COE) or flat nose.* The driver is seated on top of the front axle and the engine. This design is found in Europe, where overall truck lengths are strictly regulated.
- *Conventionals or long nose.* The driver is seated behind the engine, as in most passenger cars or pickup trucks. This design is most common in the US and Australia.
- *Cabin beside engine (CBE)* designs also exist, but are rather rare. They can be found in harbor regions or distribution centres.

Trucks can use all sorts of engines. Light trucks have either a gasoline or diesel engine. Medium and heavy trucks use four stroke turbo diesel engines because they are durable, powerful and fuel efficient. Light trucks use the same type of transmissions as passenger cars which have either an automatic or a manual transmission. Medium and heavy trucks are equipped with a manual, automatic or semi-automatic transmission. Automatic and semi-automatic transmissions are becoming more and more common due to advances both in transmission and engine power. Manual transmissions have 8, 10 or 12 gears, while automatic or semi-automatic transmission would have anything from 5 to 12 gears.

Present-day trucks keep evolving as a result of developments in the fields of driver comfort, engine and drive-trains, safety systems and the environment. Some of these developments are enforced by legislation. For example, cleaner and more fuel efficient engines. Making fuel efficient engines also contributes to the reduction of the transportation costs. Others are to improve competitiveness of the concerning manufacturer. A trend within the development of new advanced truck systems is that these are becoming more complex and more interrelated with control engineering. The development process itself is evolving as well. Simulation models are increasingly used for research, problem solving and as an aid in decision making. Examples of simulation model applicability within the automotive industry are: virtual crash testing, durability tests, and the analysis of dynamic vehicle behaviour.

A tendency within the automotive industry is that the simulation model is increasingly preferred over the physical prototype in the research and development phase. However, it is not possible to completely replace a physical prototype with a simulation model. The main advantages of using simulation models over prototypes are: cost, time and the ease of changing system parameters. However there are some disadvantages as well. The simulation model is not as accurate as a prototype. This is often caused by the simplification of some model components. Another recurring disadvantage for every simulation model is the time-consuming validation process. Model validation is usually defined as: "substantiation that the computerized model within its domain of applicability possesses a satisfactory range of accuracy consistent with the intended application of the model" [13]. This is the definition used in this master's thesis.

As the validation of a simulation model is essential in determining the accuracy of the model, it also is a substantial part of this master's thesis. The simulation model of this master's thesis is a three-dimensional multibody simulation model of a tractor semi-trailer combination which is developed by *TNO Automotive* in association with the *Eindhoven University of Technology*. The simulation model is constructed in *SimMechanics* and consists of a number of predefined modules that makes the construction of different vehicle configurations relatively simple. An important advantage of using *SimMechanics* is that it is an extension of *MATLAB® Simulink®*. This makes that control design

1.2 Problem statement

and multibody model construction can be performed in one simulation environment (*Simulink*[®]). Another advantage of using this simulation environment is that it makes exchanging control design strategies between simulation model and vehicle prototype straightforward, as hardware control design within TNO is *Simulink*[®]-based. This tractor semi-trailer simulation model will be used for the analysis of dynamic truck behaviour for a wide range of commercial vehicle configurations due to its modular design.

1.2 Problem statement

Prior to this master's thesis, TNO Automotive in association with the Eindhoven University of Technology and DAF Trucks initiated a project for the development of a three-dimensional tractor semi-trailer multibody simulation model. In July 2006 the first version of this tractor semi-trailer multibody simulation model has been completed. Next, a wide variety of experiments are performed using a specially prepared tractor semi-trailer test vehicle. These experiments have been performed on a proving ground and consist of acceleration, braking and different steering tests. Furthermore, riding over different road surfaces and obstacles are also part of the performed experiments. Having a large amount of test vehicle data and simulation model which has not been validated, the main problem of this master's thesis can be defined as:

"The validation and improvement of a three-dimensional tractor semi-trailer simulation model that is capable of accurately predicting dynamic vehicle behaviour."

1.3 Objective

The main objectives of this master's thesis are:

- Evaluation of the *baseline* model using test truck data;
- Analysis of the simulation results and improving the model;
- Validation of the modified model.

Moreover, the following sub-objectives can be defined:

- Development of a model evaluation methodology;
- Formulation of a model evaluation algorithm.

Herein the *baseline* model is defined as the original tractor semi-trailer simulation model developed in July 2006 by TNO Automotive in association with the Eindhoven University of Technology and DAF Trucks.

1.4 Outline of the report

The report is ordered as follows. Chapter 2 reviews several truck simulation models and different approaches for model validation as found in literature. In chapter 3 an extensive description of the test vehicle and the performed experiments are given. Chapter 4 deals with the construction of the *baseline* simulation model. In chapter 5 an evaluation methodology and algorithm are presented for the evaluation of the simulation model. Using this evaluation algorithm, the *baseline* model is evaluated in chapter 6. Furthermore, some model adjustments are discussed and combined in an updated version of the *baseline* model. Further model adjustments are treated in chapter 7. Chapter 8 deals with the validation of the *final* model. This model includes the adjustments treated in the chapters 6 and 7. Finally, in chapter 9 the conclusion and recommendations are given.

Chapter 2

Vehicle simulation models and validation methods

This chapter provides an overview of the literature in the field of vehicle simulation models and how these models are validated and verified.

2.1 Vehicle simulation models

Simulation studies are commonly used for vehicle dynamics analysis. Typically, vehicle handling deals with the vehicle-driver system, and when a vehicle alone is considered it is often referred to as vehicle dynamics analysis. A simulation model helps in the understanding of a physical system. Models developed for the vehicle dynamics analysis vary greatly in their capabilities, complexity, number of degrees of freedom, and the amount of input data that is required for the simulation. Furthermore, they can vary in modelling approach. The next section discusses modelling approaches. The section afterwards treats differences between the approaches.

2.1.1 Modelling approach

When creating a vehicle model, different approaches can be adopted, depending on the intended use. The modelling approaches discussed in this section are: the lumped parameter model (LPM) approach and the multibody formulation (MBF) approach. For more information on both approaches see, [28].

Lumped parameter model

Lumped parameters are a simplification in a mathematical model of a physical system where variables that are spatially distributed fields are represented as single scalars. For example in a lumped mass modelling approach, the masses of different components are "lumped" together as one component with one mass. In a lumped parameter model approach, the analyst develops the model including its discretisation and the equations of motion (EOM). Discretisation is the process of transferring a continuous model into a discrete counterpart. This process is carried out as a first step towards making them suitable for numerical evaluation and implementation on digital computers. In physics, equations of motion are equations that describe the behaviour of a system (e.g., the motion of a body under the influence of a force) as a function of time. The term equations of motion refers to the differential equations that the system satisfies (e.g., Newton or Lagrange equations).

Multibody formulation

In the multibody formulation, the analyst builds up the model by giving the details about the bodies, their kinematic constraints and system topology, then the computer generates the equations of motion. Commonly used multibody packages for vehicle simulation models are: *ADAMS* by *MSC*

Software, SIMPACK by INTEC GmbH, Carsim/Trucksim by Mechanical Simulation Corporation and SimMechanics by The Mathworks.

2.1.2 Comparison of approaches

Below, a comparison is made between the lumped parameter model and multibody formulation approach with respect to efficiency, model adaptability, human effort and applicability.

Efficiency

The lumped parameter model approach has the advantages of allowing the analyst to include or ignore certain effects in the model development phase. These assumptions or simplifications made during model development, including those made while discretising the system, have a direct consequence for the accuracy of the simulation results. These models have only as many degrees of freedom (DOF) as are judged to be needed. Also, since many of the models are custom made, one can easily include particular forcing functions typical for the system under consideration, [28].

In a multibody formulation approach, the analyst is not able to select the number of degrees of freedom. Generally, every body is assumed to have six degrees of freedom and the unwanted degrees of freedom will be constrained, [28]. The multibody formulation approach requires matrix operations and iterative techniques to satisfy the kinematic constraints. A consequence is that these codes are computationally not very efficient and therefore the use in real-time applications, highly iterative design optimisation, or interactive use, is limited. However, the recursive multibody formulation based approach can be real-time when parallel processing is used, [15]. For more information on recursive multibody formulation see [1] and [16].

Model adaptability

In the lumped parameter model approach, the model and the equations of motion are valid for a specific vehicle configuration. If the vehicle under consideration has a different lay-out, then an equivalent vehicle has to be defined to use available equations of motion. This is very labour intensive.

In multibody formulation approach, vehicles with a different lay-out or design changes can be easily accommodated by modifying the input file that describes the vehicle components and their relations to each other.

Human effort

Formulation of the equations of motion

In the lumped parameter model approach, the analyst must put much effort in deriving the equations of motion, then coding and validating them. This process is error prone. However, software packages like *Mathematica* and *MATLAB*[®] can reduce this task.

In the multibody formulation approach, the codes are believed to function properly. Here, the analyst is relieved of equations of motion derivation, but his effort is now shifted to modelling every component in detail using a variety of predefined elements and keeping track of numerous inputs, [28].

Parameter measurement

A significant amount of analysis is required before a required input is ready for use in simulation studies. For the multibody formulation approach, the input consists of mass and inertial properties, component geometry, reference frame definitions, body types, body compliance description, topological and analytical constraints, force and motion actuation, and control laws, [15]. The lumped parame-

2.2 Validation

ter approach requires parameters of discretised elements.

Analyst's proficiency

An analyst with only the basic understanding of dynamics can derive equations of motion for simple systems. For more complex systems, basic understanding of dynamics is not sufficient for the derivation of the equations of motion. The multibody formulation approach requires an advanced user training for the multibody software package.

Applicability

In the lumped parameter model approach, by the way the model has been defined through composite parameters, it is easy to make comparison between two vehicles with different parameter values. This approach allows changes in the design to be studied directly. For example, in the investigation of the effect of rear suspension roll steer on vehicle directional response only this parameter could be changed independently of other parameters, [11].

Considering a detailed simulation model, to account for this change, suspension pickup points and suspension link lengths need to be changed in the multibody formulation approach. After these changes are made, a check is necessary to determine that these changes have not affected other suspension characteristics. However, it should be pointed out that relating the composite parameter changes to physical component changes is not an easy task.

The multibody formulation approach is most useful in determining structural loads and large motion analysis, while the lumped parameter model approach is more suitable for small motion analysis as lumping together certain model components results in inaccurate results for large motion analysis.

2.2 Validation

This section provides an overview of the literature in the field validation and verification of simulation models. Treated subjects are: subject clarification, validation difficulties and validation forms.

2.2.1 What is verification and validation?

Models can be used to predict or compare the performance of systems under various conditions. In the field of vehicle dynamics, simulation models are commonly used in vehicle handling and vehicle ride analysis. When models are used for comparison purposes, the comparison is usually made to a baseline model or to a real world system. In any of these cases the model constructor wants to know whether the model is sufficiently accurate within the domain of applicability, [9]. "*Sufficiently accurate*" is subjective and depends upon the type of analysis and objective(s).

A significant element of any simulation study should be the verification and validation (V&V) of the simulation model. Thorough V&V leads to grounds on which to place the confidence in a study's results. However, V&V is far from straightforward and is often not performed as thoroughly as it should be done, [24].

Model validation is proving that the model, within its domain of applicability, behaves with satisfactory accuracy consistent with the study objectives. In other words, in model validation, we prove that the input-output transformation of a model is a sufficiently accurate representation of the input-output transformation of the corresponding physical system, [3]. When validating a simulation model, it must also be considered that a "*wrong*" simulation model can result in sufficiently accurate input-output transformation of the corresponding physical system. Model validation deals with building the *right* model, [24].

Model verification is often defined as "ensuring that the computer program of the computerized model and its implementation are correct", [27]. In other words, building the model *right*, [3]. Computerized model verification takes place on the level of the programming language used for simulation. For more detailed information about model verification, see [27].

Figure 2.1 shows how V&V map onto the the modelling process. What it shows is that each stage in the modelling process requires, in parallel, a verification or validation process.

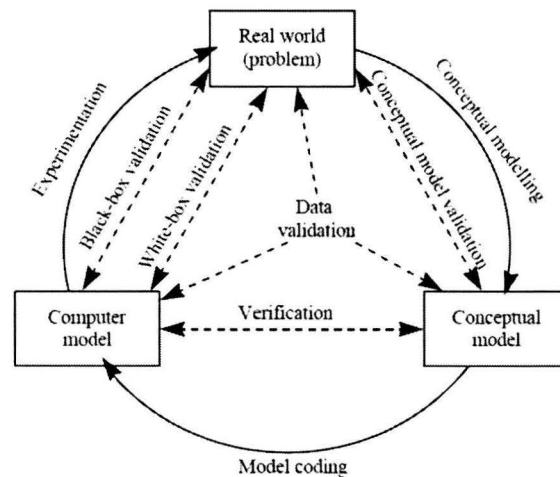


Figure 2.1: Simulation model validation and verification in the modelling process, [24].

2.2.2 The difficulties of validation

In [24], a number of problems are summarised, that arise in trying to validate a simulation model. This paragraph gives a summarised overview of these difficulties.

There is no such thing as general validity

A model is only validated with respect to its purpose. It cannot be assumed that a model that is valid for one purpose is also valid for another. A model could only be described as generally valid if it could be demonstrated that it is suitably accurate for every purpose to which it might ever be put.

There may be no real world to compare against

Many models are developed for future real world systems. As a consequence there is no real world to use for comparison. The model may be valid when it is made to represent the existing operation, but this does not guarantee that this is valid once it is representing some change to that system.

Which real world?

Different people have different interpretations of the real world, known as a world view, [10]. If people have different interpretations of the real world, which interpretation(s) should be used for developing and validating a model? A model that is valid to one person may not be valid to another. As the different real world interpretations are not very common, this is not considered as a major difficulty for the validation of the tractor semi-trailer model.

Often the real world data are inaccurate

Validation often involves a comparison of some aspects of the model. The model is run under the same conditions as the real world to see if it performs in a similar manner. There are two difficulties that arise with this procedure. First, the real world data may not be accurate. If this data is not accurate, this will result in difficulties determining whether a model's simulation results are correct. Second, even if 'accurate' real world data does exist, one must bear in mind that these are only samples which

2.2 Validation

in itself creates uncertainty. This means that the real world-to-model comparison is a comparison of two samples. Although statistical procedures can be used to determine whether these two samples are similar, these only provide a probabilistic and not a definitive answer.

There is not enough time to verify and validate everything

There is simply not enough time to verify and validate every aspect of a model. The modeler's task is to ensure that as much of the model is verified and validated as possible, both in terms of the model details and the overall validity.

2.2.3 Validation methods

The remainder of this chapter will exclusively deal with model validation and not with the verification of the model. Model verification takes place on the level of the programming language used for simulation. As the adopted simulation program is suited for vehicle simulation applications, model verification is not within the scope of this thesis. The most important validation forms are summarised below and are found in the literature; [24], [2] and [27], although some may be described differently. For a detailed review on validation and verification see, [25]. There are various ways of validation, which can be defined as follows:

- *Conceptual Model Validation*: determining whether the scope and level of detail of the proposed model is sufficient for the purpose at hand, and that any assumptions are correct. The question being asked is: does the conceptual model contain all the necessary details to meet the objectives of the simulation study?
- *Data Validation*: determining whether the data required for model building, validation and experimentation are sufficiently accurate.
- *Operational validity*: primarily concerned with determining whether the model's output behaviour has the accuracy required for the model's intended purpose over the domain of its intended application, [26]. This is where most of the validation testing and evaluation takes place. The computerised model is used in operational validity and thus any deficiencies found can be due to an inadequate conceptual model, an improperly programmed or implemented conceptual model on the computer, or due to invalid data. Operational validity can be subdivided into *White-box Validation* and *Black-box Validation*.
 - *White-box Validation*: determining that the basic parts of the computer model represent the corresponding real world elements with sufficient accuracy. This is a detailed, or micro, check of the model, in which the question is asked: does each part of the model represent the real world with sufficient accuracy.
 - *Black-box Validation*: determining that the overall model represents the real world with sufficient accuracy. This is an overall, or macro, check of the model's operation, in which the question is asked: does the overall model provide a sufficiently accurate representation of the real world system?

Figure 2.1 shows the different validation methods in the modelling process. In this master's thesis a combination of the above-mentioned validation methods is adopted. However, the main focus lies on the operational validity.

2.2.4 Operational validity

As stated before, operational validity is determining whether the simulation model's output behaviour has the accuracy required for the model's intended purpose. This brings about a lot of validation testing and evaluation. Any deficiencies found during this phase may be caused by what was developed in any of the steps that are involved in developing the simulation model including developing the system's theories or having invalid data.

According to [27], the classification of the operational validity can be done as depicted in Table 2.1. A major question concerning operational validity is whether the system is observable. The meaning of an "observable system" in this context is that it is possible to collect data on the operational behaviour of the system. Comparison means comparing the simulation model output to either the output behaviour of the system or another model. "Explore model behaviour" denotes to examine the output behaviour of the simulation model using appropriate validation techniques, including parameter variability-sensitivity analysis.

Table 2.1: Operational Validity Classification, [27].

	Observable System	Non-Observable System
Subjective Approach	<ul style="list-style-type: none"> • Comparison using graphical displays • Explore model behaviour 	<ul style="list-style-type: none"> • Explore model behaviour • Comparison to other models
Objective Approach	<ul style="list-style-type: none"> • Comparison using arithmetical tests and procedures 	<ul style="list-style-type: none"> • Comparison to other models using arithmetical tests

To be able to obtain a high degree of confidence in the simulation results an observable system is desirable. Data collected from the system can be compared to the results of the simulation when it is run under the same conditions. As the system concerning this study is observable and data for several different sets of experimental conditions are available, the focus lies on the operational validity for an observable system.

2.2.5 Operational validation techniques

Informal V&V techniques are among the most commonly ones used. They are called informal because the tools and approaches used rely heavily on human reasoning and subjectivity without consistent mathematical formalism, [3]. In [27] and [26] these techniques are defined as 'subjective' techniques. Some subjective validation techniques are listed below. For a more detailed review on the different validation techniques see [27] and [26].

Comparison to other models: Various results (e.g., outputs) of the simulation model being validated are compared to results of other (valid) models.

Face Validity: Asking individuals knowledgeable about the system whether the model and/or its behaviour are reasonable.

Turing Tests: Individuals who are knowledgeable about the operations of the system being modelled are asked if they can discriminate between system and model outputs.

Historical Data Validation: If historical data exists (or data collected on a system specifically for building and testing a model), part of the data is used to build the model and the remaining data are used to determine whether the model behaves as the system does.

Objective validation techniques are techniques involving some type of statistical test or mathematical procedure. A combination of objective and subjective techniques is generally used. The validation technique used for this master's thesis (chapter 5) is also a combination of subjective and objective techniques.

Chapter 3

Test vehicle and experiments

As mentioned in chapter 1, *TNO Automotive* in association with the *Eindhoven University of Technology* is developing a simulation model of a tractor semi-trailer combination. To obtain confidence in the simulation results, the vehicle simulation model must be validated. The validation is performed by comparing simulation and experimental data for different road tests. Experimental data is obtained from a real tractor semi-trailer combination. This tractor semi-trailer combination is referred to as the '*Trucklab*' from this point on. In this chapter the specification and configuration of the *Trucklab* and the experiments performed are discussed.

3.1 Test vehicle



Figure 3.1: *Trucklab* test vehicle.

The *Trucklab* configuration, depicted in Figure 3.1, consists of a two-axle tractor coupled to a three-axle semi-trailer. A semi-trailer is a trailer without a front axle. A large proportion of its weight is supported by the tractor or by a detachable front axle assembly known as a dolly. This paragraph provides an overview of the *Trucklab* configuration. At first the tractor and subsequent the semi-trailer will be discussed.

3.1.1 Tractor

The tractor has the most common configuration, i.e. the 4×2 tractor configuration. This means the tractor has 2 rigid axles, a steered front and a driven rear axle. The front and rear axles are suspended with leaf springs and air springs respectively. The cabin is air suspended with respect to the chassis and is positioned above the engine. The drive line consists of a six cylinder diesel engine connected to a manual 12 speed gearbox. In figure 3.2 a side view of the tractor is given.

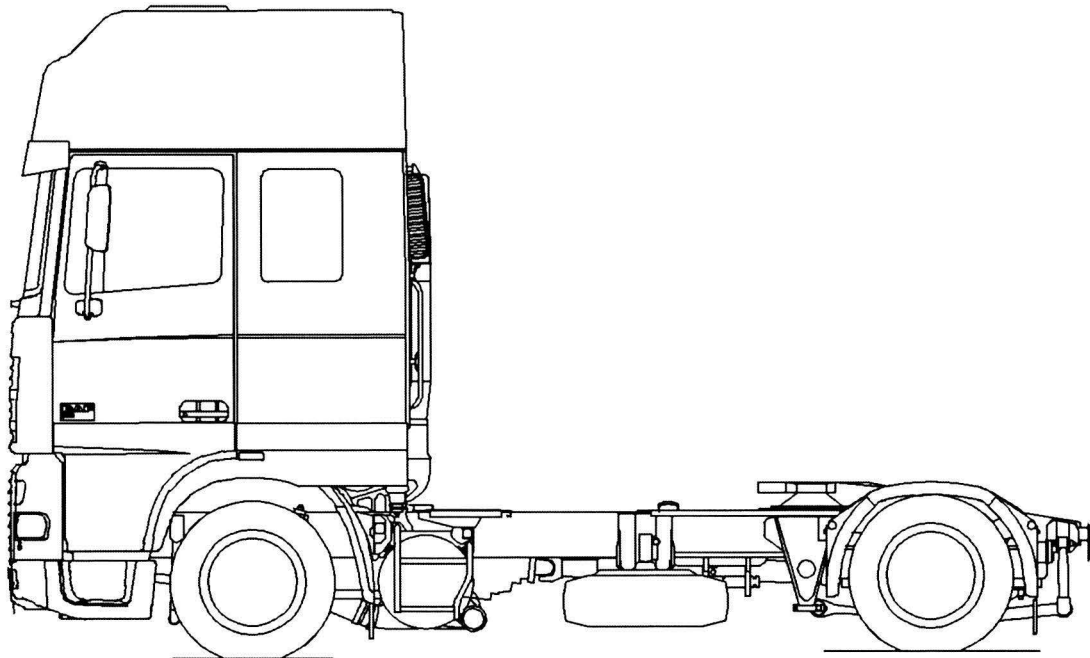


Figure 3.2: DAF FT XF95 (side view), [21].

3.1.2 Semi-trailer

For the experiments, discussed in section 3.2, two identical semi-trailers are used. The semi-trailers differ in loading condition, one trailer is fully loaded and the other is empty. The laden semi-trailer is loaded by means of 26 containers, each filled with scrap iron and an average weight of 1100kg. The semi-trailer is constructed out of a closed superstructure, three rigid axles and a chassis framework serving as a 'backbone'. The trailer axles are suspended with respect to the trailer chassis by air-springs and dampers. The total weight of the laden *Trucklab* configuration is slightly over 40 tons, which is the maximum allowed vehicle weight, better known as Gross Combined Weight Rating or GCWR. The unladen *Trucklab* configuration has a total vehicle weight of around 15 tons.

3.1.3 Data acquisition system

The *Trucklab* is equipped with a data acquisition system. Data acquisition is the sampling of continuous signals to generate data that can be manipulated by a computer. Data acquisition involves acquisition and processing of signals to obtain desired information. The sampling rate of the acquisition system is 200 Hz.

Figure 3.3 depicts the system architecture of the *Trucklab* data acquisition system. The components of this system are discussed in the following sections.

3.1 Test vehicle

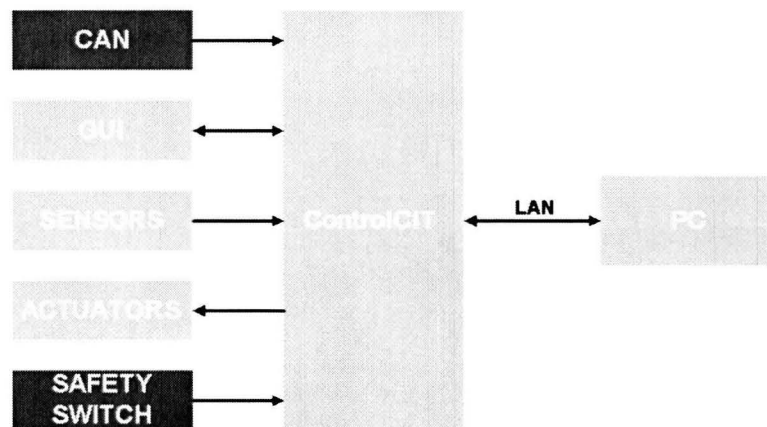


Figure 3.3: Data acquisition system architecture.

ControlCIT

ControlCIT is an acronym for Control Computer for Intelligent Transport Systems and is developed by *TNO Automotive*. The *ControlCIT* aims to provide a platform, consisting of computer software and hardware, for the design, evaluation and real-time implementation of control systems for intelligent transport systems. In this case the *ControlCIT* gathers, processes and forwards the sensor signals to the connected computer.

The *ControlCIT* hardware is a so-called Generic Controller and is a *PC/104* based system. *PC/104* (or *PC104*) is an embedded computer standard controlled by the *PC/104 Consortium*. Communication with vehicle sensors and actuators is established by a vehicle-specific interface box, which consist of *PC/104*-systems, automotive IO-modules and/or dedicated hardware modules stacked together like building blocks.

CAN

The tractor is standard equipped with a Controller Area Network or *CAN*. *CAN* is a broadcast, differential serial bus standard for connecting electronic control units or *ECUs*. This network is also used for sending sensor signals to control systems. Some of these signals are made available and are send to the *ControlCIT*. Available signals are vehicle forward velocity, steering wheel angle and tractor chassis yaw velocity.

GUI

GUI is an abbreviation for Graphical User Interface and is an information display for the driver. This device is not in operation.

Sensors

The tractor is fitted with acceleration, angle velocity and height sensors. Figure 3.4 is a schematic overview of the sensor positions. The vertical acceleration sensors placed on the cabin and chassis are positioned directly above and underneath the cabin suspension struts.

The vertical axle acceleration sensors are placed on the axle body near the primary suspension struts. For the vertical displacement measurement angular position sensors are used. These measured angles are converted into a vertical displacement. The 3-axis chassis acceleration sensor is mounted on a chassis crossbeam near its center of gravity and the 3-axis cabin acceleration and 3-axis angular velocity sensor is located within the cabin compartment in the longitudinal plane of symmetry. The exact sensor positions are included in Appendix A.1. The *Trucklab* sensor specifications are given in Table 3.1.

Actuators

System actuators can be controlled by the *ControlCIT*. In this case no additional actuators are used.

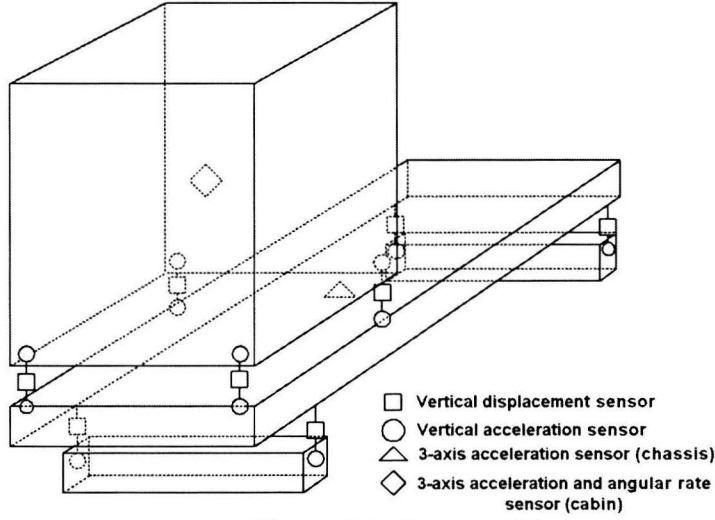


Figure 3.4: Sensor positioning.

 Table 3.1: *Trucklab* sensor specifications.

sensor	measuring range	deviation	zero g drift
vertical acc. sensor (axle)	$\pm 10g$ [m/s^2]	$\pm 0.01g$ [m/s^2]	$\pm 0.5g$ [m/s^2]
vertical acc. sensor (chassis cabin)	$\pm 4g$ [m/s^2]	$\pm 0.01g$ [m/s^2]	$\pm 0.2g$ [m/s^2]
3-axis acc. sensor (chassis)	$\pm 4g$ [m/s^2]	$\pm 0.01g$ [m/s^2]	$\pm 0.2g$ [m/s^2]
3-axis acc. and 3-axis ang. vel. sensor (cabin)	$\pm 2g$ [m/s^2]	$\pm 0.03g$ [m/s^2]	not specified
	± 100 [deg/s]	± 2 [deg/s]	-
vertical displacement sensor	± 55 [deg]	± 2.0 [deg]	-

Safety switch

In case of an emergency, when using actuators, the *ControlCIT* switches to a predefined failure mode.

PC

Acquisition software is installed on a pc which allows the pc operating system to recognise the acquisition hardware and programs to access the signals being gathered and processed by the hardware. A Local Area Network or *LAN* connects the *ControlCIT* with the PC. The utilised software is *MATLAB*[®] Simulink[®].

3.2 Experiments

With the *Trucklab* different experimental tests have been performed on a proving ground which is specially prepared for truck testing purposes. The aim of these tests is to gain an insight into vehicle behaviour when the *Trucklab* is subjected to different tests. The obtained experimental data is used for the evaluation and validation of the tractor semi-trailer simulation model.

The experimental tests can be subdivided into two groups; road excitation input and driver controlled manoeuvres. With road excitation the road surface provides the excitation of the vehicle and with driver controlled manoeuvres the driver is responsible for the excitation. The sections below give a detailed description of the experiments performed.

3.2.1 Road excitation

For this type of testing the *Trucklab* is driven over several road surfaces and obstacles with a laden and unladen configuration and different velocities. Road excitation is split up into two categories; excitation from the road surface and excitation by discrete obstacles.

3.2 Experiments

Road surface

At the proving ground, an area is accommodated with straight road sections with different surfaces. These surfaces consist of undulating asphalt, concrete slabs, brick road, Belgian blocks and smooth asphalt. In Table 3.2, the vehicle velocities and loading conditions for every type of road surface is given.

Table 3.2: Vehicle velocities and loading conditions for riding over different road surfaces.

road surface	velocity [km/h]	Trucklab loading condition
undulating asphalt	60 and 80	laden and unladen
concrete slabs	60 and 80	laden and unladen
brick road	40 and 50	laden and unladen
Belgian blocks	50	laden and unladen
smooth asphalt	60 and 80	laden and unladen

The velocities given in Table 3.2 are initial vehicle velocities and are kept constant for every section of road. The combination of velocity and road surface result in high frequency road excitation.

Discrete obstacles

Discrete obstacles are used to initiate large amplitude roll motions of the vehicle. To initiate rolling motions, the obstacles are placed on the right hand track of a flat road surface. The shape and dimensions of the obstacles are displayed in the figures 3.5, 3.6 and 3.7. In Table 3.3, the initial *Trucklab* velocities and loading conditions for the discrete obstacles are given.

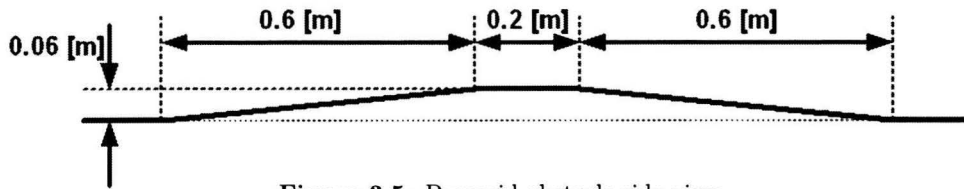


Figure 3.5: Pyramid obstacle side view.

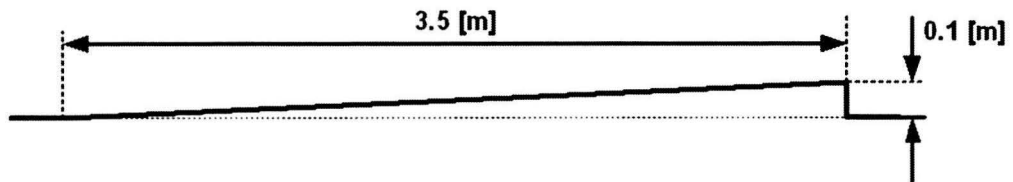


Figure 3.6: Step down obstacle side view.

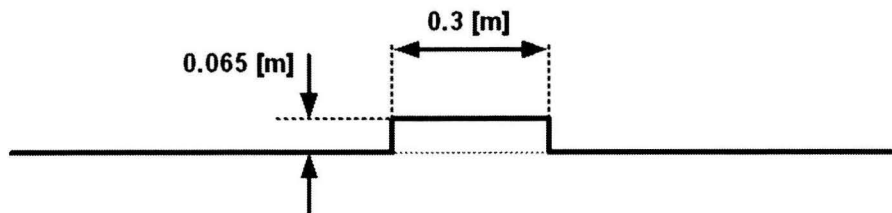


Figure 3.7: Threshold obstacle side view.

Table 3.3: Vehicle velocities for riding over the discrete obstacles.

obstacle	velocity [km/h]	Trucklab loading condition
pyramid	5, 7.5, 10, 12.5 and 15	laden
step down	5 (walking pace)	laden
threshold	5 (walking pace)	laden

3.2.2 Driver controlled manoeuvres

Besides vehicle testing on different road surfaces, driver controlled manoeuvres are performed. The objective of this type of testing is to obtain insight in longitudinal and lateral acceleration levels, suspension travel and pitch, roll and yaw rates when subjected to frequently occurring driving manoeuvres. These tests are carried out with the laden *Trucklab* configuration and consist of accelerating, braking and steering. Below, a short description of the manoeuvres is given.

Accelerating

Two different acceleration tests are performed. For the first acceleration test the vehicle is accelerating from a standstill up to the maximum velocity in first gear on a level road. After reaching the maximum velocity in first gear the clutch is disengaged. Changing gears is intentionally avoided because the simulation model is not equipped with a detailed drive line model. The second acceleration test is performed on a six per cent road slope with a low initial speed (walking pace), subsequently the throttle is applied to reach maximum engine revs in first gear.

Braking

There are two types of braking manoeuvres; normal and heavy braking. For a normal braking the maximum longitudinal deceleration is $\pm 1.5 \text{ m/s}^2$ and the maximum deceleration for heavy braking is $\pm 5 \text{ m/s}^2$. The initial velocity of a braking manoeuvre is set to 60 km/h. During these brake tests the *Trucklab* anti-lock brake system (ABS) is switched off and the brakes remain applied after the vehicle comes to a standstill. The anti-lock brake system is switched off because it affects the vehicle behaviour when braking (suspension deflections and stopping distance).

Steering

The steering manoeuvres consist of three different tests; the step steer, double lane change and circle test. For step steer testing the initial vehicle velocity is 50 km/h and subsequently a step of 60 deg. is applied to the steering wheel. This results in a very abrupt change of vehicle direction. With double lane change testing the change of direction is more gradually. The initial speed is set at 50 km/h and next a sinusoidal motion with an amplitude of 60 deg. is applied to the steering wheel. For a double lane change test, two consecutive lane changes are carried out, making the vehicle end up in the same lane as it started the first lane change from. The last steering manoeuvre is a circle test. For this test the vehicle is starting from a complete standstill and is gradually accelerating, when driving in a circle with a fixed radius, up to a lateral acceleration of about 5 m/s^2 . This test is carried out clockwise and anti-clockwise. For these steering manoeuvres the *Trucklab* safety systems, as *Vehicle stability Control* (VSC) which assists the driver, are switched off.

3.2.3 Experimental data

The data of every experimental test, described in the previous chapters, is stored as an *MATLAB*® Level 5 MAT-file. Level 5 MAT-files are compatible with *MATLAB*® versions 5 and up. The total amount of data is approximately 350 MB distributed over 145 files. Each individual data file corresponds with a single test and consists of 45 sensor data channels. The first two characters of a filename are a number followed by a letter. Each number and letter combination corresponds to one of the experimental tests mentioned earlier. A list with the character combinations and their corresponding experimental test is included in Appendix A.2. Furthermore, a list with channel names is included in Appendix A.3.

Chapter 4

Baseline simulation model

The simulation model is based on the multibody formulation approach, see section 2.1.1, and the adopted multibody software package is *SimMechanics*. Furthermore, the first version of the model was constructed in the absence of experimental data and is defined as the *baseline* simulation model.

In this chapter the tractor semi-trailer simulation model is discussed. The utilised multibody software package, simulation model construction, adopted coordinate system and excluded elements and phenomena are discussed.

4.1 SimMechanics

The adopted multibody simulation software package is *SimMechanics*. This package is a toolbox in *Simulink*[®], within the *MATLAB*[®] environment, with tools for three-dimensional modelling and simulating mechanical systems. *SimMechanics* simulates the motion of mechanical devices and generates motion variables associated with this motion. It provides tools for building mechanical models that include bodies, joints, coordinate systems and constraints. Furthermore, it is possible to connect *SimMechanics* blocks with *Simulink*[®] blocks to include nonmechanical, multidomain effects in the mechanical models. *SimMechanics* automatically creates three-dimensional animations of the constructed mechanical system. With the *MATLAB*[®] *Virtual Reality Toolbox* a connection can be made to a VRML environment for more advanced animations.

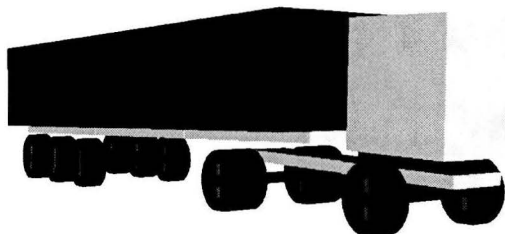


Figure 4.1: Virtual Reality visualisation.

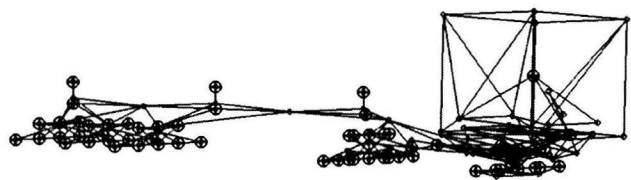


Figure 4.2: SimMechanics visualisation.

Figure 4.1 and figure 4.2 display the three-dimensional animation of the tractor semi-trailer model in the *VirtualRealityToolbox* and the default *SimMechanics* visualisation respectively. When constructing a highly complex multibody model, the use of the *Virtual Reality Toolbox* is preferred over the standard animation, as the different model components and their movements are better distinguishable.

4.2 Model construction

In this paragraph a description is given of the simulation model as it is constructed by *TNO Automotive* in association with the *Eindhoven University of Technology*. This vehicle model consists of a number of predefined modules which are stored in a *Simulink*[®] library file called the *trucklib*. Using predefined modules makes the construction of different truck configurations straightforward; furthermore, changing module specific parameters is also very simple. Examples of stored modules are: cabin, chassis, drive line, axles and driver.

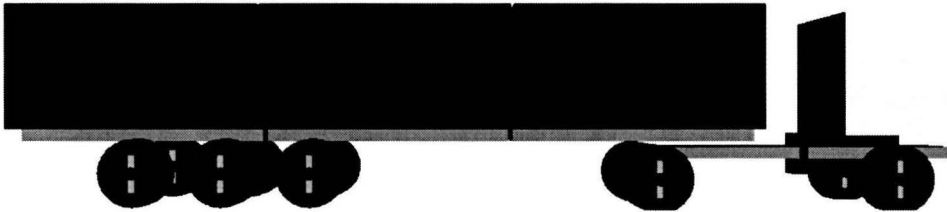


Figure 4.3: Tractor semi-trailer simulation model, side view in virtual reality.

Figure 4.3 displays the three-dimensional tractor semi-trailer model. The model contains 27 bodies connected by joints, springs and dampers. Each body adds 6 degrees of freedom, but constraints and joints reduce the final model to 45 degrees of freedom.

4.2.1 Chassis

The tractor chassis consists of two rigid bodies interconnected by a torsional spring and has 7 degrees of freedom. The spring represents the chassis torsional stiffness. Spare wheel, fuel tank and battery carrier are part of tractor chassis bodies, and are not modelled as individual rigid bodies fixed to a chassis body. The tractor chassis module serves as the backbone of the simulation model to which the other modules are connected. The trailer chassis consists of three bodies interconnected by torsional springs representing the chassis torsional stiffness. The trailer chassis has 4 degrees of freedom with respect to the tractor chassis.

4.2.2 Cabin

The tractor cabin is modelled as one rigid body with 6 degrees of freedom with respect to the tractor chassis. The cabin front suspension consists of two air-spring/damper elements in combination with an anti-roll bar simplified as an torsional spring. The cabin rear suspension consists of two air-spring/damper elements. The cabin suspension is equipped with a levelling control system.

4.2.3 Drive line

The engine block and transmission are represented by a rigid body which is suspended with respect to the tractor chassis by flexible engine mounts and has 6 degrees of freedom. The engine and transmission are connected to the rear axle by a drive axle body and serves as a reaction rod for engine torque. The engine itself, gearbox and final reduction are modelled as a *Simulink*[®] control block which is directly linked to the drive axle wheels. This drive line model is a highly simplified representation of reality.

4.2.4 Axles

The front or steering axle is modelled as a rigid body. A revolute joint connects the wheel with the upright body and serves as a wheel bearing. Another revolute joint connects the upright body with the axle body and serves as steering axis. These two revolute joints provides the steering axle wheels with 2 degrees of freedom. Steering angles of the wheels are a constrained motion enforced by the steering

4.3 Coordinate systems

wheel. The axle body has 2 degrees of freedom with respect to the chassis body; vertical translation and a rotational degree of freedom around the x-axis of the vehicle coordinate system (rolling motion). The suspension consist of two springs and dampers and a anti-roll bar modelled as a torsional spring.

The rear or driven tractor axle is modelled as a rigid body with two tyres on each axle end. The tyres are connected to the axle body by revolute joints and have 1 degree of freedom (wheel rotation). Same as the front axle, the axle body has 2 degrees of freedom with respect to the chassis body. Elements used for the suspension are: two springs, two dampers and an anti-roll bar in the form of a torsional spring. The rear axle is connected to the engine and transmission by a rigid drive axle body and serves as a reaction rod for the engine torque.

The trailer axle is modelled as a rigid body with 2 degrees of freedom with respect to the chassis. Two springs, two dampers and a torsional spring connect the axle body with the chassis. Furthermore, the axle is equipped with two tyres and brake torque is also directly imposed to the revolute joint connecting axle and wheels. Each wheel has 1 degree of freedom with respect to the axle body.

MF-Tyre is tyre model used in the vehicle model. *MF-Tyre* is part of TNO Delft-Tyre model which is a semi-empirical tyre model. Semi-empirical tyre modelling has the advantage that the resulting tyre model tends to be accurate and fast, but it relies on tyre measurements. The TNO Delft-Tyre model adopts the *Magic Formula* of professor Pacejka for the description of the tyre forces and moments. The *MF-Tyre* model can be used for handling simulations and can account for tyre dynamics up to 8 Hz. For more information on this subject see [5], [7] and [22].

4.2.5 Other model components

Driver

The driver is modelled as a *Simulink*[®] control system and serves as a simulation model operator. Control system outputs are brake pedal position, throttle pedal position, steering wheel angle.

Trailer load

The total trailer load is evenly distributed over the complete trailer chassis length and consists of three bodies. Every load body is rigidly connected to a trailer chassis body.

Sensors

To be able to compare simulation and experimental data, the *Trucklab* sensor positions are measured and adopted in the simulation model. The sensors used in the simulation model are standard *SimMechanics* body and joint sensors. In Appendix A.3 a list of simulation model signal names and their corresponding *Trucklab* counterparts is included.

4.3 Coordinate systems

This paragraph describes two types of adopted coordinate systems; an earth-fixed and a vehicle coordinate systems.

Earth-fixed coordinate system

The *earth-fixed* coordinate system (X,Y,Z) is a right-hand orthogonal axis system fixed on the earth. The X and Y-axis are in a horizontal plane and the Z-axis is directed upward (Figure 4.4). The initial positions of all model components are defined with respect to the *earth-fixed* coordinate system.

Vehicle coordinate system

The *vehicle* coordinate system (X',Y',Z') is a right-hand orthogonal axis system fixed in a vehicle such that, with the vehicle moving steadily in a straight line on a level road, the x-axis is substantially

horizontal, points forward and is in the longitudinal plane of symmetry. The y-axis points to the driver's left and the z-axis points upward (Figure 4.4).

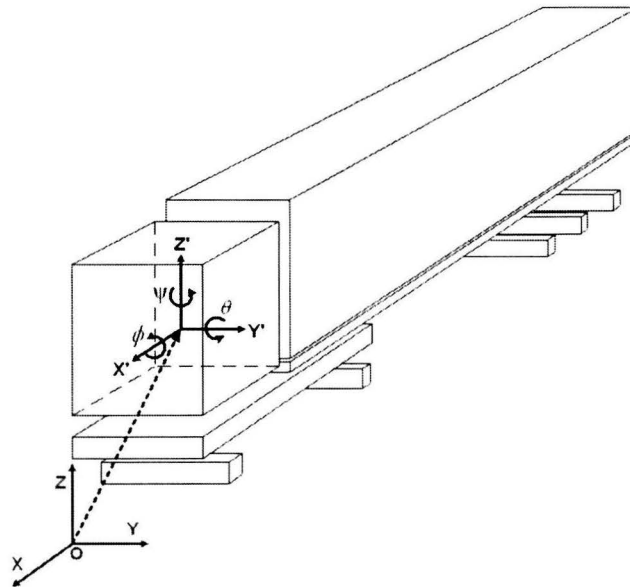


Figure 4.4: The *earth-fixed* and *vehicle* coordinate system.

Figure 4.4 displays the *earth-fixed* and *vehicle* coordinates system with the roll ϕ , pitch θ and yaw ψ rotations.

4.4 Excluded elements and phenomena

The simplest possible model adequately describing the studied phenomena is sought. Many features in actual vehicles are excluded or lumped together. Steering system linkages, suspension geometry, frame flexibility and aerodynamic forces are not included in the *baseline* simulation model. Steering system linkages and suspension geometry are excluded to limit the model size and complexity. Detailed frame flexibility is excluded to improve simulation speed; moreover, it is not straightforward to model a flexible frame in *SimMechanics*. Aerodynamic forces are also not included.

4.5 Simulation data

For the simulation of a test, measured experimental data is used in order to perform a similar test as performed with the *Trucklab*. The measured experimental data consists of vehicle velocity and steering wheel angle. By using measured experimental data for each simulation, there is a direct link between a experimental data file and a simulation data file. The simulation signals are sampled at a rate of 100 Hz and stored as a structure in a *MATLAB*® MAT-file. The filename includes the simulation model name, type of test and corresponding experimental data filename.

Chapter 5

Model evaluation method

In order to quantify the mismatch in vehicle behaviour between the *Trucklab* and simulation model, an evaluation method is developed. This method implies comparing *Trucklab* and simulation model sensor data, when subjected to the experiments mentioned in section 3.2. In addition, this method is also used for comparing *baseline* model results with the results of an adapted version of the simulation model in order to demonstrate the effects of implemented adjustments, see chapter 6 and 7. The *baseline* model is defined as the original simulation model developed by *TNO Automotive* in association with the *Eindhoven University of Technology*, dated July 2006. The construction of the *baseline* model is discussed in chapter 4.

The comparison of sensor data can be performed in either the time or frequency domain. To restrict the amount of work, solely time domain signals are considered. As a consequence, the experiments involving riding over different road surfaces are not included in the model evaluation process. Notice that the experiments involving riding over discrete obstacles are included.

Because of the enormous amount of experimental data it is not feasible to perform the model evaluation by hand. For this purpose an evaluation algorithm is developed. This algorithm makes use of the evaluation method, explained in section 5.1, and computerises the evaluation process. In section 5.2 the evaluation algorithm is treated.

5.1 Methodology

A suitable methodology for the evaluation of the simulation model is essential. For example, simply comparing experimental and simulation data using graphics is not suitable due to the large amount of experimental data; moreover, this approach is subjective. Subjectivity is not desirable because this makes the model evaluation dependent on one individual person. The methodology adopted for the model evaluation consists of comparing signal data by means of statistical measures. Statistical measures are used to assess the sensor data in an objective manner. Complete objectivity is desirable, because this makes the model evaluation independent of the individual person using the methodology, but this can not entirely be achieved. The usage of weight factors in combination with statistical measures add some subjectivity to the methodology. The adopted statistical measures and weight factors are discussed in the sections below.

In order to be able to compare simulation and experimental sensor data, the first step is to synchronise simulation and experimental data. By doing so, the initial contact between vehicle and a discrete obstacle, for example, occur at the same time. After this a time interval is indicated containing the sensor data of the performed test. This interval is applied to each sensor data channel of the considered test. Subsequently, statistical measures are utilised to quantify the level of correspondence

between the signals for the indicated time interval. These statistical measures are based on computing the *root mean square*. The *root mean square* is a statistical measure of the magnitude of a varying quantity. In section 5.1.1 the adopted statistical measures are explained. The level of correspondence between two signals is reflected by a score and is computed for each signal relevant for the considered experiment. The computed score varies between zero and one, where zero represents the minimum and one represents the maximum score. In the end a final signal score is computed for each signal of every experiment. The final signal score of a considered experiment is the average of the individual test scores for that particular signal. Finally, the model evaluation is presented as a bar chart for every experiment containing the average and standard deviation of the signal scores.

5.1.1 Statistical measures

For time domain signal comparison adapted statistical measures are deduced from existing measures as *root mean square (RMS)* and *root mean squared error (RMSE)* [4]. First, existing statistical measures are explained before discussing their deduced ones.

The *root mean square*, also known as the *quadratic mean*, is a statistical measure of the magnitude of a varying quantity and is computed by taking the square root of the mean of the squared values for a collection of n values $\{g_1, g_2, g_3, \dots, g_n\}$. The root mean square is computed by:

$$g_{rms} = \sqrt{\frac{1}{n} \sum_{i=1}^n g_i^2}, \quad (5.1)$$

where the computed value has the same unit as the values in the considered collection.

The *root mean squared error*, is a quadratic scoring rule which measures the average magnitude of the error. This value is computed by taking the square root of the average of the squared differences between each computed value (f_i) and its corresponding reference value (g_i):

$$e_{rms} = \sqrt{\frac{1}{n} \sum_{i=1}^n (f_i - g_i)^2} = \sqrt{\frac{1}{n} \sum_{i=1}^n e_i^2}, \quad (5.2)$$

where the computed *root mean squared error* value has the same unit as the actual and predicted values. Note that for the comparison of the computed and the reference signals both signals must have the same sample rate.

The adopted statistical measures for the model evaluation methodology are deduced from (5.1) and (5.2) and are called *weighted root mean square*, and *weighted root mean squared error*, respectively. The *weighted root mean square* is computed by:

$$\bar{g}_{rms} = \sqrt{\frac{1}{n} \sum_{i=1}^n w_i g_i^2} \quad (5.3)$$

The *weighted root mean squared error* is computed by:

$$\bar{e}_{rms} = \sqrt{\frac{1}{n} \sum_{i=1}^n w_i (f_i - g_i)^2} = \sqrt{\frac{1}{n} \sum_{i=1}^n w_i e_i^2} \quad (5.4)$$

Equations (5.3) and (5.4) differ from (5.1) and (5.2) because a weight factor is added for every error and signal value. The weight factors are specified in an additional array $w = \{w_1, w_2, w_3, \dots, w_i\}$. With the addition of weight factors, specific intervals can be marked as significant or insignificant. Significant intervals have a far greater impact on the computed *weighted root mean square* and *weighted root mean squared error* values than insignificant intervals. An example of an insignificant interval is a

5.1 Methodology

section mainly containing noise. By assigning weight factors the contribution of noise is limited. In the upper left graph of Figure 5.1, insignificant intervals are indicated for the vertical axle acceleration when riding over a discrete obstacle. The lower left graph displays the weight factors used for the computation of the *weighted root mean square* and *weighted root mean squared error* values for the vertical acceleration signal. Note that the weight factor values for the insignificant intervals are not equal to zero but very small. Figure 5.1b displays the weight factors of every sample for the vertical axle acceleration of Figure 5.1a. The significant area is coloured gray and both insignificant areas are coloured white.

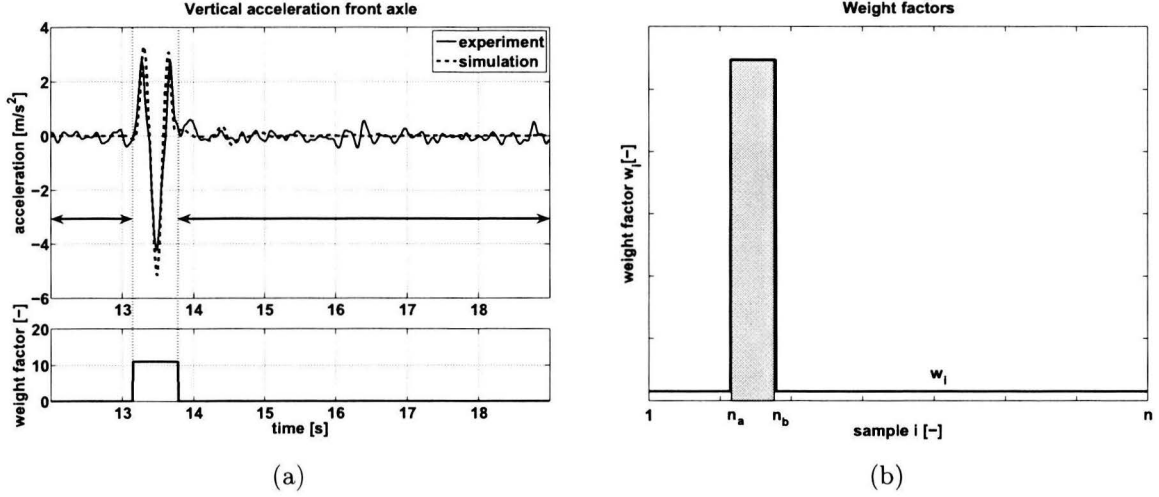


Figure 5.1: Insignificant signal sections and weight factors.

The weight factor values for the significant and insignificant intervals are determined using the following two equations:

$$k \left(\frac{1}{f} \sum_{i=1}^{n_a} w_i + \frac{1}{f} \sum_{i=n_b}^n w_i \right) = \frac{1}{f} \sum_{i=n_a}^{n_b} w_i, \quad (5.5)$$

$$\frac{1}{n} \sum_{i=1}^n w_i = 1, \quad (5.6)$$

where f is the sample frequency and k is a ratio between the summation of the significant and the summation of the insignificant areas. Equation (5.5) states there is a fixed ratio k between the significant and insignificant areas. The expression left of the equal sign in (5.5) is the summation of the areas under w_i where the weighing is low, multiplied with a factor k . The expression right of the equality sign is the summation of the areas under w_i where the weighing is high. The factor k is a predefined (large) ratio between the two areas and makes that the contribution of the insignificant sections (noise) is always limited, even if the duration of the significant section is very short compared to the duration of the insignificant sections. The value of k is determined by testing a wide range of factors and is finally set to 10^4 for obtaining evaluation scores that give a fairly accurate indication of the match between measurements and simulation. Higher values for k show no significant improvement with respect to the score computation.

Solving (5.5) yields a ratio between the high and low weight factors for the significant and insignificant areas respectively. In order to determine the high and low weight factor values, an additional equation must be introduced which is (5.6). Equation (5.6) is determined based on a situation where the error between two signals is considered constant, $e_i = C$. For this situation, solving (5.4) must yield $\bar{e}_{rms} = C$, regardless of the chosen weight factors. When the error is considered constant, (5.4) can be rewritten as:

$$\bar{e}_{rms} = C \sqrt{\frac{1}{n} \sum_{i=1}^n w_i} \quad (5.7)$$

The result of (5.7) depends on the square root of the mean of the chosen weight factors. When the average of the adopted weight factors is equal to one, the computed *weighted root mean squared error* value is equal to C . Because of this the weight factor average must be equal to one (5.6). Solving (5.5) and (5.6) yields the correct weight factor values.

5.1.2 Score computation

For the quantification of the level of correspondence between two signals, a score is computed using the computed *weighted root mean square* and *weighted root mean squared error* values (5.8).

$$score = 1 - \frac{\sqrt{\frac{1}{n} \sum_{i=1}^n w_i (f_i - g_i)^2}}{\sqrt{\frac{1}{n} \sum_{i=1}^n w_i g_i^2}} = 1 - \frac{\bar{e}_{rms}}{\bar{g}_{rms}}, \quad \bar{g}_{rms} \neq 0 \quad (5.8)$$

The score is computed by subtracting the relative error from one, where the relative error is defined as the quotient of the *weighted root mean squared error* and *weighted root mean square* of the reference signal. This yields a maximum score of one, when the relative error is equal to zero, and a score of zero when the relative error is equal to one. Note that the score can be less than zero in the case of *weighted root mean square* value of the reference signal being less than the *weighted root mean square error* value. In this case the score is set to zero.

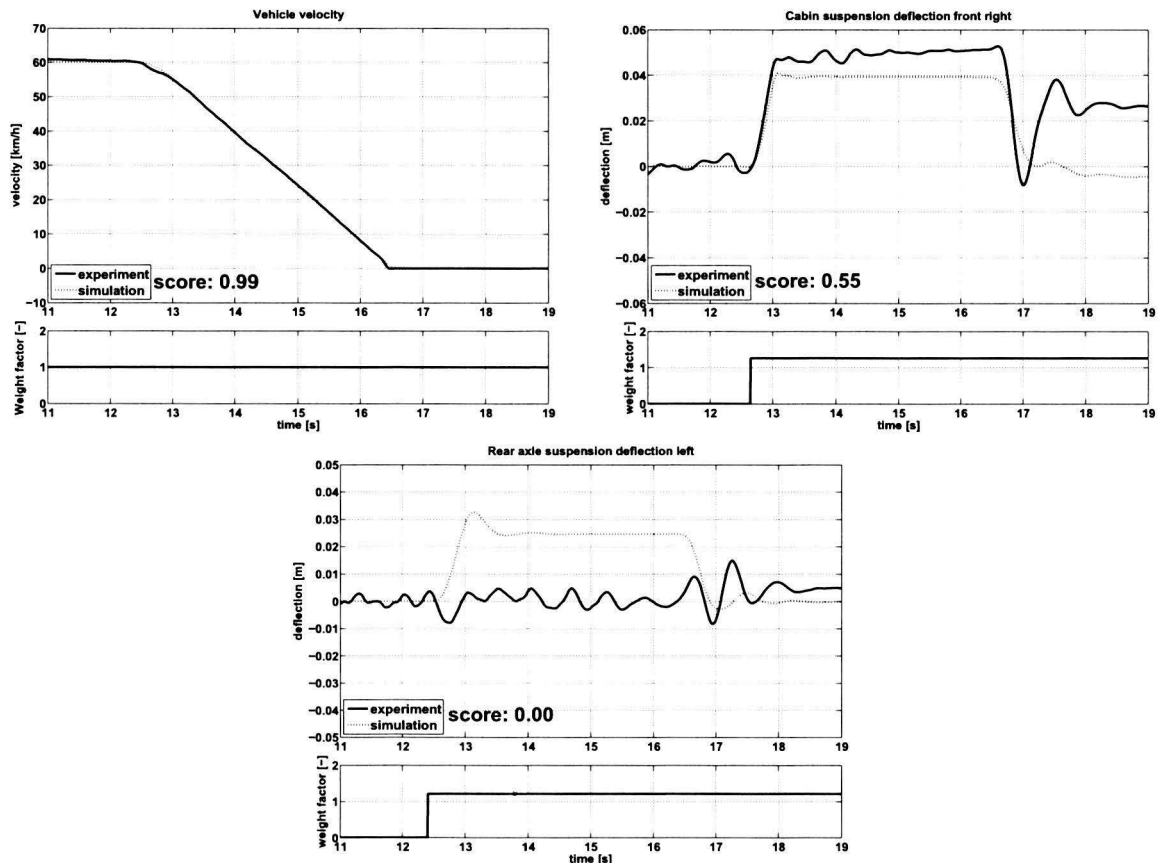


Figure 5.2: Evaluation scores for three different signals.

5.2 Algorithm implementation

Figure 5.2 displays three signals of a heavy braking experiment with their corresponding weight factors and computed scores using (5.8).

5.1.3 Evaluation signals

Not every sensor signal has the same level of relevancy for a particular experiment. For example, evaluating the roll velocity signal of the cabin is not relevant for a braking experiment. Based on the level of relevancy, a selection of sensor signals for every experiment is made which is used for the model evaluation. Appendix B.2 gives an overview of the relevant sensor signals for every experiment.

5.2 Algorithm implementation

For the evaluation process an algorithm is developed and implemented using *MATLAB*[®]. This algorithm computes the signal scores for every test of each type of experiment. The results are presented as bar graphs containing the average signal scores for every experiment. The data used for the computation of the scores is stored as *MATLAB*[®] MAT-files in order to be able to compare the evaluation results of a certain model with the results of a future version of the simulation model. This algorithm is subdivided into different parts, where each part performs a number of specific task within the process. Figure 5.3 displays a schematic overview of the evaluation algorithm.

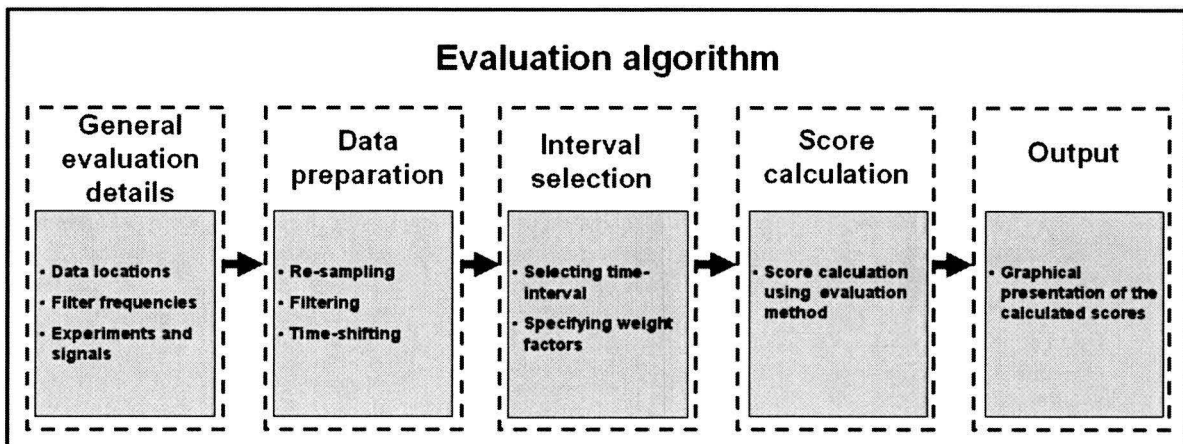


Figure 5.3: Schematic evaluation algorithm overview.

In the next sections an extensive description of each part of the algorithm is given.

5.2.1 General evaluation details

The first step of the evaluation process is to specify the required information. This information consists of specifying; data locations of simulation and experiment results, filter frequencies and experiment specific information.

5.2.2 Data preparation

The next part is the data preparation. The required simulation and experimental data is loaded and stored in a *MATLAB*[®] data structure. Experimental signal names are adopted as general signal names, therefore the simulation signal names are replaced with the names used in the experiments. Subsequently, three more data preparation operations are performed, which are discussed below.

Re-sampling

The sampling rate of the experimental and simulation data is 200 Hz and 100 Hz respectively. To be

able to compare experimental and simulation results for a certain time interval, the sampling rates of the experimental and simulation data must be the same, because this evens up the amount of data points for the considered interval. Increasing the sampling rate of the simulation data is not an option because this will result in a large increase of computing time. Instead, the experimental data is re-sampled with the standard *MATLAB*[®] function called *resample.m* to a sampling rate of 100 Hz.

Filtering

All the experimental sensor data contain a certain amount of noise. Sensor data collected from the *Trucklab* CAN is already filtered and therefore contain less noise than other *Trucklab* sensor data. To lower the undesired signal noise and simultaneously preserve valuable signal information, the data is filtered by a 15 Hz low-pass filter. The data is filtered with the standard *MATLAB*[®] function called *filtfilt.m*. Advantages of using this function is that it causes no phase distortion and it minimises start-up and ending transients. A cutoff frequency of 15 Hz removes a considerable amount of noise and preserves the frequency range of the dominant vehicle excitation modes to a large extent. Examples of dominant vehicle excitation modes are; vehicle roll, front axle bounce and rear axle bounce. The frequencies of the dominant vehicle modes are taken from literature on vehicle dynamics [5]. For an overview of the dominant vehicle modes see Appendix B.1. To ensure a fair comparison later on, the simulation data is filtered with the same filter. N.B., the evaluation results deteriorate severely for cut-off frequencies much higher than 15 Hz. Higher cutoff frequencies are accompanied by more noise and therefore deteriorating the computed scores.

Time-shifting

The initial contact between vehicle and road obstacle, applying the brakes or a steering wheel angle occur at different times for the experiments and simulations. This results in a time difference between experimental and simulation data. This time difference is eliminated by shifting the simulation data in time. For this time-shifting of simulation data, a *time-shift signal* is indicated for every type of experiment. An example of a *time-shift signal* is the vertical axle acceleration for experiments involving riding over a discrete obstacle. Appendix B.4 provides an overview of the *time-shift signals* for every type of experiment.

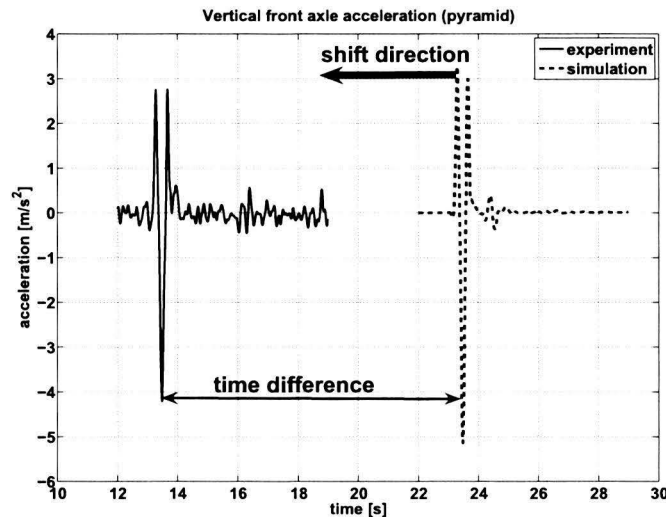


Figure 5.4: Time difference between experiment (solid) and simulation (dashed).

For the *time-shift signal* the time difference between experimental and simulation is determined and used for the elimination of the time difference of the other sensor data channels of the considered test. The time-shift factor is determined by computing the difference between the experimental and simulation data at every sampled time instant when the simulation data shifts over the experimental

5.2 Algorithm implementation

data. The time instant at which the error is minimal determines the time-shift factor. The time-shift factors are calculated whenever a specific model is evaluated using the algorithm. In Figure 5.4 the vertical front axle acceleration and the time difference are displayed for riding over a discrete obstacle (pyramid).

5.2.3 Interval selection

The next step of the evaluation algorithm is the interval selection. This interval represents the domain of interest for a concerned test. For each test an interval is selected by indicating the beginning and end of the domain of interest, see Figure 5.5. Figure 5.5 displays the interval selection for the experiment of riding over a discrete obstacle. The selected interval is applied to every relevant signal of the concerned test.

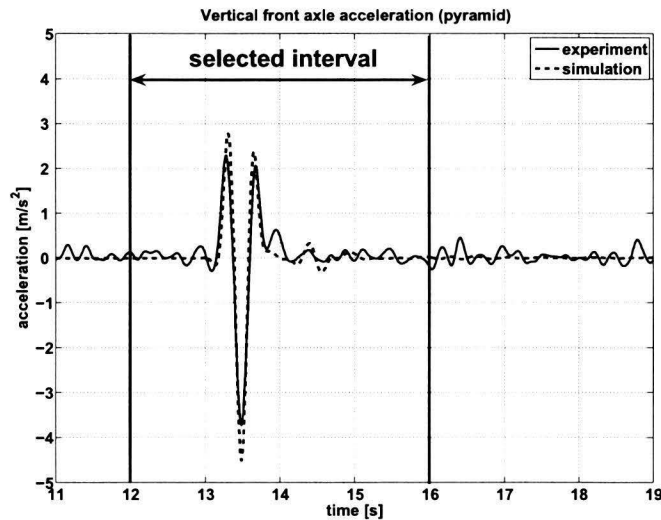


Figure 5.5: interval selection.

The next step is to subdivide the selected interval into significant and insignificant sections. This is done for every relevant sensor signal of the considered test. For the significant and insignificant sections the weight factors are computed as explained in section 5.1.1. The specified intervals of all the tests are stored in a *MATLAB*[®] data file. These intervals are adopted whenever a simulation model is evaluated using the *Trucklab* data of the experiments discussed in chapter 3. For every new set of *Trucklab* data, new intervals are specified.

5.2.4 Score calculation

This part of the evaluation algorithm computes the signal scores of all the performed tests using (5.8) stated in section 5.1; moreover, final signal scores are computed for each type of experiment. These final signal scores are averages of the signal scores of the individual tests because each experiment consists of multiple tests. To minimise the effects of noise on the calculated scores, the *RMS* value of the sensor noise of each signal is determined and subtracted from the *RMS* value of the experimental sensor signals. The *RMS* value of the signal noise is determined with sensor data originating from an experiment where the *Trucklab* is in standstill with the engine running. In Appendix B.3 the sensor noise *RMS* values for the used sensor data channels is given. Two important contributors to the signal noise are: the engine and the used *Trucklab* sensors (sensor noise).

5.2.5 Output

The output of the evaluation algorithm consists of bar graphs, one graph for each experiment. In these graphs the average signal evaluation scores are displayed. Figure 5.6 displays the average evaluation

scores of the relevant sensor signals for an acceleration test on a level road. The relevant sensor signals for each type of experiment are discussed in section 5.1.3. By examining the evaluation plots, the deficiencies in the simulation model can be indicated. A computed evaluation score of 1 denotes a perfect match between experiment and simulation. A score of 0 or close to 0, means there is a profound mismatch between the experimental and simulation sensor signals.

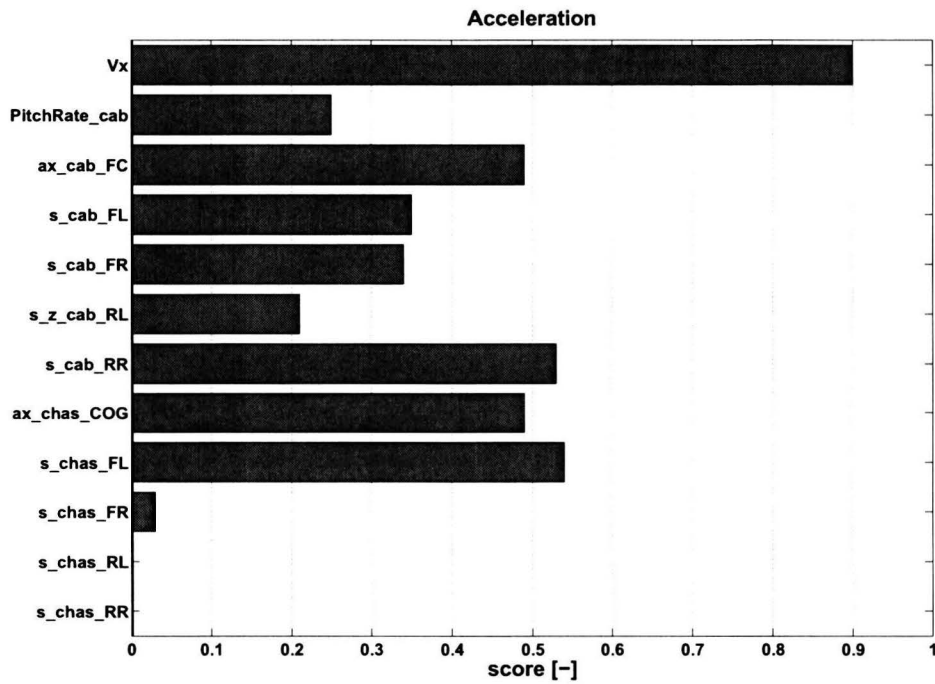


Figure 5.6: Bar graph of the evaluation scores for the acceleration test.

Chapter 6

Baseline model analysis

In this chapter the *baseline* model is analysed. The *baseline* model is defined as the original tractor semi-trailer simulation model, status: July 2006, as it is developed by *TNO Automotive* in association with *Eindhoven University of Technology*. The construction of this *baseline* model is discussed in chapter 4. The analysis is performed to review the differences with the experiments. By means of this analysis the weakness and strength of the simulation model is indicated. The objective is to improve the weakness of the simulation model by parameter tuning and implementing adjustments. Some of the model weaknesses require only minor adjustments to the simulation model and are therefore relatively simple to improve. Other weaknesses require a more profound study of the simulation model and its results in order to find the cause and appropriate model adjustments. The latter is discussed in chapter 7.

In the first section of this chapter the *baseline* model is evaluated using the evaluation algorithm of section 5.2. Based on these evaluation results small model adjustments are implemented and discussed in sections 6.2 through 6.6. In section 6.7 an updated version of the *baseline* model is introduced. This version of the simulation model contains the adjustments discussed in this chapter and is referred to as *reference* model from this point on. This model is called *reference* model as it is used as a reference for the model adjustments of chapter 7.

6.1 Evaluation scores

For the *baseline* model analysis many simulations are performed. Each simulation represents a test performed with the *Trucklab* test vehicle. This experimental and simulation data is used for the evaluation of the simulation model. In this section the *baseline* model is evaluated using the algorithm discussed in section 5.2. This algorithm compares the experimental and simulation data and computes a score to quantify the match or mismatch. Based on the computed scores of this evaluation algorithm, the weaknesses of the *baseline* model are indicated.

The results of the evaluation algorithm are presented in tabular form, see Table 6.1. This table contains the average signal scores of the *baseline* model for each type of experiment. Each column contains the average signal scores of a performed experiment with the exception of the last column. This column represents average scores computed over all the performed experiments. A gray field in Table 6.1 means that the concerning sensor signal is not evaluated for that particular test. Note that only the relevant sensor signals for each experiment are evaluated, see section 5.1.3.

After a closer examination of the results of Table 6.1, the sensor signals can be classified into three categories. The first category holds the sensor signals with a uniform score for each experiment being above average on a scale of 0 to 1. For example, the longitudinal vehicle velocity (V_x) has an average

score of 0.97 and all the scores of the concerning distribution are close to the average value. Other sensor signals belonging to this category are: the steering wheel angle (SWheel_Angle); the longitudinal cabin acceleration (ax_cab_FC) and the longitudinal chassis acceleration (ax_chas_COG).

Table 6.1: Baseline model evaluation scores.

			Experiments									average score	
			pyramid	step down	threshold	acceleration	normal braking	heavy braking	circle	double lane change	stepsteer		
signals	cabin	ang.	Vx	0.98	0.96	0.96	0.90	0.97	0.99	0.99	0.99	0.99	0.97
			SWheel_Angle							0.94	0.99	0.98	0.97
		ang.	RollRate_cab	0.13	0.00	0.01				0.14	0.59	0.53	0.23
			PitchRate_cab	0.36	0.03	0.12	0.25	0.16	0.30				0.20
			YawRate_cab	0.09	0.12	0.00				0.81	0.88	0.83	0.46
			acc.	az_cab_FL	0.34	0.04	0.09						
		az_cab_FR		0.40	0.07	0.08							0.18
		az_cab_RL		0.28	0.11	0.12							0.17
		az_cab_RR		0.40	0.27	0.26							0.31
		ax_cab_FC					0.49	0.75	0.81				0.68
		ay_cab_FC		0.08	0.00	0.01				0.66	0.67	0.61	0.34
		az_cab_FC											
		defl.		s_cab_FL	0.30	0.07	0.07	0.35	0.60	0.59	0.20	0.19	0.16
			s_cab_FR	0.37	0.08	0.10	0.34	0.61	0.59	0.02	0.25	0.17	0.28
			s_z_cab_RL	0.14	0.12	0.00	0.21	0.61	0.74	0.19	0.20	0.26	0.27
			s_cab_RR	0.25	0.00	0.14	0.53	0.58	0.75	0.20	0.23	0.24	0.32
	chassis	ang.	YawRate_chas	0.00	0.00	0.00				0.81	0.81	0.82	0.41
			acc.	az_chas_FL	0.46	0.03	0.07						
		az_chas_FR		0.53	0.08	0.11							0.24
		az_chas_RL		0.47	0.09	0.14							0.23
		az_chas_RR		0.50	0.22	0.22							0.31
		ax_chas_COG					0.49	0.80	0.87				0.72
		ay_chas_COG		0.00	0.00	0.00				0.70	0.70	0.64	0.34
		az_chas_COG											
	axles	defl.	s_chas_FL	0.13	0.08	0.01	0.54	0.58	0.67	0.62	0.71	0.69	0.45
			s_chas_FR	0.23	0.22	0.03	0.03	0.50	0.66	0.59	0.75	0.71	0.41
			s_chas_RL	0.18	0.00	0.00	0.00	0.00	0.00	0.36	0.00	0.00	0.06
			s_chas_RR	0.04	0.00	0.00	0.00	0.00	0.00	0.02	0.20	0.11	0.04
		acc.	az_axle_FL	0.65	0.00	0.00							0.22
			az_axle_FR	0.54	0.00	0.00							0.18
			az_axle_RL	0.50	0.00	0.00							0.17
			az_axle_RR	0.45	0.00	0.00							0.15

The second category contains the sensor signals with a wide spread variation of scores. A representative example is the yaw velocity of the cabin (YawRate_cab) where the scores are low for experiments involved with riding over discrete obstacles. However, the scores of the experiments with regard to steering manoeuvres on the other hand, have respectable scores. Other sensor signals belonging to this category are; lateral cabin acceleration (ay_cab_FC), yaw velocity chassis (YawRate_chas) and lateral chassis acceleration (ay_chas_COG).

6.2 Updating model parameters

The third and last category holds the sensor signals with an uniform low score for each experiment. For example, the vertical axle accelerations. Other signals belonging to this category are; the vertical suspension deflection sensor signals of axles and cabin, vertical accelerations of chassis and cabin, the roll and pitch velocity of the cabin. Because of the low scores, the sensor signals belonging to this category are considered as the weaknesses of the *baseline* model. In the following sections and in the next chapter, the causes of the model weaknesses are studied and improved, whenever feasible, by implementing adjustments to the *baseline* model.

6.2 Updating model parameters

The first step of improving the simulation model requires the verification of the adopted *baseline* model parameters. As stated earlier, the *baseline* model has been constructed before the exact configuration of the *Trucklab* test vehicle was known. Consequently, a considerable number of the model parameters had to be estimated as their exact values were unknown at the time of construction. An example of such a parameter is the wheelbase of the tractor. Other model parameters were already available and are originating from the manufacturer of the *Trucklab* test vehicle. Examples of available parameters are the spring stiffnesses and damper constants of the primary and cabin suspension.

For the verification of the estimated model parameters, measurements are carried out on and with the *Trucklab*. For the determination of the static *Trucklab* axle loads and total weight, the *Trucklab* is placed on a weighing machine. The measurements are used as a reference for the simulation model. By adjusting the weight and longitudinal centre of gravity position of the tractor chassis and primary suspension pre-loads, the correct total weight and a good approximation of the axle loads are obtained for the solo tractor. Next, the weights and longitudinal centre of gravity positions of the trailer components and the spring pre-loads of the trailer axles are adjusted to obtain the correct total weight and good approximation of the axle loads for the tractor semi-trailer model. In table 6.2 the static axle loads for the *Trucklab*, *baseline* model and the *reference* model are displayed. Note that a good approximation of the axle loads with respect to the measurements, result in a good approximation of the longitudinal centre of gravity position of the simulation model.

Table 6.2: Static axle loads for tractor with semi-trailer and solo tractor.

tractor with semi-trailer				solo tractor			
	<i>Trucklab</i> (measurements)	<i>baseline</i> model	<i>reference</i> model		<i>Trucklab</i> (measurements)	<i>baseline</i> model	<i>reference</i> model
Front axle load [kg]	6860	7419	6851	Front axle load [kg]	5230	5430	5231
Rear axle load [kg]	12680	11569	12740	Rear axle load [kg]	2250	2306	2255
Trailer axle load (1) [kg]	7250	7033	7243	Totaal [kg]	7480	7736	7486
Trailer axle load (2) [kg]	7080	7100	7031				
Trailer axle load (3) [kg]	6700	7167	6705				
Totaal [kg]	40570	40288	40570				

For the determination and verification of position parameters, for example the fifth wheel coupling position, measuring tape is used. All the changes in parameter value are included in the *reference* model treated in section 6.7.

6.3 Modelling errors

The next step in the analysis of the *baseline* model is to check the simulation model on possible errors which can result in unexpected simulation results. Possible modelling errors are located by verifying the block parameters of the used *SimMechanics* bodies and joints. Every single body connection is checked for the correct *Origin Position Vector* and reference coordinate system. The joint parameters are checked for the correct *Axis of Action* and reference coordinate system. Below, two modelling errors of the *baseline* model are discussed.

Fifth wheel coupling

The first modelling error is the vertical position of the fifth wheel coupling. As a result of a wrong reference coordinate system for the fifth wheel coupling connection of the tractor chassis body, the fifth wheel coupling is positioned 0.25 m above the road surface instead of 1.15 m.

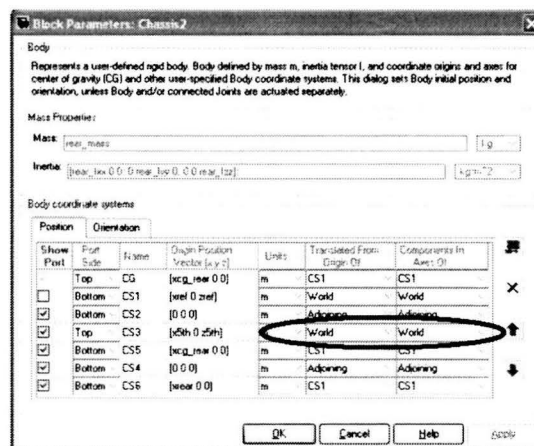


Figure 6.1: *SimMechanics* body block parameters of tractor chassis body.

Figure 6.1 displays the *SimMechanics* block parameters of the tractor chassis body. Encircled is the reference coordinate system for the fifth wheel connection *cs3*. This reference coordinate system is set to *world* (*earth-fixed*) instead of *cs1* (*body-fixed* or *vehicle*) coordinate system, where *cs1* is defined as the tractor chassis reference point. Figure 6.2 is a schematic view of two situations with different fifth wheel coupling positions.

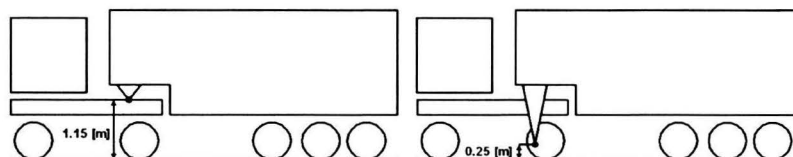


Figure 6.2: Schematic view of two fifth wheel coupling positions.

The difference in fifth wheel coupling heights has a large effect on the tractor primary suspension deflection. The correct fifth wheel coupling height is responsible for a large improvement with respect to the primary suspension deflections when accelerating and braking.

Position revolute joints trailer chassis

As discussed in section 4.2.1, the semi-trailer chassis bodies are interconnected by two revolute joints. Due to a miscalculation the joints were not positioned correctly. Instead both joints were situated 1 m behind the fifth wheel coupling. The correct and incorrect positions are indicated in Figure 6.3. The axis of rotation of the revolute joints is exactly parallel with the longitudinal axis as can be seen in Figure 6.3. This makes a wrong longitudinal component of the revolute joint position a displacement

6.4 Tyre model

along the axis of rotation. Changing the longitudinal position of a revolute joint by shifting it over its axis of rotation has no effect on the simulation results because this has no effect on the equilibrium of forces and moments acting on the trailer.

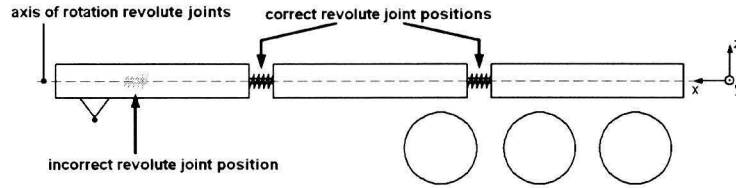


Figure 6.3: Schematic view of the *baseline* trailer construction with correct and incorrect revolute joint positions.

A practical tool in preventing and detecting modelling errors is a decent model visualisation environment that is directly linked to the simulation environment. With a proper model visualisation environment, both modelling errors would have been detected when the first simulations were performed. Because of the poor standard *SimMechanics* visualisation the modelling errors remained undetected.

6.4 Tyre model

In section 4.2.4 the adopted tyre model is discussed. This model is called the *TNO Delft-Tyre model*. When using this tyre model, the user has two choices. The first choice is the so-called *MF-Tyre* model. This model is appropriate for handling simulations (tyre dynamics up to 8 Hz) on a smooth long wavelength road surface. Under these conditions the tyre model gives a good approximation of the forces and moments acting on a tyre. An additional advantage of using this model is that it has a relatively low computation time.

The second choice is the *MF-Swift* model. This model is more complex than the *MF-Tyre* model due to the addition of an enveloping model making it suitable for riding over short wavelength road obstacles. This enveloping model is a special filter that takes care of the envelopment properties of the tyre and the variation in effective rolling radius that occurs when the tyre rolls over a short obstacle. Figure 6.4 gives a schematic overview of the *MF-Swift* model. This model can account for tyre dynamics up to 60-80 Hz. A disadvantage of using this model is that it has a relatively high computing time.

Both tyre models depend on measurements performed with real tyres. Using these tyre measurement data, parameters are determined for the description of the forces and moments of the tyre models. For more information on this subject see [5], [7] and [22].

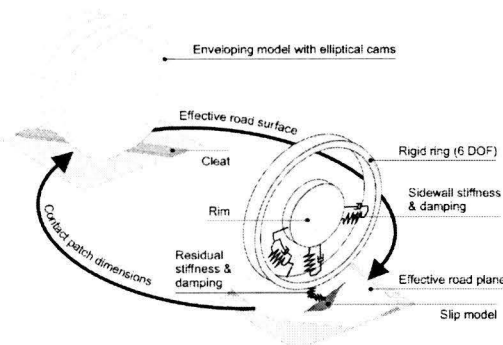


Figure 6.4: Schematic overview of the *MF-Swift* model, with rigid ring and enveloping model, [7].

The *baseline* model uses *MF-Tyre* as tyre model. For the experiments carried out on a flat road surface as braking and accelerating, this model is sufficiently accurate. For the experiments with regard to

riding over road obstacles this model is not sufficiently accurate. This is confirmed by the evaluation scores of section 6.1 and the simulation results of these experiments. Figure 6.5 displays the vertical axle acceleration for the *Trucklab* and simulation model. The left graph displays simulation results using the *MF-Tyre* model, the right graph displays the simulation results using the *MF-Swift* model.

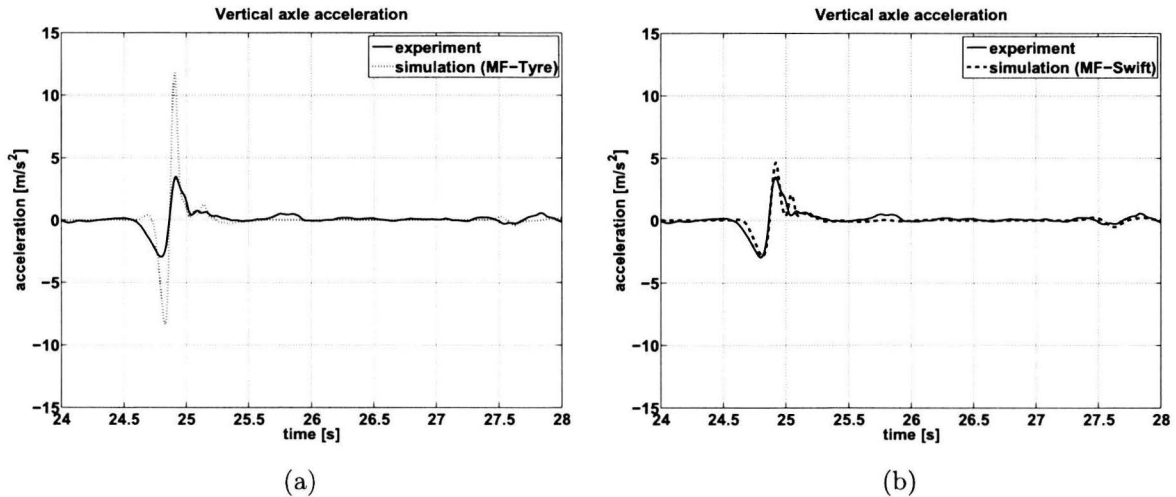


Figure 6.5: Discrete obstacle (step down) experiment. Vertical front axle accelerations for *MF-Tyre* (a) and *MF-Swift* (b).

Examining the results displayed in Figure 6.5 it can be seen that the simulation model using the *MF-Swift* model gives a much better estimation of the vertical axle accelerations with respect to the measured *Trucklab* data. This improvement in estimating the vertical axle accelerations by using the *MF-Swift* model, is observed for every experiment with regard to riding over road obstacles. Other experiments show no improvements by using a different tyre model. Because of this and the increase in computing time, the *MF-Swift* model is solely used for the road obstacle experiments, the other experiments use the *MF-Tyre* model.

6.5 Sensor modification

In the sections 3.1.3 and 4.2.7 the utilised sensors for the acquisition of experimental and simulation data are treated. Besides the correct sensor positions, it is fundamental that the *Trucklab* and simulation model sensors measure the same quantities under similar conditions. After comparing the *Trucklab* and simulation model sensors, a fundamental difference in measuring longitudinal and lateral accelerations for the *Trucklab* and simulation model came forward. These quantities are measured for the tractor cabin and chassis. The difference between the *Trucklab* and the standard *SimMechanics* sensors, used for measuring the longitudinal and lateral accelerations, is that the *SimMechanics* acceleration sensors do not account for the acceleration due to gravity. This results in different readings for the *Trucklab* and simulation model sensors when these sensors are attached to tilting bodies. For example, when the *Trucklab* is riding on a slope the *Trucklab* sensor has a different reading for the longitudinal and vertical accelerations compared to the *SimMechanics* sensor.

In Figure 6.6 a schematic view is given of the sensor used for measuring the longitudinal and lateral chassis and cabin acceleration. The sensor consists of a known mass m and three springs with a known spring constant k . By measuring the spring deflection u and using *Newton's Second Law of Motion*: $F = ma$ and $F = ku$, the acceleration a of mass m is calculated.

For the *Trucklab* sensor (Figure 6.6) the vertical acceleration reading in static position is -9.81 m/s^2 (the acceleration due to gravity). The sensor reading of the standard *SimMechanics* acceleration sensor,

6.5 Sensor modification

under the same conditions, is 0 m/s^2 . This difference can be overcome by subtracting 9.81 from the *SimMechanics* acceleration sensor reading, but this is only legitimate when the sensor is kept exactly horizontal. Horizontal means that the bottom plane of the sensor housing is aligned with the xy -plane of the *earth-fixed* coordinate system. For the situations where the sensor is attached to a body that is slightly tilting, the latter solution is no longer legitimate. To match the *Trucklab* and the standard *SimMechanics* acceleration sensor readings, the *SimMechanics* acceleration sensor is modified. This modification implies: determining the orientation of the body attached to the sensor using a rotation matrix; and recalculating the sensor readings.

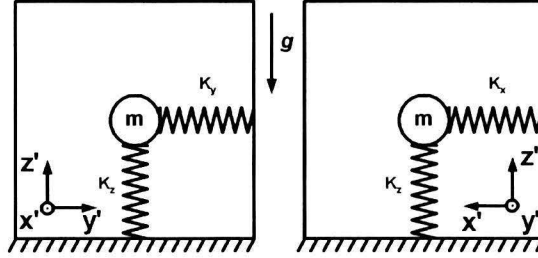


Figure 6.6: Schematic frontal (left) and side (right) view of *Trucklab* acceleration sensor.

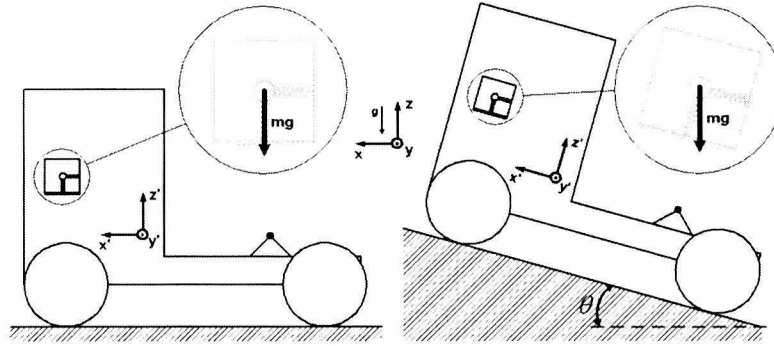


Figure 6.7: Schematic *Trucklab* view when riding on a flat (left) and sloped road (right).

The *SimMechanics* acceleration sensor modification is illustrated for the situation of riding with a constant velocity on a sloped road (Figure 6.7) where the acceleration sensor has a pitch angle. In Figure 6.8 a schematic view of the *Trucklab* acceleration sensor with a pitch angle θ is displayed. The vertical and longitudinal acceleration sensor readings are indicated by a_z and a_x respectively. The vertical acceleration due to gravity is indicated by g and has a magnitude of -9.81 m/s^2 . Due to the construction of the *Trucklab* sensor, the vertical acceleration reading in a tilted position is equal to a_z , which is smaller than g . Moreover, an additional lateral acceleration reading a_x occurs for this situation. However, when the *SimMechanics* acceleration sensor is subjected to an equal pitch angle θ the readings for a_x and a_z are zero.

To calculate the correct sensor readings for the situation of a pitch angle, the orientation (rotation matrix) of the *SimMechanics* body block is required. The rotation matrix can be generated by *SimMechanics*, but is determined by hand for this situation using Figure 6.9. Figure 6.9 displays the rotation of frame \bar{e}^1 to \bar{e}^2 , where these frames correspond to the *Earth-fixed* and *vehicle* coordinate systems respectively. The transformation from \bar{e}^1 to \bar{e}^2 can be described by:

$$\bar{e}^2 = \underline{R}(\theta)\bar{e}^1 = \begin{bmatrix} \cos(\theta) & 0 & \sin(\theta) \\ 0 & 1 & 0 \\ -\sin(\theta) & 0 & \cos(\theta) \end{bmatrix} \bar{e}^1, \quad (6.1)$$

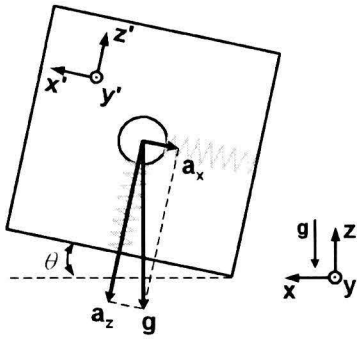


Figure 6.8: *Trucklab* acceleration sensor with small pitch angle θ .

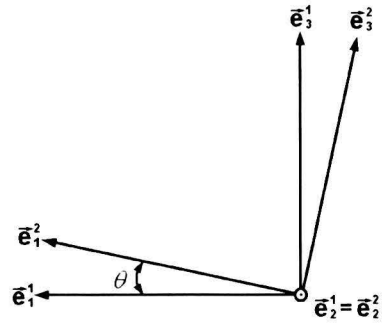


Figure 6.9: Description of the rotation of a frame \underline{e}^1 to \underline{e}^2 .

where $\underline{R}(\theta)$ is the rotation matrix. Note that in this example the rotation matrix is only a function of the pitch angle θ , because the yaw ψ and roll ϕ angles are equal to zero. In order to match the *Trucklab* and *SimMechanics* acceleration sensor readings, the absolute gravitation acceleration vector with respect to the *Earth-fixed* coordinate system is transferred to the *vehicle* coordinate system to obtain the a_x and a_z readings of Figure 6.8, using (6.1).

$$\begin{bmatrix} -9.81 \sin(\theta) \\ 0 \\ -9.81 \cos(\theta) \end{bmatrix} = \begin{bmatrix} \cos(\theta) & 0 & \sin(\theta) \\ 0 & 1 & 0 \\ -\sin(\theta) & 0 & \cos(\theta) \end{bmatrix} \begin{bmatrix} 0 \\ 0 \\ -9.81 \end{bmatrix} = \begin{bmatrix} a_x \\ a_y \\ a_z \end{bmatrix} \quad (6.2)$$

The result of (6.2) are the sensor acceleration readings when the truck is riding on the sloped road of Figure 6.7 with a constant velocity. When the truck is riding on the sloped road and is accelerating at the same time, the absolute vehicle acceleration vector must be added to the absolute gravitation acceleration vector. The resulting acceleration vector is then multiplied with the rotation matrix. Note that a similar approach holds for the situations of a roll angle ϕ or a combination of roll and pitch angles. However, these situations require different rotation matrices \underline{R} .

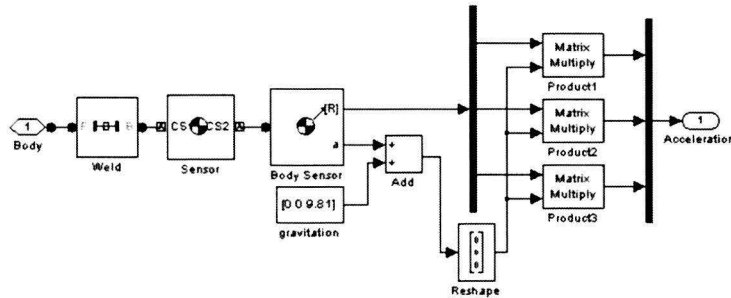


Figure 6.10: Modified *SimMechanics* acceleration sensor.

Figure 6.10 displays the modified acceleration sensor. The sensor consist of a sensor body connected to a standard *SimMechanics* body acceleration sensor. It can be seen that the absolute vehicle acceleration vector is added to the absolute gravitation acceleration vector before multiplying with the rotation matrix.

6.6 Driver model

In section 4.2.5 the driver of the simulation model is discussed. The driver is modelled as a *Simulink*[®] control system and serves as a simulation model operator. For the reproduction of the *Trucklab* experiments, the driver model makes use of experimental sensor data. This sensor data consists of the vehicle velocity and the steering wheel angle. Before a simulation is performed, the latter sensor data

6.6 Driver model

is uploaded into *MATLAB*[®] and filtered. By this way of simulating with measured inputs, the simulation results are directly linked to the experimental data file for almost every type of experiment.

For experiments concerning braking manoeuvres there is no direct connection between experimental and simulation data. The *baseline* model brake tests are carried out with an initial vehicle velocity of 60 km/h and after a certain period of time the brakes are applied by specifying by a percentage of the maximal brake torque. The brake torque percentage is specified before a brake test is carried out and is maintained constant, when applied, for the remainder of the simulation. An experimental data file is linked to a simulation data file by matching the velocity profiles. Figure 6.11 displays the velocity profiles for the *Trucklab* and *baseline* model when performing a heavy braking test.

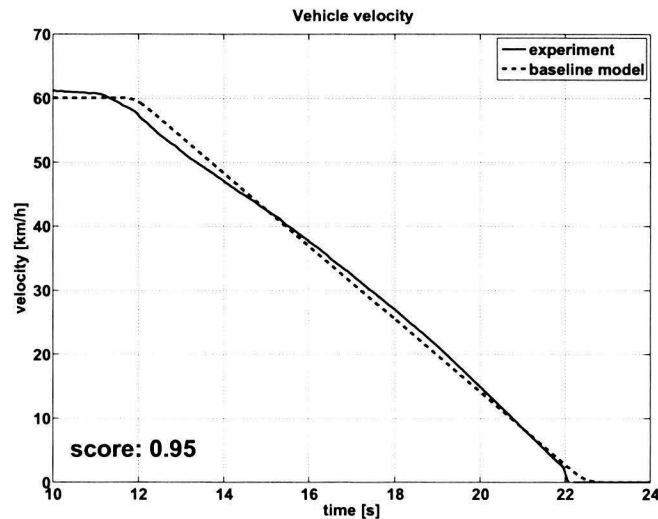


Figure 6.11: Normal braking experiment. Vehicle velocity, *Trucklab* (solid) and *baseline* model (dashed) vehicle velocity profiles.

When comparing the two velocity profiles of Figure 6.11 it is clear that the velocity profile of the *baseline* model is not an accurate representation of the *Trucklab* velocity profile during a braking manoeuvre. This mismatch is caused by the fact that the brake torque is considered constant for the simulation model, what results in a linear velocity profile. The *Trucklab* velocity profile is less smooth compared to the simulation model. This can be the result of small brake pedal position variations during braking. Maintaining a constant brake pedal position is not feasible for the *Trucklab* driver, particularly for normal braking experiments where the duration of the manoeuvre is longer than for a heavy braking manoeuvre.

To improve the consistency of these velocity profiles, the driver model of the *baseline* model is adjusted. The driver model is expanded by adding a brake torque controller for the braking experiments. Because of the lack of *Trucklab* brake pressure data, other available *Trucklab* sensor signals are used to control the brake torque. Figure 6.12 depicts the brake torque controller. Note that this brake torque controller directly links the simulation results to an experimental data file because experimental sensor data is used for the operation of the simulation model.

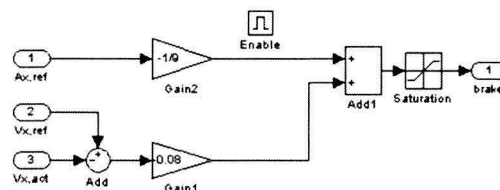


Figure 6.12: Brake torque controller in *Simulink*[®].

The controller uses three signals for its input. These signals are the measured longitudinal acceleration a_{xref} and velocity v_{xref} and the actual simulation model velocity v_{xact} . The values for $gain_1$ and $gain_2$ are determined using trial and error until the simulation model velocity profile matched the experimental velocity profile for every test of heavy and normal braking experiments. By this adjustment to the driver model, the simulation model is able to make an accurate reproduction of the velocity profile of an experimental test.

Figure 6.13 displays the vehicle velocity profiles for the *Trucklab* and the adjusted *baseline* model. The experimental velocity profile is the same as displayed in Figure 6.11. The simulation model with adjusted driver model results in an improved reproduction of the *Trucklab* velocity profile, as can be seen in Figure 6.13.

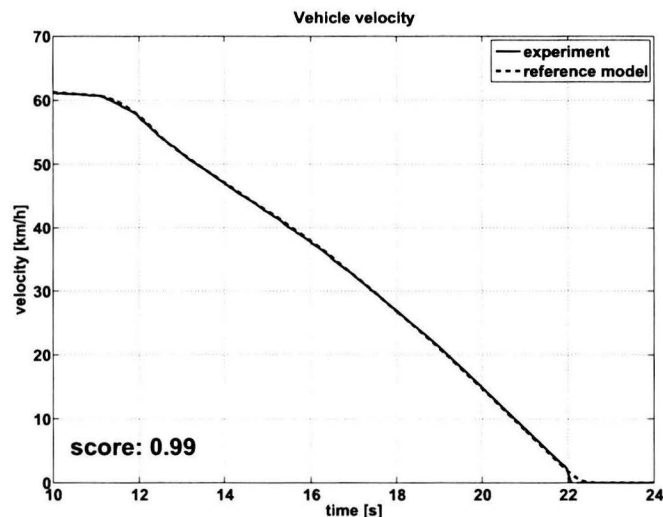


Figure 6.13: Normal braking experiment. Vehicle velocity, *Trucklab* (solid) and *reference* model (dashed) vehicle velocity profiles.

6.7 Evaluation *reference* model

In this section the *reference* model is evaluated. In Appendix C.1 the evaluation results of the *reference* model are included. The evaluation scores of the *reference* model are compared to the *baseline* model evaluation scores by means of bar graphs for each experiment.

The evaluation graphs of Appendix C.1 show that large score improvements are achieved when riding over discrete obstacles, particularly for the threshold (Figure 6.14) and stepdown experiments. These score improvements are caused by the implementation of the *MF-Swift* tyre model. The signal scores for riding over the *pyramid* obstacle show a smaller improvement compared to the other two discrete obstacle experiments. This is a result of the shape of the obstacle in combination with the enveloping model included in *MF-Swift*.

For evaluation of the *reference* model, the sensor signals are subdivided into three groups: axles; chassis and cabin. Each group is discussed in the following sections.

6.7.1 Axles

As stated before, the implementation of the *MF-Swift* model into the simulation model resulted in a large improvement of the vertical axle accelerations and the primary suspension deflections for the discrete obstacle experiments. The primary suspension deflections for the other experiments show improvements as well as some minor decrease of evaluation scores. This is mainly the result of

6.7 Evaluation reference model

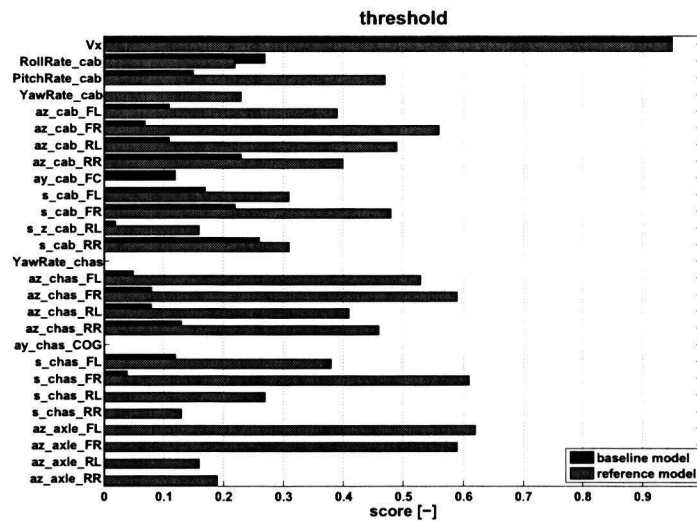


Figure 6.14: Discrete obstacle experiment (threshold). Evaluation scores, *baseline* model (black) and *reference* model (gray).

adjusting the model parameters discussed in section 6.2. Striking about the axles are the zero and very low scores of the rear axle suspension deflection for the acceleration, normal braking, heavy braking and circle experiments. Figure 6.15 displays the rear axle left side suspension deflections for heavy braking (a) and acceleration (b). There is a large mismatch between *Trucklab* and *reference* model. The cause of this mismatch is not clear, therefore a more profound study of the simulation model is necessary.

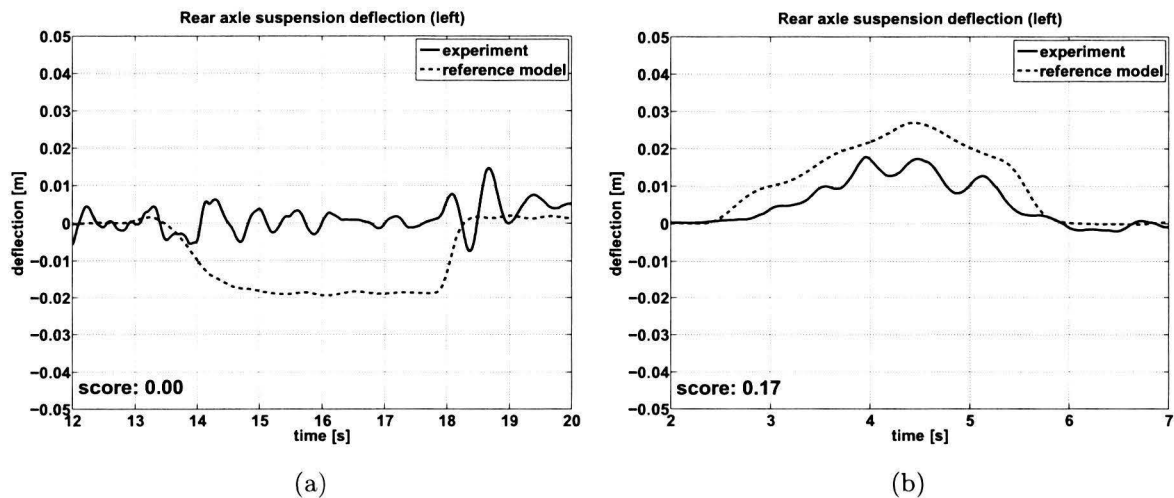


Figure 6.15: Rear axle suspension deflections left for heavy braking (a) and acceleration (b), *Trucklab* (solid) and *reference* model (dashed). Positive deflection corresponds to compression.

6.7.2 Chassis

The vertical acceleration of the chassis show also a lot of improvement. This is directly the result of using the *MF-Swift* tyre model. The longitudinal and lateral chassis accelerations and the chassis yaw velocity show the same trend in evaluation scores. These signals have very low scores for the discrete obstacle experiments in contrast to respectable high scores for the other experiments. This is caused by the fact that, for the discrete obstacle experiments, the sensor values of the experimental signals are small compared to the noise level of the concerning *Trucklab* sensor. This creates a high level of uncertainty for these signals and therefore can not be reproduced accurately by the simulation model. For example, the maximum measured lateral chassis acceleration value for riding over the pyramid

obstacle is 0.02 m/s^2 in contrast to a deviation of $\pm 0.01 \text{ g m/s}^2$ for the concerning acceleration sensor. Because of this, there are no model adjustments that are able to improve these scores.

6.7.3 Cabin

The vertical cabin accelerations are improved as a result of using the *MF-Swift* tyre model. The longitudinal and lateral cabin accelerations have low scores for the discrete obstacle experiments in contrast to the respectable high scores for the other experiments. Examination of the cabin suspension deflections shows that there is a considerable mismatch between *Trucklab* and simulation model. Figure 6.16 displays the mismatch of the cabin suspension deflections at the front left (a) and rear left (b) for a heavy braking experiment. The cause of this mismatch is not clear and therefore a profound study of the cabin suspension is required.

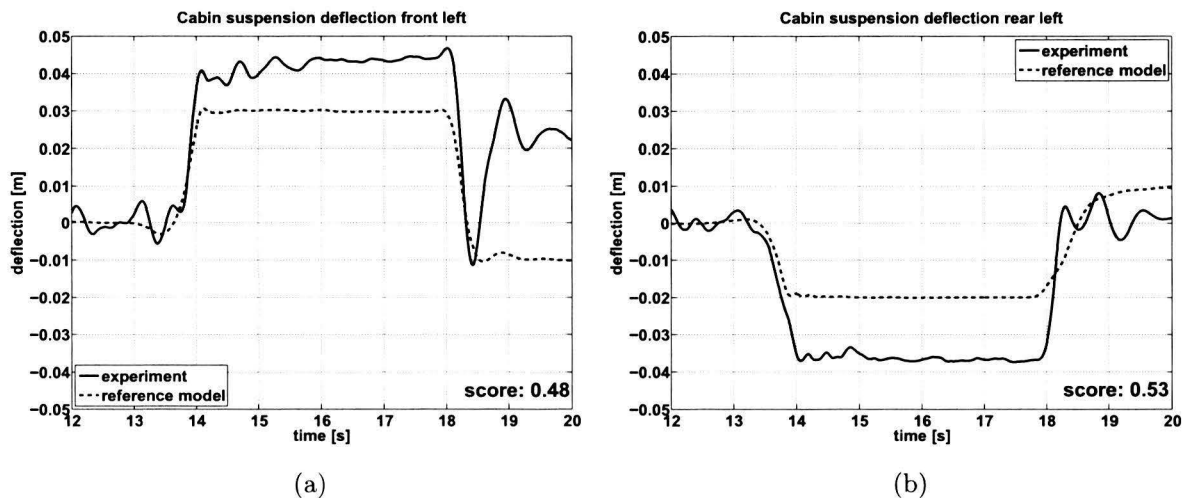


Figure 6.16: Heavy braking experiment. Cabin suspension deflections front left (a) and rear left (b), *Trucklab* (solid) and *reference* model (dashed). Positive deflection corresponds to compression.

After evaluating the *reference* model it can be concluded that the *reference* model gives a more accurate match between *Trucklab* and simulation model data. Clear improvements are achieved with respect to the vertical axle, chassis and cabin accelerations. However, large mismatches between *Trucklab* and simulation model are observed for the rear axle suspension deflections and the cabin suspension deflections.

6.8 Summarising this chapter

In this chapter the *reference* model is presented. This model differs from the *baseline* model by the implementation of the following model adjustments:

- **Model parameter update:** the *baseline* model parameters are verified using measurements and data originating from the manufacturer of the *Trucklab* test vehicle.
- **Modelling errors:** the *baseline* model is checked for possible modelling errors. The detected errors are: the wrong fifth wheel coupling height; and the wrong position of the revolute joints of the semi-trailer chassis.
- **Tyre model:** the adopted tyre model for riding over discrete obstacles is changed from *MF-Tyre* to *MF-Swift*. *MF-Swift* has an enveloping model making it suitable for riding over short wavelength road obstacles.
- **Sensor modification:** the standard *SimMechanics* acceleration sensor is modified to match the *Trucklab* longitudinal and lateral acceleration readings for tractor cabin and chassis.

6.8 Summarising this chapter

- **Driver model:** The driver model is adjusted by implementing a brake torque controller for a more accurate match of the measured and simulated velocity profiles during a braking manoeuvre.

After evaluating the *reference* model it can be concluded that this model gives a more accurate match between *Trucklab* and simulation model with respect to the vertical axle, chassis and cabin accelerations. However, large mismatches between *Trucklab* and simulation model are observed for the rear axle suspension deflections and cabin suspension deflections.

Chapter 7

Model modifications

In chapter 6 the *baseline* simulation model is evaluated. Moreover, first adjustments are made and implemented in an updated version of the *baseline* model called *reference* model. However, it can also be seen that there is still room for further improvement. The adopted approach for further improvement of the simulation model is based on the *bottom-up* method. This means that the implementation of adjustments starts at the bottom (axles) and ends at the top (cabin) of the simulation model. This approach is adopted as it is fundamental to start with making improvements at the "input-side" of the system. An inaccurate response of components at the "input-side" automatically result in inaccurate outputs. For example, a mismatch in vertical axle accelerations for riding over a discrete obstacle due to an inadequate tyre model makes an accurate match for the vertical cabin accelerations impossible as the "input" is incorrect.

In the following sections, the simulation model aspects in need of further improvement are discussed. Treated aspects are: the rear axle suspension; the brake system; the steering system; and the cabin suspension respectively. The *reference* model, discussed in chapter 6, is used as a reference for the implemented adjustments. Note that this *reference* model is the same in each section.

7.1 Rear axle suspension

As can be seen in section 6.7.1 there is a large mismatch between the *Trucklab* measurements and the simulation results of the *reference* model for the rear axle suspension deflection. In order to find the cause for this large difference, the rear axle suspension is examined both for the *Trucklab* and *reference* model. Subsequently, adaptations are made to the *reference* model to improve the rear axle suspension deflection.

7.1.1 Trucklab

The *Trucklab* is equipped with a rigid rear axle that is driven by the engine. This axle is suspended by air-springs and non-linear dampers in combination with two lower trailing arms and an upper A-arm. The air-springs are connected to a compressor to control the ride height at the rear. A schematic view of the *Trucklab* rear axle configuration is displayed in Figure 7.1. In order to restrict the rolling motion an anti-roll bar is mounted behind the rear axle. This suspension geometry allows two degrees of freedom for the axle with respect to the chassis: a vertical translation and a rolling motion.

7.1.2 Simulation model

The modelled rear axle suspension is a simplified representation of a tractor rear axle suspension. Figure 7.2 is a schematic frontal view of this modelled rear axle suspension. The rear axle has also two degrees of freedom with respect to the chassis body. These degrees of freedom are a vertical

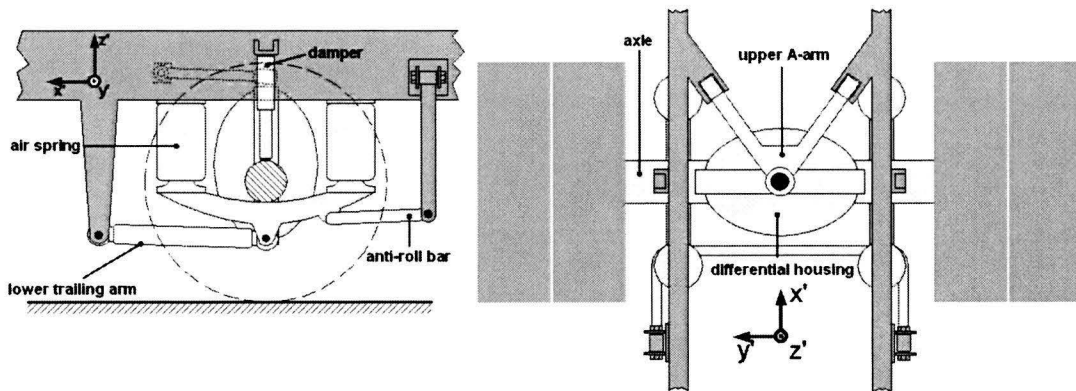


Figure 7.1: Schematic side (left) and top view (right) of the *Trucklab* rear axle suspension geometry.

translation along the z' -axis and a rotational degree of freedom ϕ around the x' -axis of the vehicle coordinate system. The axle and chassis bodies are connected by means of a *SimMechanics Custom Joint*. The suspension consists in vertical direction of one spring and a non-linear damper in parallel on each side. To constrain the rolling motion ϕ , a torsional spring is added, which represents the anti-roll bar.

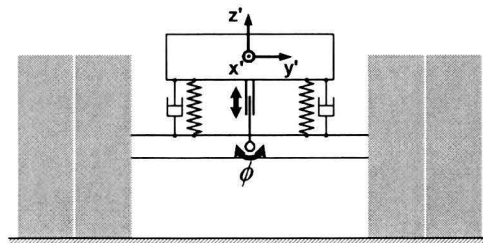


Figure 7.2: Schematic frontal view of the rear axle suspension geometry of the *reference* simulation model.

7.1.3 Analysis

Figures 7.3 and 7.4 display the rear axle suspension deflection for a braking and an acceleration experiment respectively. It can be seen that there is a large mismatch between the *Trucklab* and *reference* model for both experiments.

Figure 7.3 shows there is a considerable amount of negative suspension deflection for the *reference* model in contrast to the *Trucklab* suspension. Instead, the *Trucklab* makes a small oscillating motion around its equilibrium point (deflection = 0 m). The deflections of the *reference* model are solely the result of weight transfer when the brakes are applied. The brake force and brake torque acting on the rigid axle have no effect on the primary suspension deflections as a result of the simplified suspension. The *Trucklab* has approximately the same amount of weight transfer but the deflection of the rear axle is counteracted by an anti-rise effect (Figure 7.5) that is the result of the *Trucklab* suspension geometry (suspension pole location) in combination with the brake force and brake torque acting on the axle housing. Based on rear axle geometry measurements, the *Trucklab* suspension pole location is estimated at 20 m in front of the rear axle at a height of approximately 2 m.

For the acceleration experiment (Figure 7.4) the difference in rear axle suspension geometry is responsible for the difference in primary suspension response. When accelerating, the *Trucklab* suspension geometry (suspension pole location) in combination with the drive force and drive torque acting on the rear axle housing results in an anti-squat effect (Figure 7.5). Because of this, the rear axle

7.1 Rear axle suspension

suspension deflection is smaller for the *Trucklab* than for the *reference* model. Furthermore, a small oscillation is observed for the *Trucklab* suspension deflection. The exact cause of these low frequency oscillations is unknown. It is not likely that these oscillations are caused by the *Trucklab* braking system or drive line, as this is also observed for the front and rear axle suspension deflections of other experiments.

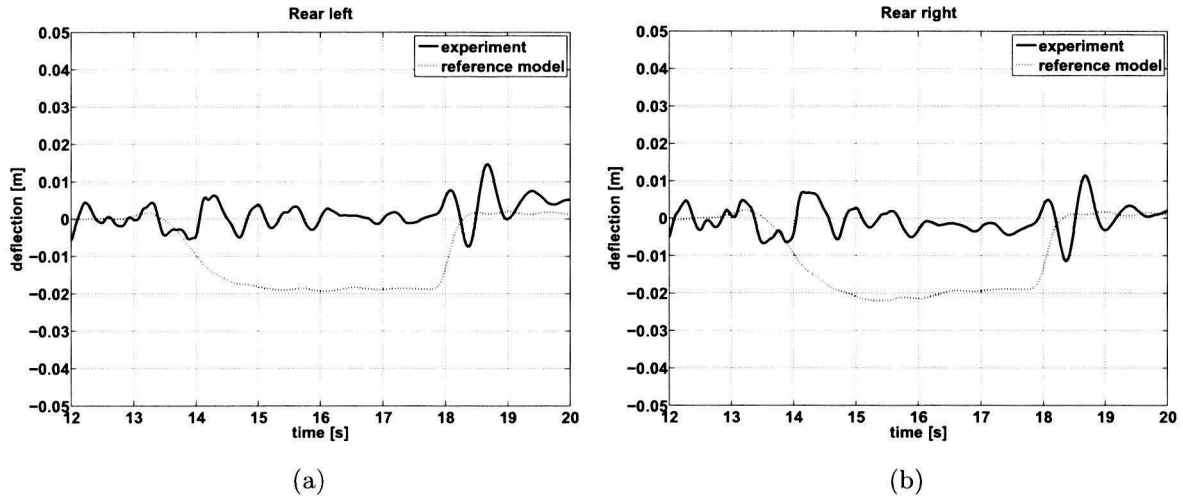


Figure 7.3: Braking experiment. Rear axle suspension deflection left (a) and right (b), *Trucklab* (solid) and *reference* model (dotted). Positive deflection corresponds to compression

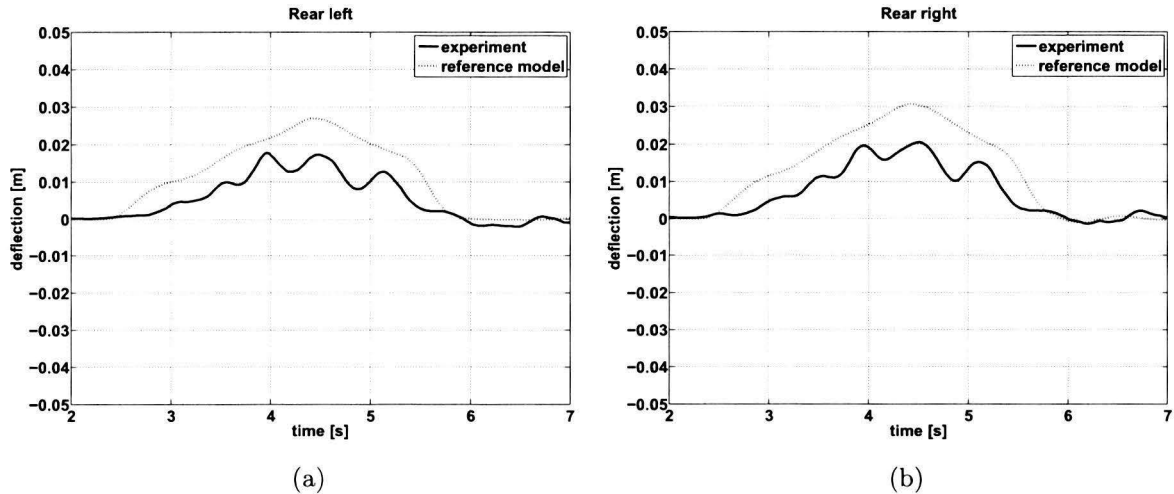


Figure 7.4: Acceleration experiment. Rear axle suspension deflection left (a) and right (b), *Trucklab* (solid) and *reference* model (dotted). Positive deflection corresponds to compression

7.1.4 Model adjustments

In order to improve the match between *Trucklab* and simulation with regard to the rear axle suspension deflection, the *Trucklab* suspension geometry (Figure 7.1) is measured and implemented in the simulation model. This simulation model is referred to as the *adapted* model for the remainder of this section. To study the differences between the rear axle suspensions of the *reference* and *adapted* model, some tests are performed. In the first test the wheel centre path as a function of the suspension travel is investigated.

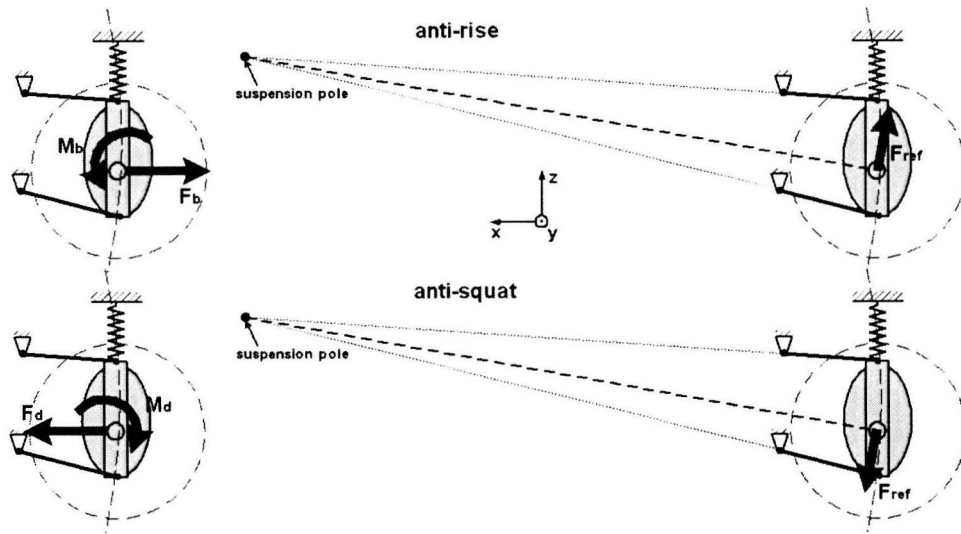


Figure 7.5: Schematic view of the rear axle anti-rise and anti-squat effects.

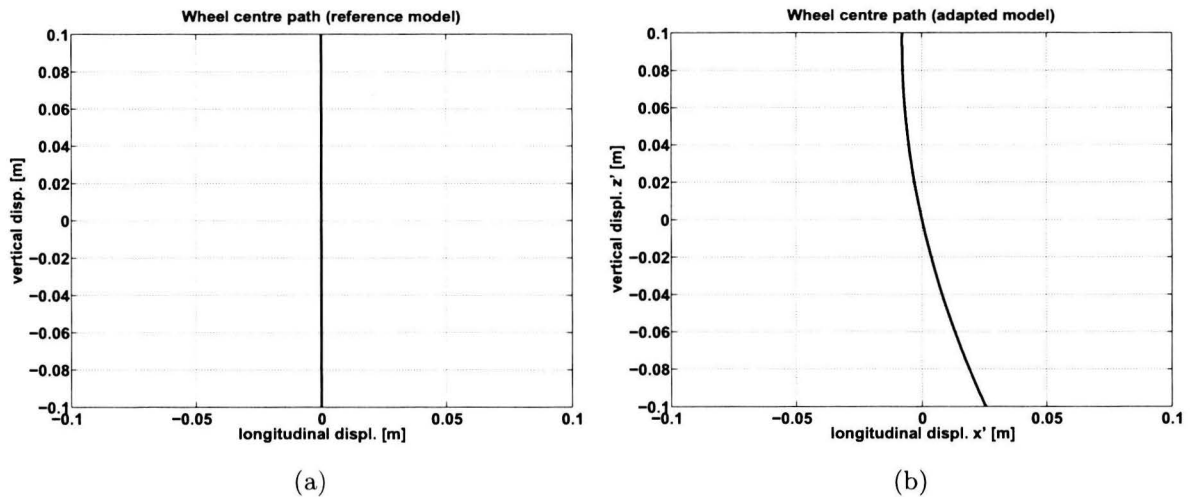


Figure 7.6: Rear axle wheel centre path for the *reference* model (a) and *adapted* model (b).

Figure 7.6 displays the wheel centre paths for the *reference* and *adapted* simulation model in the $x'z'$ -plane of the *vehicle* coordinate system. Point $(0,0)$ represents the static position of the rear axle suspension. It can be seen that the wheel centre path of the *reference* model is a straight line parallel to the z' -axis of the *vehicle* coordinate system. This is the results of the single translational degree of freedom in z' -direction. The wheel centre path in the $x'z'$ -plane of the *adapted* model is an arc of circle with its centre of rotation (rear axle suspension pole) in front of the rear axle. This curved wheel centre path is a direct result of using two lower trailing arms and one upper A-arm in the suspension geometry.

The second test to indicate the difference between the rear axle suspension of the *reference* and *adapted* models involves the rolling motion ϕ of the chassis. The suspension geometry as depicted in Figure 7.1 is subjected to a phenomenon called *roll steer*. *Roll steer* is a self-steer-effect of an axle, initiated when there is a difference in suspension deflection between the left and right side of the vehicle (body roll). It is used to increase or decrease the vehicle's turning ability in proportion to the roll angle caused by cornering. Because it affects the steering handling characteristics when cornering it is also known as *roll oversteer* and *roll understeer* respectively, [17]. For more information on this subject see [17] and [19].

7.2 Brake system

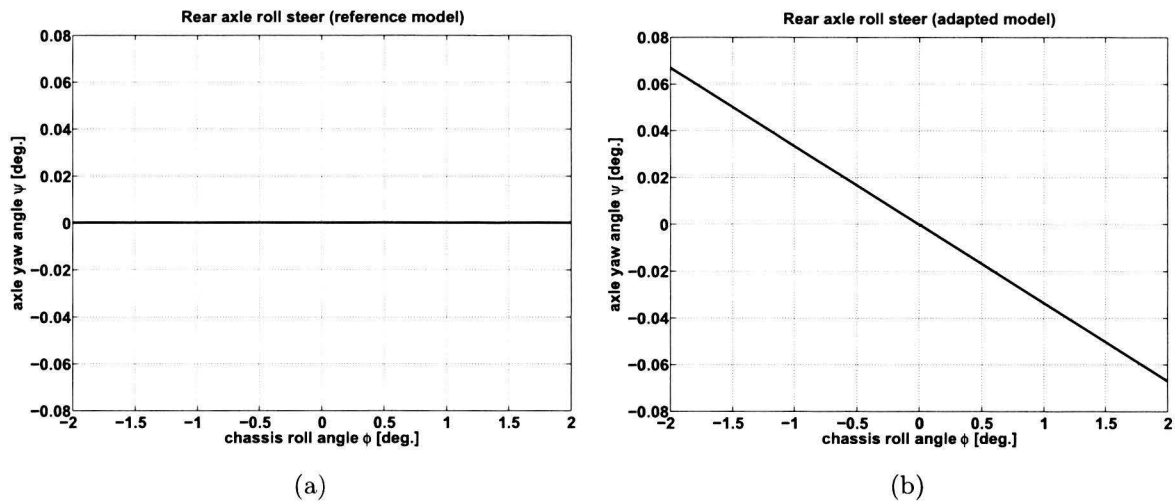


Figure 7.7: Rear axle roll steer for the *reference* model (a) and *adapted* model (b).

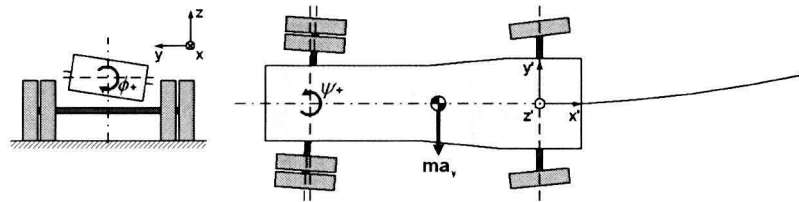


Figure 7.8: Rear axle roll steer during steady state cornering for the *adapted* model.

Figure 7.7a shows that $\psi = 0$ for every value of ϕ . This means there is no relation between the chassis roll angle and the rear axle yaw angle as a result of the absence of a suspension geometry. Figure 7.7b displays the rear axle yaw angle ψ as a function of the chassis roll angle ϕ for the *adapted* model. It can be seen that the implemented *Trucklab* suspension geometry causes a yaw angle for the rear axle. Figure 7.8 displays a schematic view of the roll steer effect for the *adapted* simulation model. The *adapted* suspension geometry results in a rear axle steer effect during cornering. Note that the roll steer is very small and therefore the effect on steering handling characteristics is minimal.

7.1.5 Evaluation

Figures 7.9 and 7.10 display the rear axle suspension deflections for a heavy braking and acceleration experiments respectively. The result of implementing a rear axle suspension geometry with anti-rise/anti-squat effects is clear. The simplified rear axle suspension of the *reference* model is not sufficiently accurate for predicting the suspension deflection as the anti-rise and anti-squat effects are not included. A large improvement is achieved with regard to the primary suspension deflection for the braking and acceleration experiments; still, there is room for further improvement. The primary suspension deflections when braking (Figure 7.9) also depend on the adopted brake force distribution. Therefore, the brake system is discussed in the next section.

7.2 Brake system

Braking of a fully loaded commercial vehicle results in a large load transfer between the axles. The load transfer is largely responsible for the amount of suspension travel of the various axles during a braking manoeuvre. A braking parameter that affects the load transfer and therefore the suspension travel is the brake force distribution. The *Trucklab* braking system uses a variable brake force distribution in contrast to the *reference* model braking system which uses a fixed brake force distribution. In this

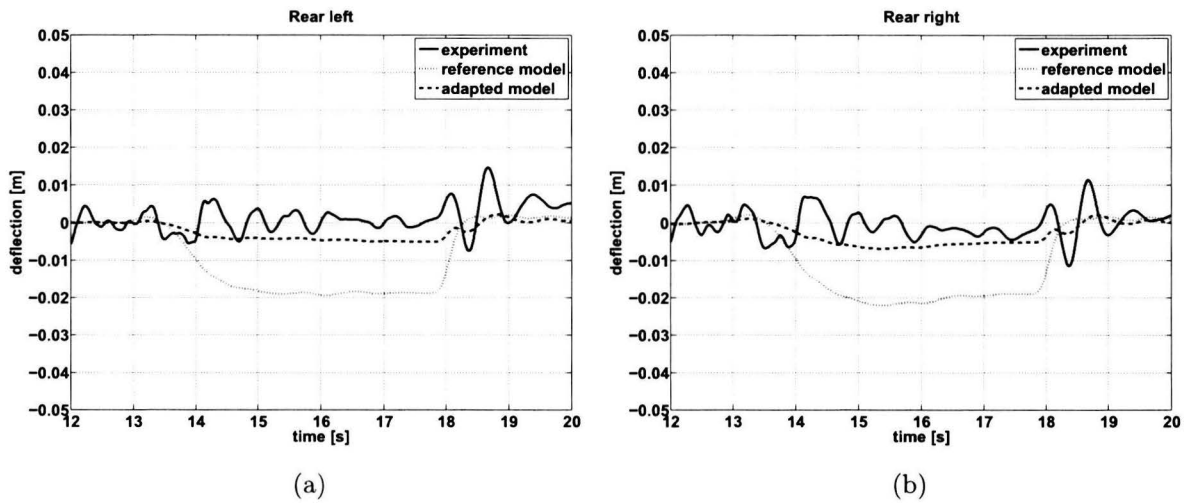


Figure 7.9: Heavy braking experiment. Rear axle suspension deflection left (a) and right (b), *Trucklab* (solid), *reference model* (dotted) and *adapted model* (dashed). Positive deflection corresponds to compression

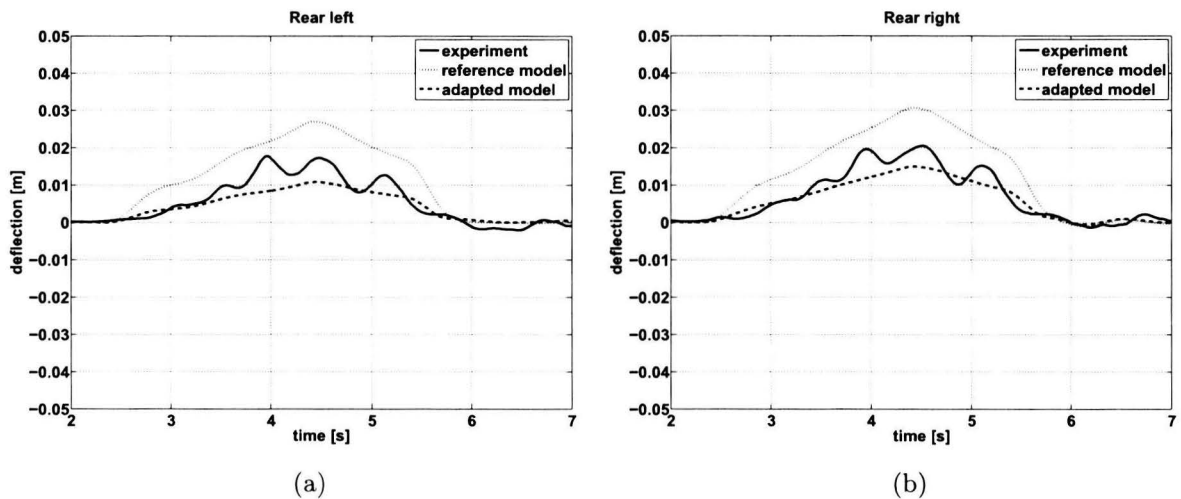


Figure 7.10: Acceleration experiment. Rear axle suspension deflection left (a) and right (b), *Trucklab* (solid), *reference model* (dotted) and *adapted model* (dashed). Positive deflection corresponds to compression

section the *Trucklab* and *reference model* braking systems are discussed. Subsequently, the model adjustments are discussed.

7.2.1 Trucklab

The *Trucklab* is equipped with a complicated braking system. Besides the primary task of braking, the system also contains safety features as *Electronic Stability Control* (ESC); *Anti-lock Braking System* (ABS) and an *Acceleration Slip Regulation* (ASR). These latter safety systems are used to assist the driver in critical situations as suddenly swerving to avoid an obstacle. The intervention of these safety systems can avoid accidents in everyday traffic but is undesirable when performing the experiments of section 3.2 on a proving ground. For that reason these safety systems are switched off during the tests. For more information on this subject see [8]. Switching off these safety systems also reduces the complexity of the braking system.

7.2 Brake system

The *Trucklab* brakes are operated using pressurised air. This brake system is better known as an air brake system. This air brake system is also accommodated with a variable brake force distribution to meet the legally required deceleration level for every loading condition by avoiding unnecessary premature wheel lock-up. To adjust the brake force for the different loading conditions of the axles, a brake force control system is used. This system calculates the brake force distribution by minimising the differential slip between the various axles. Another and more traditional approach to control the brake force distribution is the load-dependent brake force distribution. This is typically a mechanical control system using *Load Sensing Valves* (LSV's) on the various axles to adjust the braking forces. Note that the variable brake force distribution does not prevent the wheels from locking-up, it only avoids unnecessary premature wheel lock-up. To prevent the wheels from locking-up the *Trucklab* is equipped with an *Anti-lock Braking system* (ABS). For more information on the subject of truck braking systems see [5], [8] and [18].

7.2.2 Simulation model

The brake system of the *reference* simulation model uses a fixed brake force distribution control system. This distribution is optimised for the fully loaded condition of the *reference* model. Other loading conditions as an tractor with empty trailer and a solo tractor do not meet the legally required deceleration level using this brake force distribution. In order to determine the performance of the *reference* model braking system, a straight-line braking test is performed with three loading conditions for this model. These loading conditions are: a fully loaded tractor-semi trailer combination (*reference* model); an empty tractor-semi trailer combination; and a solo tractor configuration. The brake test is performed on a level surface with an initial vehicle speed of 80 km/h. During the straight-line braking manoeuvre the brake force is increased to reach the highest possible deceleration.

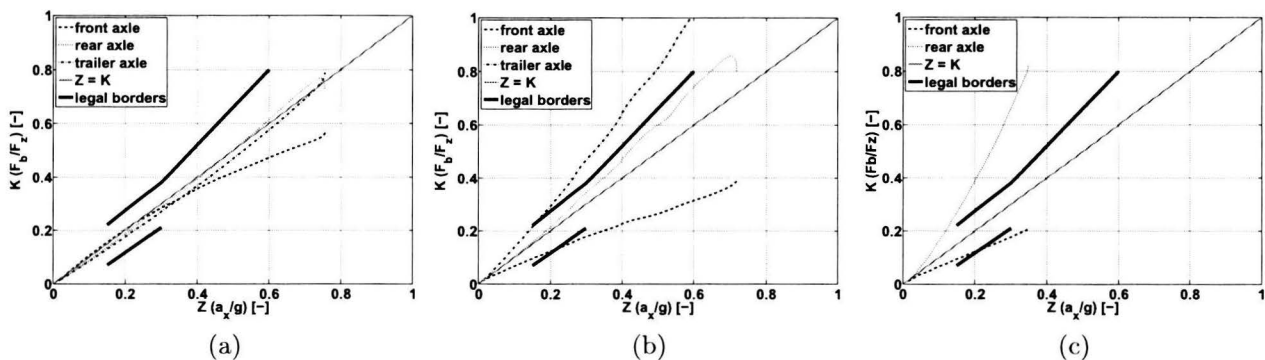


Figure 7.11: Tyre-road friction utilisation for the fully loaded (a), empty trailer (b) and solo tractor (c) configurations of the *reference* model.

Figure 7.11 displays the tyre-road friction utilisation for the fully loaded, empty trailer and solo configuration of the *reference* model. The horizontal axis of these graphs represents the dimensionless deceleration Z , defined as the longitudinal vehicle deceleration a_x divided by the gravitational acceleration g . The vertical axis represents the required road friction coefficient K and is defined as the total axle brake force F_b divided by the total axle normal force F_z . Figure 7.11 displays the dimensionless deceleration as a function of the required road friction coefficient for three vehicle axles: the front; the rear; and the trailer axle. Only one trailer axle is displayed as the total axle brake force and normal force are considered to be the same for each trailer axle. Besides the axles, the legal borders [20] and the optimum braking force distribution ($Z = K$) are displayed. For straight-line braking on a level surface in the absence of any aerodynamic effects, optimum braking in terms of maximising vehicle deceleration is defined by $Z = K$. For the optimum condition, the brake force F_b is given by:

$$F_b = \mu F_n \quad (7.1)$$

where μ and F_n are the road friction coefficient and normal force respectively. Examining Figure 7.11, it can be seen that the fixed brake force distribution is optimised for the fully loaded configuration of the *reference* model. The rear axle of the solo tractor configuration has almost instant wheel lock-up; moreover, the front and rear axles do not stay within the legal borders. For the empty trailer configuration the front and trailer axle do not stay within the legal borders. Clearly, the fixed brake force distribution of the *reference* model does not meet the legal requirements with regard to braking.

7.2.3 Model adjustments

As the *Trucklab* does meet the legal requirements, the braking system of the *reference* model is adapted. Therefore a variable brake force distribution is implemented. This adapted version of the *reference* model is referred to as the *adapted* model for the remainder of this section.

The variable brake force distribution is based on the minimisation of the differential slip between the various axles [7] as adopted for the *Trucklab* braking system. The differential slip is calculated by [6]:

$$\kappa_{fr} = \frac{\Omega_{front} R_{front} - \Omega_{rear} R_{rear}}{\Omega_{front} R_{front}} \quad (7.2)$$

$$\kappa_{tt} = \frac{V_{tractor} - \Omega_{trailer} R_{trailer}}{V_{tractor}} \quad (7.3)$$

$$V_{tractor} = \frac{\Omega_{front} R_{front} + \Omega_{rear} R_{rear}}{2} \quad (7.4)$$

where κ_{fr} and κ_{tt} are the differential slip between the tractor front and rear axle and between the tractor and trailer respectively. These equations are used in the brake force control strategy of the *adapted* model. This control system measures the angular wheel velocity Ω_i of the three axles. The angular velocity for every wheel of a particular axle is considered to be the same, as only straight-line braking is considered. Subsequently the differential slip values are computed using the measured angular velocities and the effective rolling radius R_i of each wheel. This effective rolling radius is also considered to be the same for each tyre of a particular axle because the normal forces are almost the same. The differential slip is a measure for the amount of brake force for the rear tractor and trailer axles. These differential slip values are multiplied with a brake moment gain G in order to make the output of the brake force controller a realistic brake moment value that can be applied to the wheels. The controller equations are:

$$M_{b_{rear}} = \frac{\Omega_{front} R_{front} - \Omega_{rear} R_{rear}}{\Omega_{front} R_{front} + 1} G \quad (7.5)$$

$$M_{b_{trailer}} = \frac{V_{tractor} - \Omega_{trailer} R_{trailer}}{V_{tractor} + 1} G \quad (7.6)$$

where $M_{b_{rear}}$ and $M_{b_{trailer}}$ are the braking torques for the rear tractor axle and trailer axles respectively. The brake moment gain G has an arbitrarily determined value of $-1.5e^6$ Ns/rad. Note the addition of 1 to the denominator in order to prevent the division by zero for $\Omega = 0$.

With the *adapted* model the same brake tests are performed as with the *reference* model in order to determine its performance. Figure 7.12 displays the tyre road friction utilisation for the fully loaded (a), empty trailer (b) and solo tractor (c) configurations of the *adapted* model.

When comparing the tire-road friction utilisation graphs for the *reference* (Figure 7.11) and *adapted* (Figure 7.12) simulation models, it can be seen that the braking system with variable brake force distribution affects the braking results for all three configurations. A large improvement is observed

7.2 Brake system

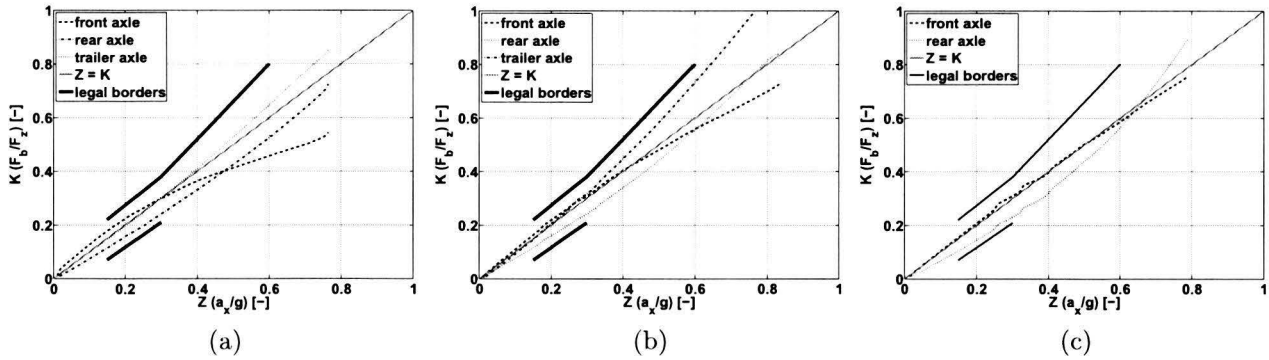


Figure 7.12: Tyre-road friction utilisation for the fully loaded (a), empty trailer (b) and solo tractor (c) configurations of the *adapted* model.

for the empty trailer (b) and solo tractor (c) configurations. These configurations stay within the legal borders for the *adapted* model in contrast to these configurations of the *reference* model. Comparing the fully loaded model configurations it can be seen that the rear tractor axle is braking less hard and the trailer axle is braking harder for the *adapted* simulation model. The brake force for the front axle remains almost unaffected. This change in brake force for rear tractor axle and trailer axes affects the primary suspension deflections of these axes.

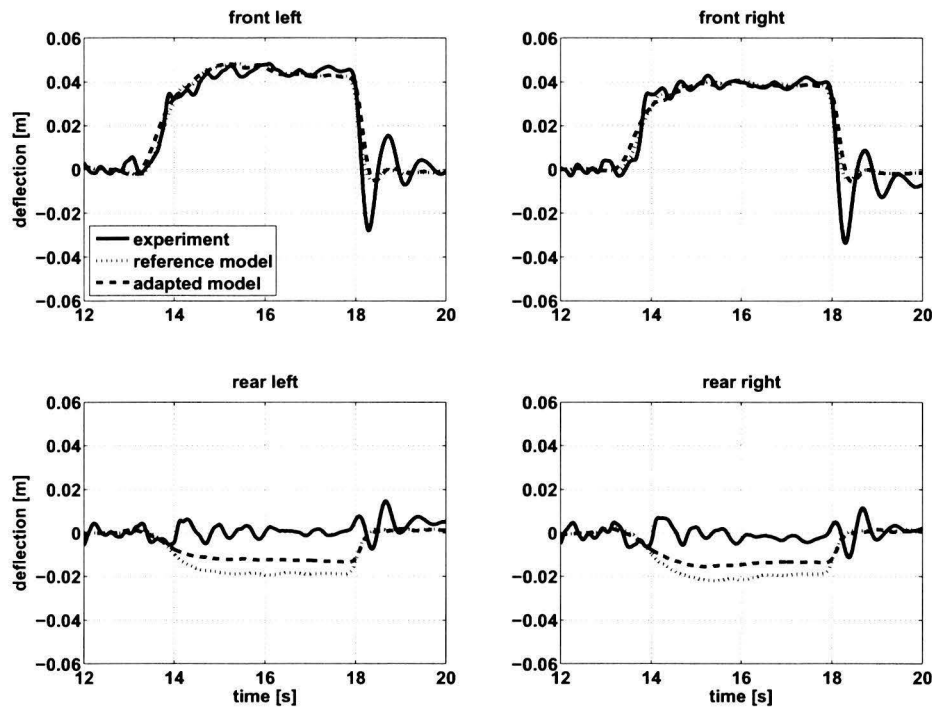


Figure 7.13: Braking experiment. Axle suspension deflection, *Trucklab* (solid), *reference* model (dotted) and *adapted* model (dashed). Positive deflection corresponds to compression.

Figure 7.13 displays the axle suspension deflections for a braking manoeuvre. It can be seen that the rear axle suspension deflection is smaller for the *adapted* model using the variable brake force distribution. This is a direct result of reducing the rear axle brake force. It can also be seen that the front axle suspensions remains almost unaffected. The combination of the variable brake force

distribution and the suspension geometry of section 7.1 result in an improved rear axle suspension deflection, as will be shown in the validation of the braking manoeuvre in chapter 8.

7.3 Steering system

In this section the steering system is treated. An accurate representation of the steering system model is required as it affects the handling of the vehicle. Therefore the *Trucklab* and simulation model steering systems are evaluated. The comparison of both systems shows that there is a difference in steering results and in construction between *reference* model and *Trucklab*. In order to make the steering system of the model more accurate and more consistent with the *Trucklab*, the *reference* model is adjusted.

7.3.1 Trucklab

The *Trucklab* front axle is equipped with a steering system which is commonly used on light and heavy trucks. The steering wheel is connected to the steering gearbox by means of a long rod called the steering column. When turning, the steering column is slightly twisted due to the moments acting on both ends of the column. This shows that the steering column is slightly flexible. The purpose of the steering box is to rotate the pitman arm which controls the steering angle of the left wheel. The steering gearbox is mounted to the tractor chassis and provides the reduction between the rotational input from the steering wheel and the rotational output of the pitman arm; moreover, it assists the driver in turning the wheels. The pitman arm is connected to the steering arm of the upright of the left wheel by the steering rod. The right wheel is steered from the left wheel via the track rod linkage. This configuration of the steering system is known as a rear-steer-configuration because the track rod linkage, connecting the left and right wheels, is located behind the wheel centre. Figure 7.14 is a schematic view of the *Trucklab* steering geometry.

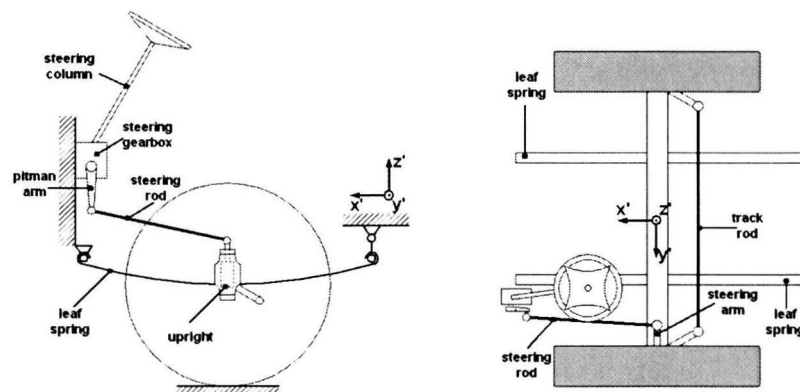


Figure 7.14: Schematic side view (left) and top view (right) of the *Trucklab* steering configuration.

The kinematic geometry of the linkages between upright and track rod and the track rod linkage is not a parallelogram (which would produce equal left and right steer angles), but rather a trapezoid (Figure 7.16) to more closely approximate "Ackerman" geometry which steers the inside wheel δ_i to a larger angle than the outside wheel δ_o . The Ackerman geometry is illustrated in Figure 7.15. The approximation of the Ackerman geometry is also clearly visible in the top view of the schematic *Trucklab* steering configuration in Figure 7.14.

From analysis of the triangles it can be shown that the outer δ_o and inner δ_i wheel steer angles for the Ackerman geometry are calculated by:

7.3 Steering system

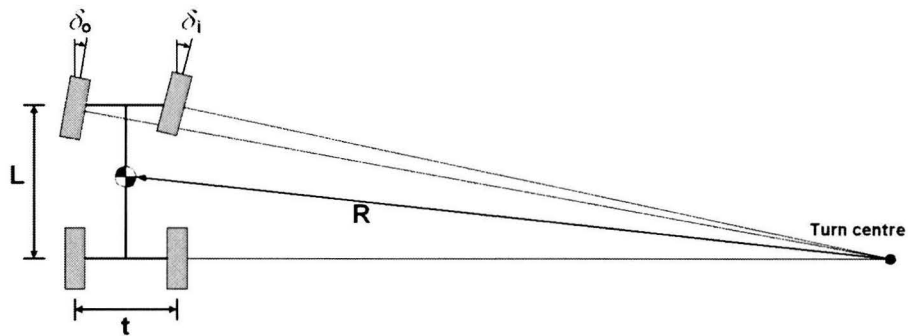


Figure 7.15: Ackerman turning geometry.

$$\delta_o = \tan^{-1} \left(\frac{L}{R + t/2} \right) \cong \frac{L}{R + t/2} \quad (7.7)$$

$$\delta_i = \tan^{-1} \left(\frac{L}{R - t/2} \right) \cong \frac{L}{R - t/2} \quad (7.8)$$

For small angles, as are typical for high speed turning, the arctangent of the angle is very nearly equal to the angle itself (in radians), justifying the approximations shown on the right side of the equations.

Perfect *Ackerman* steering is difficult to achieve with practical linkage designs, but is closely approximated by the trapezoidal arrangement as shown in Figure 7.16. When the wheels steer right or left, the asymmetry in the geometry causes the inside wheel to steer to a larger angle than the outside wheel. For more information on the subject of steering systems see [14] and [23].

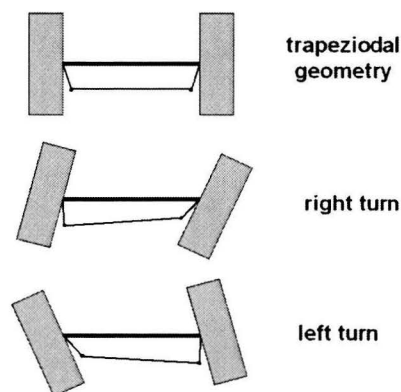


Figure 7.16: Ackerman turning geometry.

7.3.2 Simulation model

The *reference* simulation model is not equipped with a steering system geometry like the *Trucklab*, instead a simplified steering system is used. This simplified steering system steers the vehicle by means of directly imposing an angle to the steering axis of each wheel. The wheel steer angle is calculated by multiplying the steering wheel angle by the steer ratio. Both wheels have the same prescribed steering angle. The steer ratio is estimated by matching the chassis yaw velocity of the simulation model with the experimental results for the lane change and step steer experiments. For the performance of the steering experiments with the simulation model, the *Trucklab* steering wheel angle and forward velocity signals are measured inputs for the simulation model.

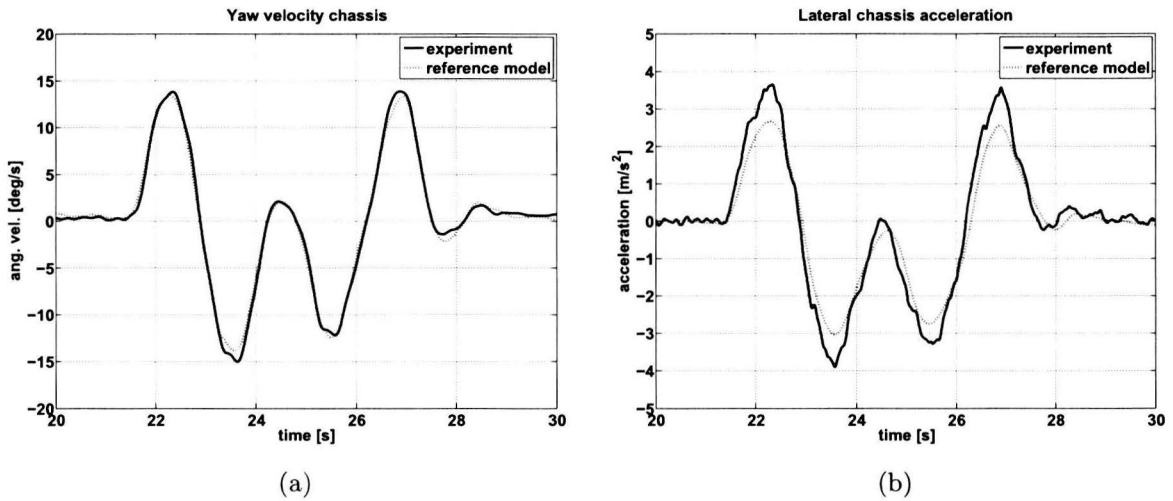


Figure 7.17: Double lane change experiment. Yaw velocity chassis (a) and lateral chassis acceleration (b), *Trucklab* (solid) and *reference model* (dotted).

Figure 7.17 displays the yaw velocity and lateral acceleration for a double lane change experiment. It can be seen that the *reference model* and the *Trucklab* show an accurate match regarding the chassis yaw velocity. Comparing the lateral chassis acceleration, it can be seen that the peak lateral acceleration values are higher for the *Trucklab*. The difference in lateral acceleration peak values is approximately 1 m/s^2 for the lane change experiment. This difference is substantial compared to peak values of $\pm 4 \text{ m/s}^2$. The difference in lateral acceleration is probably caused by the difference in steer ratios for the *Trucklab* and *reference model*. After matching the chassis yaw velocity of the simulation model with the experimental results, the steer ratio of the simulation model is set to $\frac{1}{30}$. This is much smaller than the *Trucklab* steer ratio of $\frac{1}{20}$ as specified by the *Trucklab* manufacturer.

7.3.3 Model adjustments

To obtain a steering system which is more accurate and more consistent with the *Trucklab* steering system, the *Trucklab* steering geometry is measured and documented. For this the steering system components are measured using measuring tape. Subsequently, the various steering system components are implemented. To compensate for the *Trucklab* steering column flexibility, a torsional spring and damper is included. The simulation model with the revised steering system geometry is referred to as "*adapted*" model for the remainder of this section. Figure 7.18 is a schematic view of the *adapted* model steering geometry.

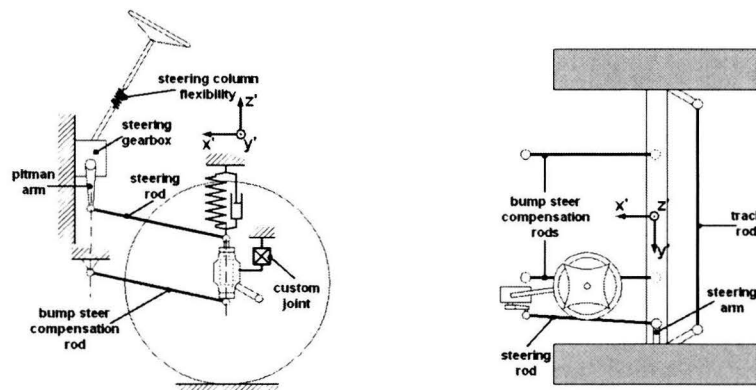


Figure 7.18: Schematic side view (left) and top view (right) of the *adapted* model steering geometry.

7.3 Steering system

Comparing Figure 7.14 and Figure 7.18, it can be seen that these configurations are not completely alike. Clearly, the main difference is the lack of leaf springs for the *adapted* model. These leaf springs are not included because accurate modelling of leaf springs is highly complex; furthermore, no measurements are available to validate an accurate leaf spring model. Simply omitting the leaf springs and replacing them with two vertical springs is no option as this will lead to a considerable amount of bump steer; moreover, no roll steer effect is introduced. In order to compensate for bump steer and to introduce roll steer, the *adapted* model is equipped with two bump steer compensation rods, one on each side of the vehicle. The combination of these rods and the vertical spring-damper elements is a simplified representation for the *Trucklab* leaf springs.

In *SimMechanics*, the bump steer compensation rods (Figure 7.18) are modelled as two massless *spherical-spherical* connectors and are symmetrically placed with respect to the vehicle centre line. The lateral distance between these rods is the same as the lateral distance between the *Trucklab* leaf springs. The bump steer compensation rods are parallel with the steering rod in the $x'z'$ -plane of the *vehicle* coordinate system; moreover, the length of the bump steer compensation rods and the steering rod are also the same. As a result of this, the bump steer is eliminated and the roll steer effect is introduced. For this adapted front axle suspension geometry, the lateral axle movement and rotation around its y' -axis are constrained with a *custom* joint between axle and chassis.

The bump steer effect for the *Trucklab* front axle is eliminated by using carefully determined leaf spring dimensions. The roll steer effect is not compensated for and is the result of using leaf springs for the *Trucklab* front axle suspension. For an explanation of the roll steer effect see section 7.1. The front axle roll steer effect of the *adapted* model is realised by the bump steer compensation rods.

As exact *Trucklab* front axle bump and roll steer measurements are not available, a comparison with simulation results is impossible. Instead, only the bump and roll steer results for the *adapted* model are displayed in Figure 7.19. It can be seen that there is no bump steer on the front axle as a result of using the bump steer compensation rods. The roll steer, displayed in the right graph of Figure 7.19 is very small. Because of the fact that the *reference* model has no steering system geometry, the front axle of this model is not subjected to bump or roll steer effects. For more information on the subject of bump and roll steer effects see [12].

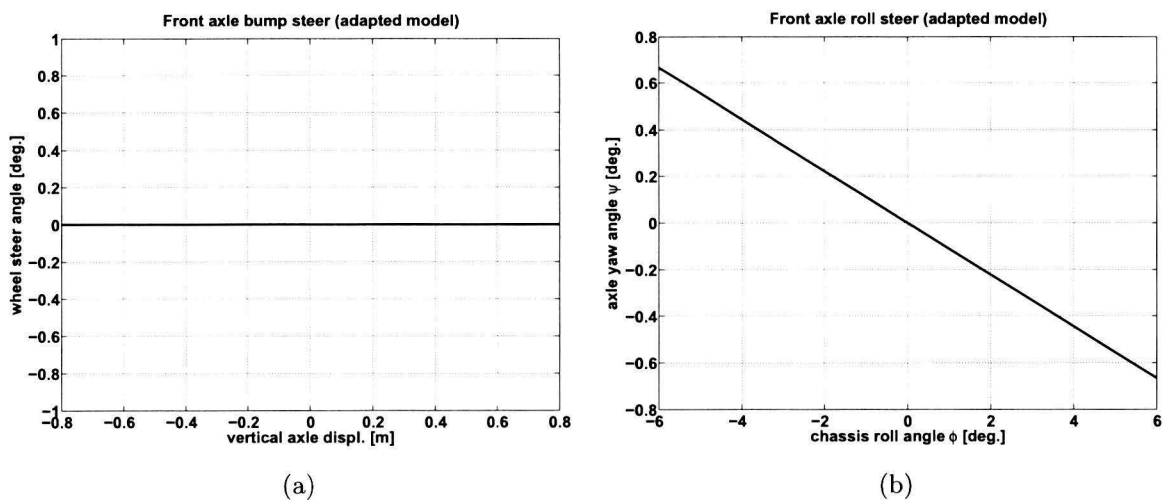


Figure 7.19: Front axle bump steer (a) and roll steer (b) for the *adapted* model.

However, adding two bump steer compensation rods also affects the front axle primary suspension deflection when braking (Figure 7.20). The added bump steer compensations rods act as two trailing arms. When the brakes are applied, the brake force F_b in combination with the trailing arms result in extra spring compression.

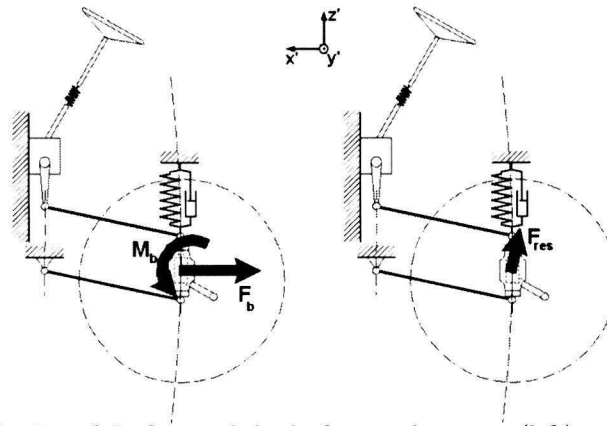


Figure 7.20: Schematic view of the front axle brake force and moment (left) and the resulting suspension force (right).

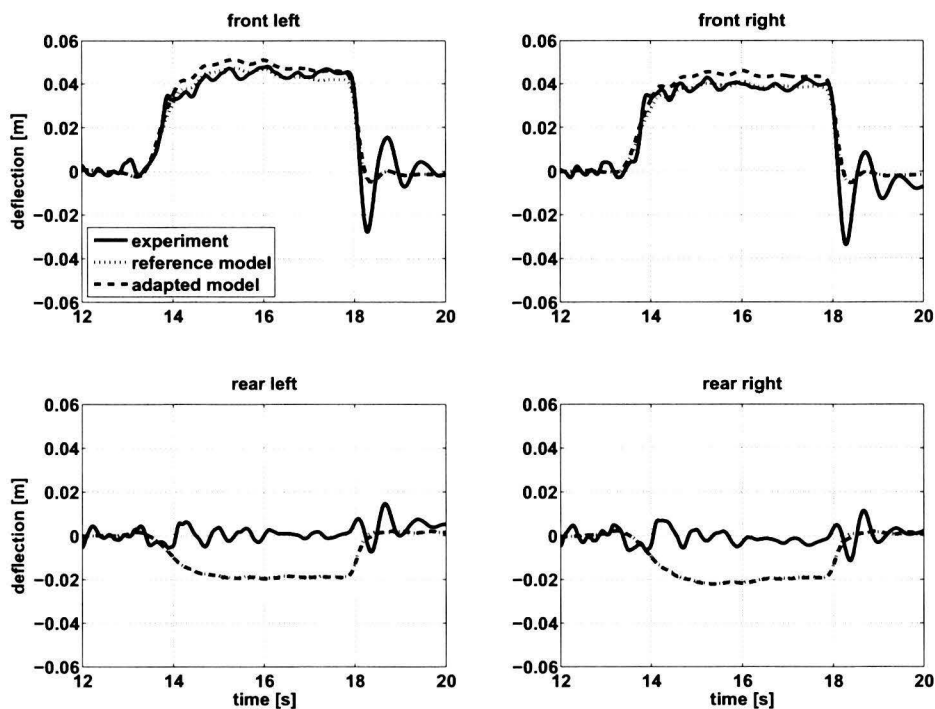


Figure 7.21: Heavy braking experiment. Axle suspension deflection, *Trucklab* (solid), *reference* model (dotted) and *adapted* model (dashed). Positive deflection corresponds to compression.

In Figure 7.21 it can be seen that the difference in front axle suspension deflection between the *reference* and *adapted* models is very small. Despite the extra spring compression, the *adapted* model still gives an accurate match between *Trucklab* and simulation.

Another important steering system parameter is the ratio between the steering wheel angle and the steer angle of the wheels, known as the steer ratio. To determine the steer ratio the steering wheel angles with their corresponding wheel steer angles for the left and right wheels are measured. Figure 7.22 displays the wheel steer angle as a function of the steering wheel angle for the *Trucklab*, *adapted* model and *reference* model.

7.3 Steering system

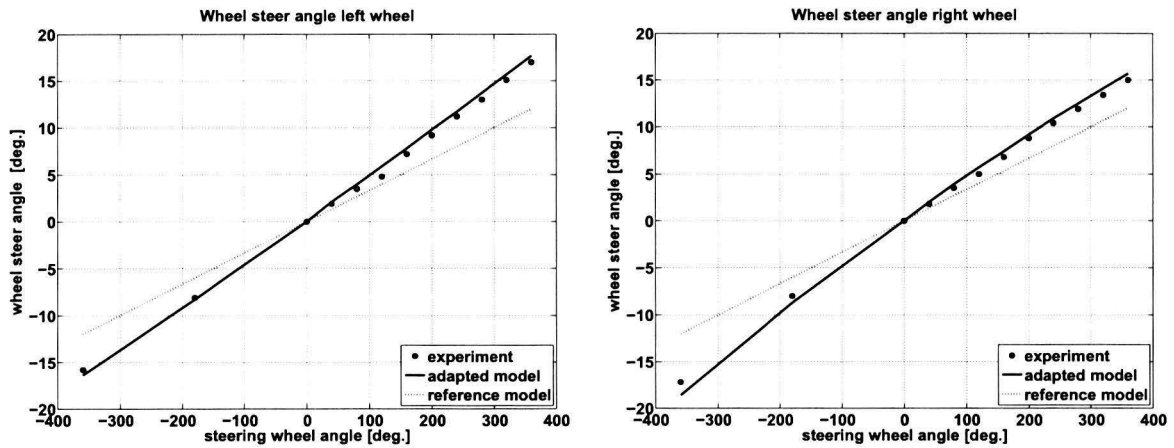


Figure 7.22: Front axle wheel steer angles for the left wheel (a) and right wheel (b), *Trucklab* (circular marker), *reference model* (dotted) and *adapted model* (solid).

Looking at Figure 7.22, it can be seen that the steering system geometry of the *adapted model* results in a more accurate approximation of the *Trucklab* wheel steer angles than the *reference model*. This also means that the steer ratio of the *adapted model* is closer to the *Trucklab* steer ratio than the *reference model*. The steer ratios for the *Trucklab*, *adapted model* and *reference model* are: $\frac{1}{21.8}$; $\frac{1}{20.6}$; and $\frac{1}{30}$ respectively.

As mentioned in the description of the adapted steering system, a torsional spring-damper element is included to account for the steering column flexibility. The effect of steering column flexibility is that it reduces the steer ratio for dynamic steering wheel input. A highly flexible steering column results in a slow response of the wheels when steering. Exact *Trucklab* steering column flexibility measurements are difficult to perform and therefore the exact stiffness and damping values are unknown. Instead, these steering column stiffness and damping parameters are determined by trial and error and tuned until the lateral chassis acceleration and yaw velocity are accurately matched with the measurements. The contribution of the added flexibility, to improve the match with the measurements, is small and is solely used to fine-tune the steer ratio for dynamic steering wheel input. The fine-tuned parameter values are 38000 Nm/rad and 500 Nms/rad for the steering column stiffness and damping respectively.

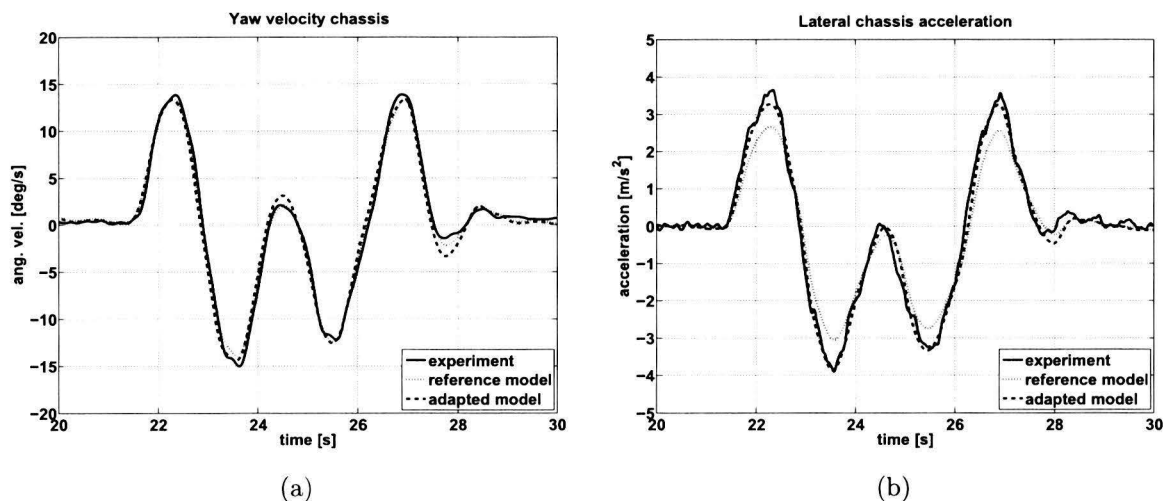


Figure 7.23: Double lane change experiment. Yaw velocity chassis (a) and lateral chassis acceleration (b), *Trucklab* (solid), *reference model* (dotted) and *adapted model* (dashed).

7.3.4 Evaluation

Figure 7.23 displays the chassis yaw velocity and lateral chassis acceleration for the *Trucklab*, *reference* model and *adapted* model for the lane change experiment. It can be seen that the adapted steering system result in a more accurate prediction of the lateral chassis acceleration when subjected to dynamic steering wheel inputs. The chassis yaw velocity is also accurately predicted. Examining the results displayed in this section, it can be concluded that the revised steering system of the *adapted* model results in an accurate prediction of the chassis yaw velocity and lateral chassis acceleration when subjected to quasi-static and dynamic steering wheel inputs. After evaluating the contribution of each implemented adjustment, it can be concluded that the combination of steering arm, steering rod, pitman arm, steering box and bump steer compensation rods has the largest contribution to improving the model. By implementing these adjustments the simulation model has a more accurate steer ratio.

7.4 Cabin suspension

As discussed in section 6.7, the cabin suspension deflection is another aspect of the *reference* model that needs closer examination. The evaluation scores for the cabin suspension are generally low, especially for the steering manoeuvres. Braking experiments on the other hand have relatively high scores for the cabin suspension deflection. Because of this large variation of evaluation scores the *Trucklab* and simulation model cabin suspension are investigated. Subsequently, adjustments are implemented to improve the match between *Trucklab* and simulation model.

7.4.1 Trucklab

The *Trucklab* is equipped with an air-suspension system for the cabin. Figure 7.24 displays the *Trucklab* cabin suspension. The suspension consists of four vertical aligned air-springs coupled to an expansion volume and compressor. Besides these vertically aligned suspension struts, the cabin is also equipped with horizontally aligned dampers at the rear side of the cabin to dampen the yaw and lateral motions of the cabin, increasing the comfort level. The expansion volume for the vertically aligned suspension struts is added to the system to obtain the required low spring stiffness. The compressor in combination with a levelling control system is included to level the cabin with respect to the tractor chassis. The levelling of the cabin is realised by adjusting the air pressure inside the front and rear air spring elements. Note that for the levelling system the front and rear suspension struts are two separated circuits. The cabin suspension is also equipped with an anti-roll bar at the front side of the cabin to restrict the rolling motion of the cabin with respect to the tractor chassis.

7.4.2 Simulation model

For the *reference* model the cabin suspension is a simplification of the *Trucklab* suspension geometry. The cabin is modelled as a single rigid body, elastically suspended in all 6 degrees of freedom with respect to the tractor chassis. The anti-roll bar is modelled as a torsional spring in the longitudinal direction of the *vehicle* coordinate system (X' -direction). The cabin levelling control system consists of two simple feed-forward controllers, one for the front and one for the rear side suspension struts of the cabin. These controllers adjust the spring pre-load to level the cabin.

Figure 7.25 displays a schematic view of the *reference* model cabin suspension. It can be seen that the four vertical spring/damper combinations, the roll stiffness, and the horizontal dampers at the rear side of the cabin are included in the simulation model. Besides these elements, additional spring/damper combinations in longitudinal (X') and lateral (Y') direction are included. These account for the flexibility in longitudinal and lateral direction of the *Trucklab* cabin mounts. For the *reference* model the aerodynamic forces acting on the cabin are not considered.

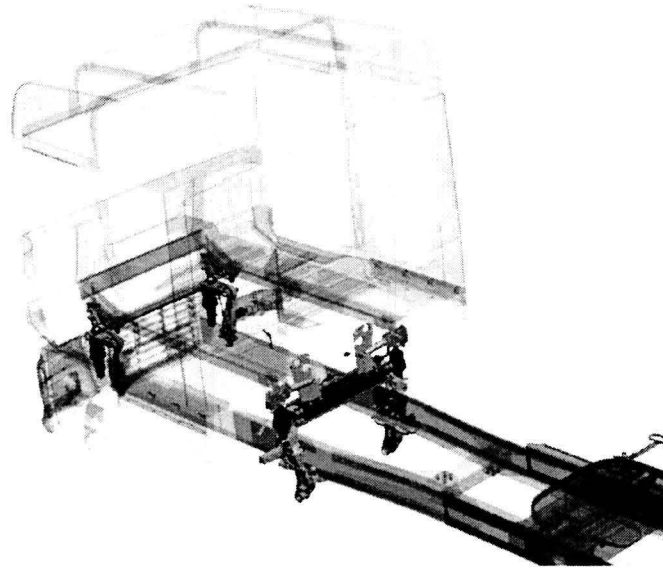


Figure 7.24: *Trucklab* cabin suspension system [5].

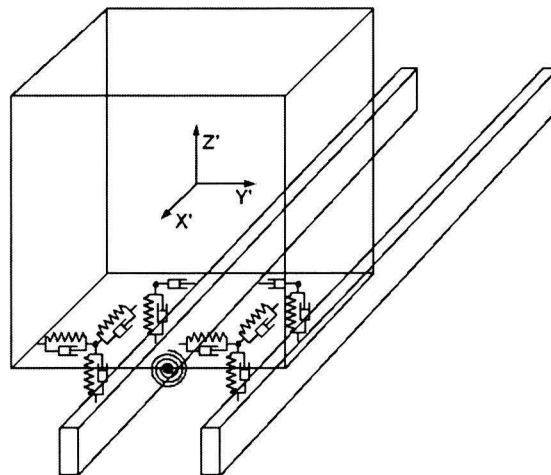


Figure 7.25: Schematic view of the *reference* model cabin suspension.

7.4.3 Analysis

As said at the beginning of this section, the cabin suspension deflection scores vary a lot in magnitude for the different experiments. Therefore the time-domain cabin suspension graphs are closely examined. Closer examination of the cabin suspension deflections when braking shows a few striking differences between *Trucklab* and *reference* model. Figure 7.26 displays the cabin suspension deflections for a braking manoeuvre. In the same figure the differences are marked by the letters: A, B and C. In the sections below, each marked difference is discussed separately.

Offset A

During the braking manoeuvre for $13.5 < t < 18.5$ seconds, there is an offset in deflection between *Trucklab* and *reference* model marked with the letter A. This mismatch is observed both for the front and rear side suspension struts. There are a few possible causes for the observed mismatch when braking. The first is the stiffness of the air-springs and/or the stiffness of the spring deflection restricting bump stops. The second possible cause is that the *Trucklab* suspension sensors were reset before the cabin was correctly levelled. This resetting was necessary due to a failing data acquisition

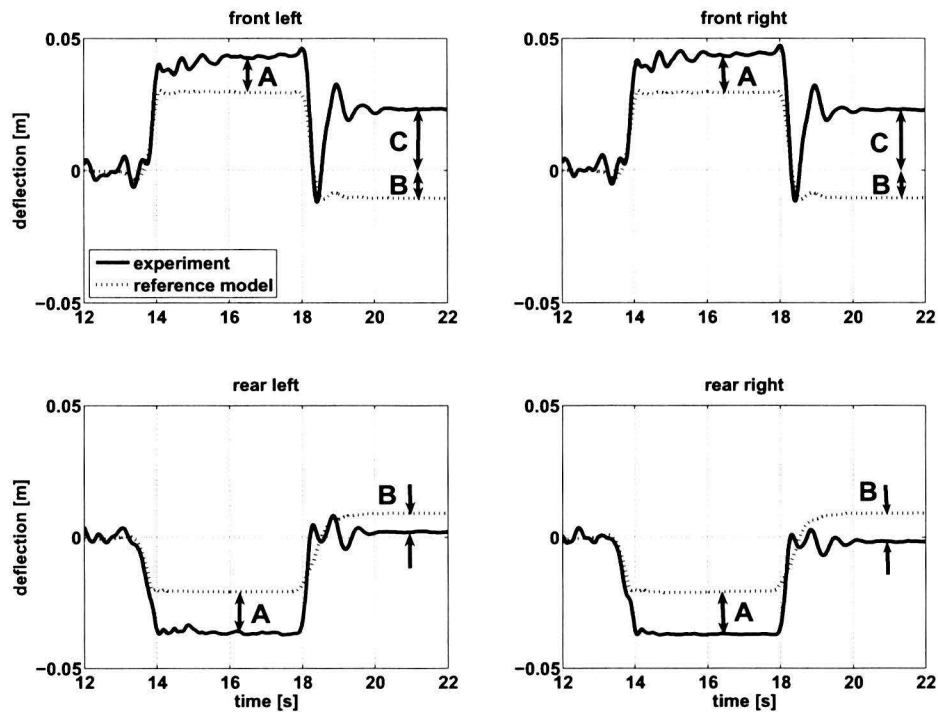


Figure 7.26: Heavy braking experiment. Cabin suspension deflection, *Trucklab* (solid) and *reference* model (dotted). Positive deflection corresponds to compression.

system. The third cause can be an incorrectly levelled *Trucklab* cabin before the brakes are applied. Due to the aerodynamic drag force acting on the *Trucklab* cabin at 60 km/h in combination with a very slow *Trucklab* levelling control, the cabin is tilted backwards resulting in more positive and negative working space for the *Trucklab* front and rear suspension struts respectively.

At $t = 18.5$ seconds the vehicle comes to a standstill. For $t = 18.5$ seconds it can be seen that there is a major mismatch between the *Trucklab* and *reference* model. The *Trucklab* and simulation model show a different suspension response. This difference is probably caused by a phenomenon called axle wind-up for the front axle which is not included for the simulation model as this requires a leaf spring model for the front axle suspension. Moreover, a simplified friction model for the brakes and tyre deformation also contributes to this mismatch in suspension response.

Offset B

For $t > 18.5$ seconds the front and rear suspension struts of the *reference* model do not return to their initial position ($t < 13.5$ seconds). Instead, the front and rear show a small negative and positive deflection respectively. This is the result of continuously levelling the cabin during the braking manoeuvre. As a result the cabin has a small negative pitch angle after coming to a standstill.

Offset C

Examining the *Trucklab* suspension response for $t > 18.5$ seconds, it can be seen that the front shows a large positive offset with respect to its initial position ($t < 13.5$ seconds). This is caused by the levelling of the cabin before braking as a result of the aerodynamic drag force acting on the cabin in combination with switching off the levelling control when the brakes are applied. Because of this the pressure inside the *Trucklab* front suspension struts is the same for $t < 13.5$ and $t > 18.5$; furthermore, this pressure is lower than when the vehicle is standing still with the levelling control switched on. After coming to a standstill, the brakes remain applied ($t > 18.5$ seconds) and therefore the levelling control remains switched off. As a result a positive deflection is observed for the front suspension struts.

7.4 Cabin suspension

Logically, the same offset is expected for the *Trucklab* rear suspension struts resulting in a negative deflection for $t > 18.5$ seconds. However, this offset is not observed for the rear suspension deflections in Figure 7.26. A possible cause for this is a malfunctioning levelling system.

7.4.4 Model adjustments

In order to obtain a better match between *Trucklab* and *reference* model more accurate with regard to the cabin suspension deflections, a number of adaptations are made. This adapted version of the *reference* model is referred to as "*adapted*" model for the remainder of this section.

At first, the cabin levelling control is switched off directly after the cabin is levelled at the beginning of each simulation. Consequently, there is no levelling of the cabin during the actual braking manoeuvre. Secondly, the aerodynamic force acting on the cabin is added to the simulation model. This aerodynamic drag force is calculated by:

$$F_d = \frac{1}{2} \rho v^2 C_d A \quad (7.9)$$

where ρ is the density of air, v is the relative vehicle velocity, A is the estimated frontal surface of the cabin (4 [m²]) and C_d is drag coefficient (0.8 [-]). The latter value is estimated based on values mentioned in literature on the subject of aerodynamics. For the relative velocity v , the longitudinal velocity of the simulation model is used.

The third adaptation is the addition of the anti-roll bar geometry. The anti-roll bar acts as a suspension geometry for the cabin suspension. The addition of a suspension geometry can affect the suspension travel and therefore the anti-roll bar geometry is added. Note that solely the physical geometry of the anti-roll bar is added, the roll stiffness itself remains represented by the torsional spring discussed earlier. In *SimMechanics* the anti-roll bar is represented by two longitudinal rods, each with a length of 27.5 cm. In Figure 7.27 is schematic side view of the cabin suspension with these rods is given. The front sides of these rods are connected to the cabin with a *revolute* joint. The rear side is connected to the chassis by a *custom* joint. This joint is a modified *spherical* joint which includes the cabin mount stiffness in longitudinal and lateral directions.

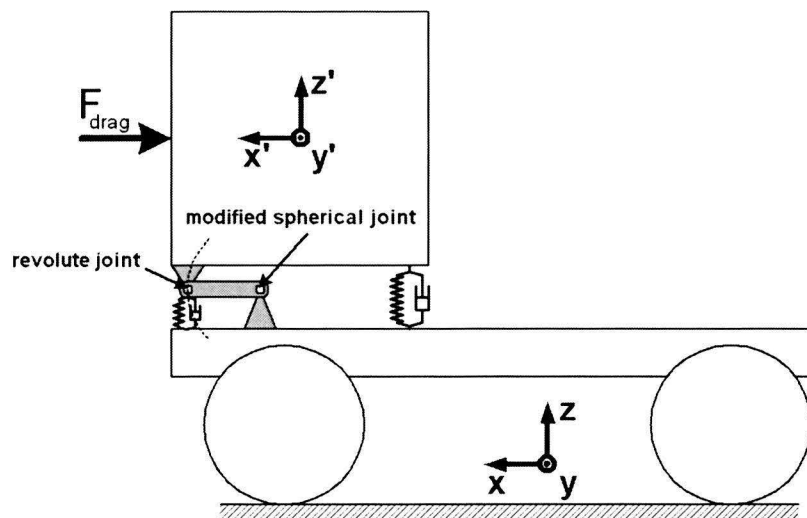


Figure 7.27: Schematic side view of the cabin suspension of the *adapted* model.

The cabin mount stiffness is moved from the front side suspension struts (*reference* model) to the longitudinal rods (*adapted* model). This prevents the longitudinal cabin mount stiffness from interfering

with the vertical suspension deflection, as small movement in x' -direction between chassis and cabin is enforced by the anti-roll bar geometry. An exact model of the anti-roll bar is not included because this involves high simulation times due to the combination of high stiffness and low body mass of the anti-roll bar.

The fourth and last model adaptation involves the spring and dampers characteristics of the front and rear cabin suspension struts. Figure 7.28 displays the normalised spring and damper characteristics of the cabin suspension for the *reference* model and *adapted* model. The spring and damper characteristics of the *adapted* model are accurately fitted on measurements performed by *TNO Automotive*. Figure 7.28 shows a lower spring stiffnesses and damping coefficients for the *adapted* model.

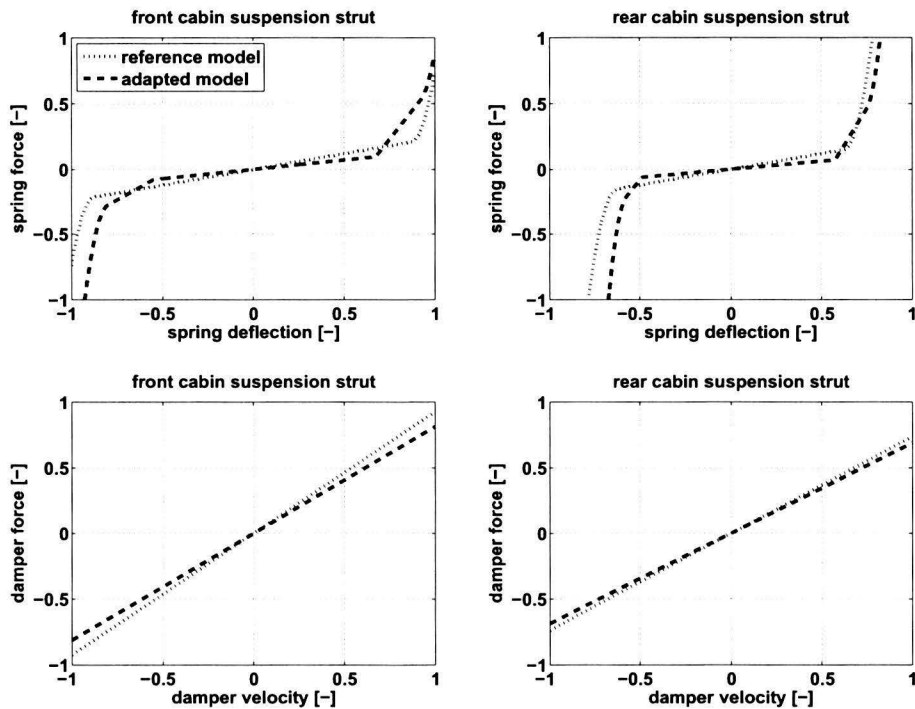


Figure 7.28: Normalised cabin suspension characteristics, *reference* model (dotted) and *adapted* model (dashed).

7.4.5 Evaluation

To demonstrate the effects of the implemented model adjustments of the *adapted* model, the cabin suspension deflection for the *Trucklab*, *reference* model and *adapted* model are shown in Figure 7.29. It can be seen that mismatch is drastically reduced for $t > 18.5$ seconds at the front of the cabin. This is the result of the switched off levelling control and the addition of the aerodynamic drag force. However, there remains a mismatch for $t < 18.5$ seconds.

Examining the rear suspension for $t > 18.5$ seconds, it can be seen that the *adapted* model responds as expected. After the vehicle has come to a standstill the rear suspension shows a negative deflection that is not observed for the *Trucklab*. To illustrate that the rear *Trucklab* cabin suspension is malfunctioning, an additional *Trucklab* braking test is performed. For this test the *Trucklab* is equipped with a different anti-roll bar; furthermore, this test is performed without semi-trailer with an initial speed of 70 km/h. Fitting a different anti-roll should have no effect on symmetric vehicle behaviour. However,

7.4 Cabin suspension

different suspension response is observed at the rear suspension struts after the vehicle has come to a standstill. The cabin suspension deflections for this test are displayed in Figure 7.30. It can be seen that rear suspension shows a negative deflection after the vehicle has come to a standstill ($t > 17$ seconds). This rear suspension response corresponds to the simulation results of the *adapted* model; furthermore it agrees with what is to be expected. This difference in suspension response for the different tests is highly remarkable; moreover, it confirms the malfunctioning of the original *Trucklab* rear cabin suspension struts.

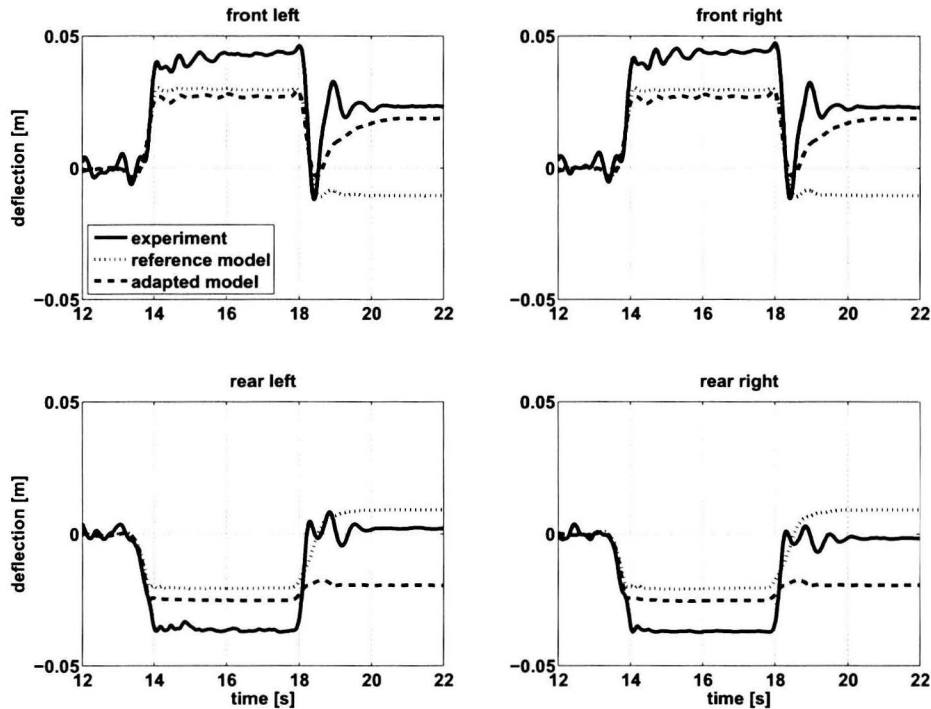


Figure 7.29: Heavy braking experiment. Cabin suspension deflection, *Trucklab* (solid) *reference* model (dotted) and *adapted* model. Positive deflection corresponds to compression.

Looking at Figure 7.29 it can also be seen that the difference between *Trucklab* and *adapted* model during the braking manoeuvre itself ($13.5 < t < 18.5$ seconds) is hardly changed both for the front and rear. The difference in deflection between the *reference* and *adapted* model is the result of the adapted spring and damper characteristics. During the braking manoeuvre, the front and rear suspension hit the bump stops for the simulation models and *Trucklab*. However, it can be seen that the *Trucklab* has more available working space for the suspension at the front and rear than the simulation models when braking. Examining the cabin suspension deflections for an acceleration experiment (Figure 7.31) show that the *Trucklab* has less working space before hitting the bump stops than the simulation models. This in combination with the accurately fitted suspension characteristics indicate that the *Trucklab* cabin is probably not correctly levelled.

During the evaluation of the four model adaptations, it appeared that the adapted cabin levelling controller is not working properly for every experiment. The controller is optimised for the braking experiments. Due to the limited amount of idle-time before braking, the controller is forced to level the cabin within the first two seconds of the simulation which is much faster than the *Trucklab*. In order to prevent peculiar cabin suspension responses, the cabin levelling controller is switched off for the other experiments. Switching off the levelling controller also results small mismatches in cabin suspension deflections as can be seen in Figure 7.32. This figure displays the cabin suspension deflection for a double lane change experiment. After evaluating the contribution of each of the four adaptations it also appeared that the contribution of the anti-roll bar geometry is insignificant; therefore, this adaptation can be left out in future model updates.

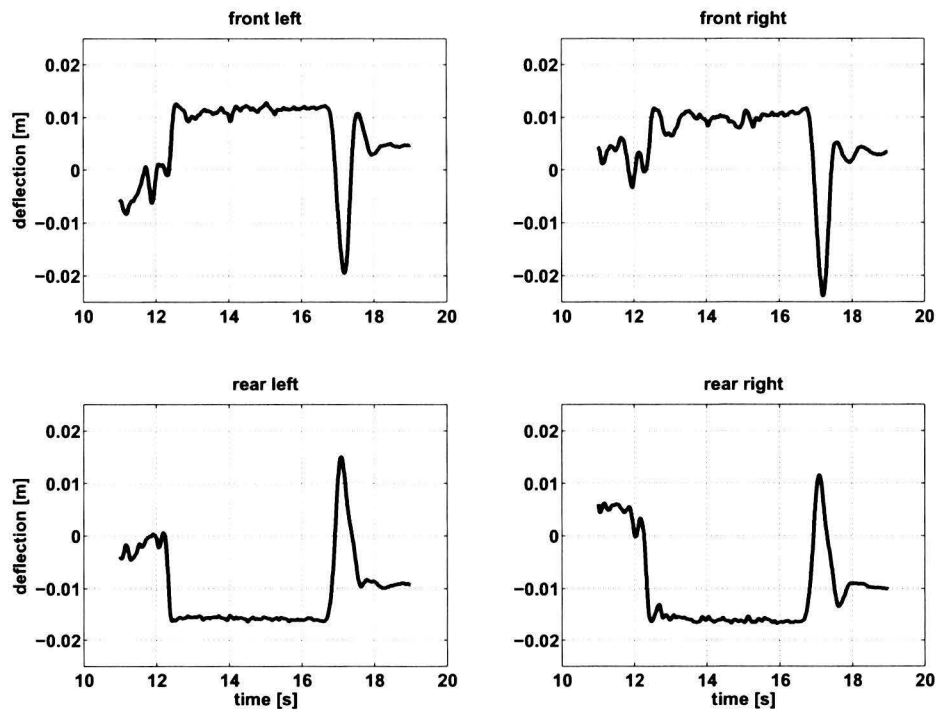


Figure 7.30: Heavy braking experiment with modified *Trucklab* cabin suspension at 70 km/h without semi-trailer. Positive deflection corresponds to compression.

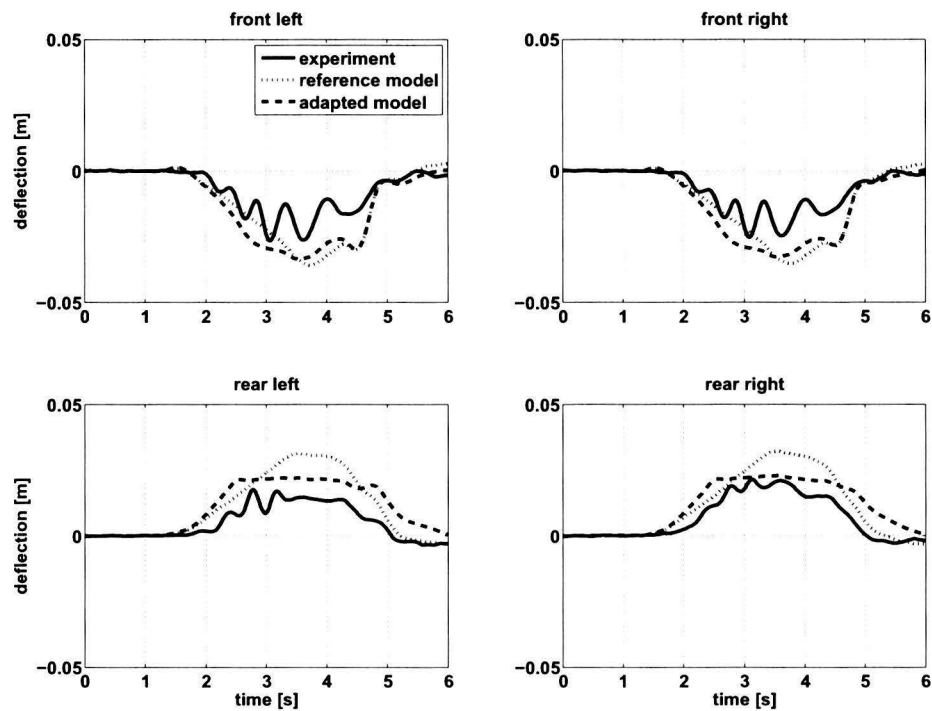


Figure 7.31: Acceleration experiment. Cabin suspension deflection, *Trucklab* (solid) reference model (dotted) and adapted model. Positive deflection corresponds to compression.

7.5 Summarising this chapter

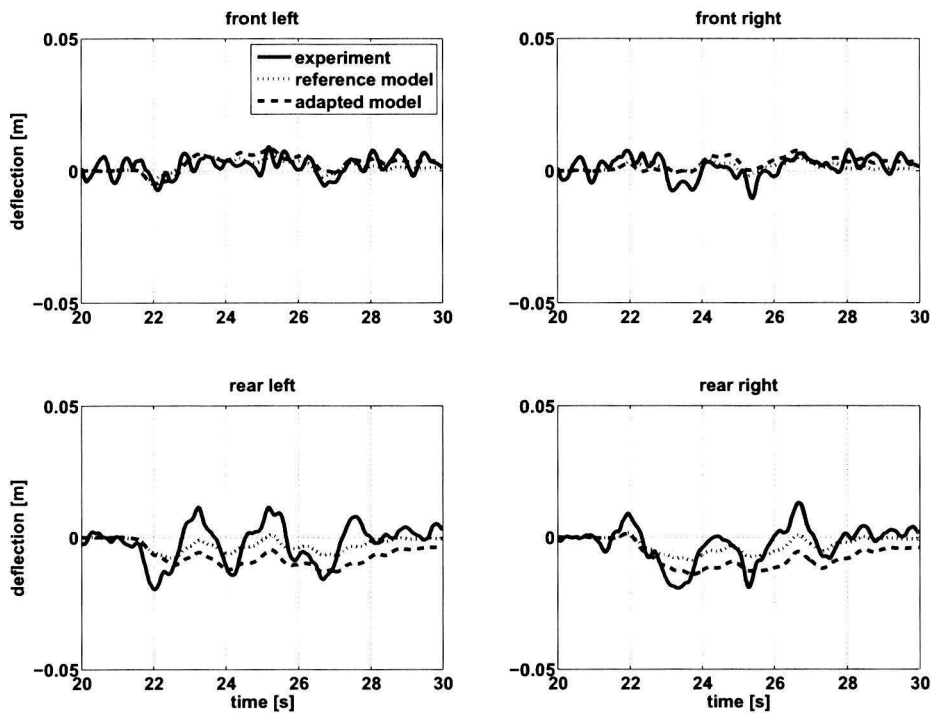


Figure 7.32: Double lane change experiment. Cabin suspension deflection, *Trucklab* (solid) *reference* model (dotted) and *adapted* model. Positive deflection corresponds to compression.

7.5 Summarising this chapter

In chapter 6 an updated version of the baseline model is presented called *reference* model. After the evaluation of this model it can be seen that there is still room for further improvement. In this chapter the model adjustments for further improvement of the *reference* model are discussed. Below, a short summary of each model adjustment is given:

Rear axle suspension

For this model adjustment the *Trucklab* rear axle suspension geometry is measured and implemented in the simulation model. This suspension geometry introduces an anti-rise effect when braking and an anti-squat effect when accelerating for the rear axle suspension. This results in a large improvement with regard to the rear axle suspension deflection for the braking and acceleration experiments. The adapted suspension geometry also introduces a small amount of rear axle roll steer. As the roll steer is very small, the effect on steering handling characteristics is minimal.

Brake system

The brake system with a fixed brake force distribution (*reference* model) is replaced by a brake system with a variable brake force distribution (*Trucklab*). The latter brake system is based on the minimisation of the differential slip between the various axles. As a result, the simulation model meets the legally required deceleration level for every loading condition. Moreover, it also improves the rear axle suspension deflection when braking.

Steering system

To obtain a steering system which is more accurate than the *reference* model steering system and more consistent with the *Trucklab* steering system, the *Trucklab* steering geometry is measured and implemented. For this implemented steering system the bump steer effect is eliminated and a roll steer effect is introduced by adding two bump steer compensation rods. These compensation rods result in

a counter steer effect on the front axle during cornering. This adapted steering geometry results in a more accurate prediction of the lateral chassis acceleration and chassis yaw velocity as the steer ratio is more accurate.

Cabin suspension

The adaptation of the cabin suspension consists of four adjustments:

- switching off the cabin levelling controller after the cabin is levelled.
- adding the aerodynamic force acting on the cabin.
- implementing the anti-roll bar geometry
- adding measured spring and damper characteristics

The first two adjustments resulted in an improved cabin front suspension response after coming to a standstill for a braking experiment. The improvement of the rear cabin suspension remains unclear as it is likely that the *Trucklab* rear cabin suspension is malfunctioning. However, the cabin levelling controller is not working correctly when performing steering experiments. Therefore, further adjustments are required.

The implementation of the anti-roll bar geometry and measured spring/damper characteristics show no large improvement with respect to the suspension response before coming to a standstill. There remains a considerable mismatch between simulation model and *Trucklab*.

Chapter 8

Model validation

In this chapter, the tractor semi-trailer simulation model including all the adjustments is validated. As stated in chapter 2, model validation is defined as: proving that the input-output transformation of the simulation model is a sufficiently accurate representation of the input-output transformation of the corresponding physical system. Beside the first objective of validating the tractor-semi trailer simulation model, the second objective is to show the achieved improvements as a result of the model adjustments discussed in chapters 6 and 7. For this purpose, a comparison is made between the *baseline* and *final* model using time domain graphs and the evaluation algorithm of chapter 5. The *baseline* model is the original tractor semi-trailer simulation model as discussed in chapter 4, the *final* model is an updated version of this *baseline* model and includes the adjustments discussed in chapters 6 and 7.

The model validation is performed by comparing *Trucklab* and simulation data of the *final* model for different types of experiments. Furthermore, *baseline* simulation model data is used to indicate the effect of the implemented model adjustments. For every type of experiment the evaluation scores for the *baseline* and *final* model and *reference* and *final* model are also compared. Some of the evaluation score graphs are included in the sections below, others are included in Appendix C.2 and Appendix C.3. For an overview of the signal names used in the evaluation figures see Appendix A.3.

8.1 Discrete obstacles

The discrete obstacle experiments consists of riding over three types of obstacles: the pyramid; the step down; and the threshold obstacle. The validation of the discrete obstacles is based on the *Trucklab* and simulation data of the threshold obstacle. Riding over this obstacle has the most severe impact on the vehicle. Because of this, the response caused by the obstacle is much larger than the noise level of the various *Trucklab* sensors.

8.1.1 Vertical accelerations

In Figures 8.1, 8.2 and 8.3 respectively the vertical axle, chassis and cabin accelerations are given. Looking at the vertical accelerations, it can be seen that the acceleration spikes induced by the obstacle can be predicted accurately for the axles, chassis and cabin of the *final* model. This holds for the right side where the obstacle is placed, as well as the left side of the vehicle. Comparing the simulation results for the *baseline* and *final* model, it can be seen that the *final* model gives a more accurate prediction of the acceleration spikes than the *baseline* model. This is mainly the result of using the *MF-Swift* tyre model for riding over the discrete obstacles.

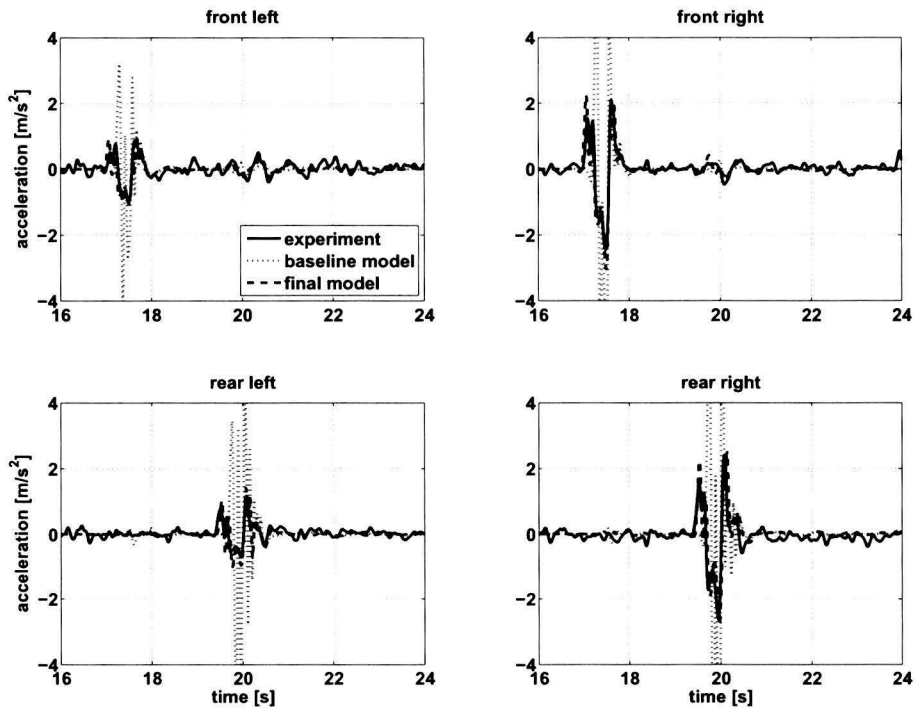


Figure 8.1: Discrete obstacle (threshold) experiment. Vertical axle accelerations, *Trucklab* (solid), *baseline model* (dotted) and *final model* (dashed).

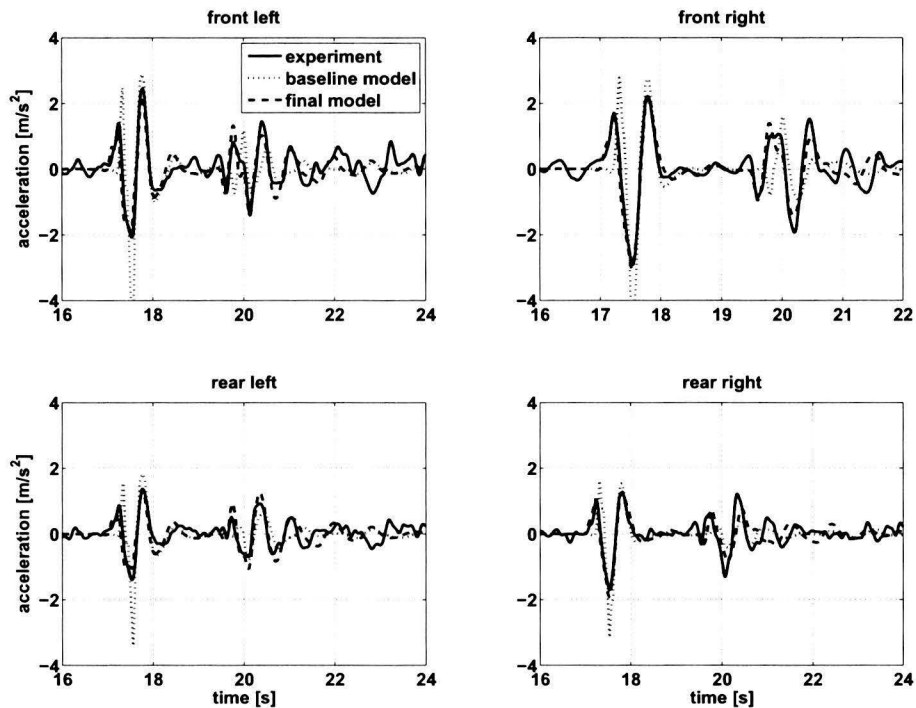


Figure 8.2: Discrete obstacle (threshold) experiment. Vertical chassis accelerations below cabin suspension struts, *Trucklab* (solid), *baseline model* (dotted) and *final model* (dashed).

8.1 Discrete obstacles

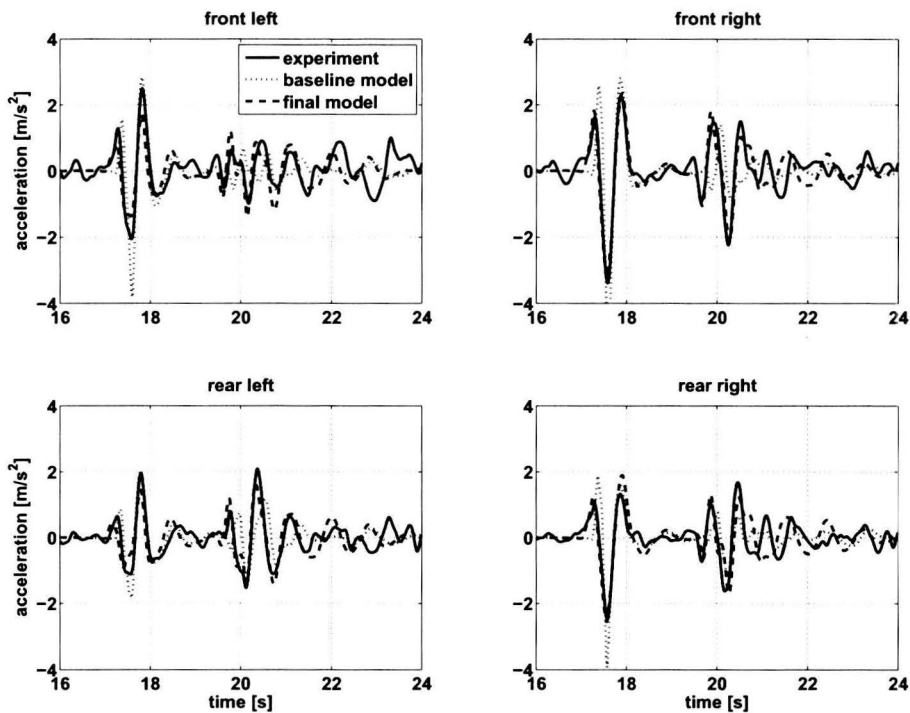


Figure 8.3: Discrete obstacle (threshold) experiment. Vertical cabin accelerations above cabin suspension struts, *Trucklab* (solid), *baseline model* (dotted) and *final model* (dashed).

8.1.2 Suspension deflections

Figure 8.4 displays the axle suspension deflection when riding over the threshold obstacle. It can be seen that the deflection spikes induced by the obstacle can be accurately predicted. Clearly perceptible is the improvement with respect to the *baseline model*. However, for $t > 21$ seconds the difference between *Trucklab* and simulated response for the front and rear axle is increasing; furthermore, a time shift occurs. It can be seen that the *Trucklab* suspension responses for front and rear axles are opposite phased that means a pitching motion of the chassis. This can be the result of cabin movement induced by the obstacle.

The response of the cabin suspension (Figure 8.5) shows that the response of the front left, front right and rear right suspension is simulated quite accurately when the front and rear wheels cross the obstacle. The rear left suspension shows a considerable error between *Trucklab* and simulation when the front and rear wheels cross the obstacle. What causes this error on the rear left suspension strut is still unclear. For $t > 21$ seconds a mismatch appears between *Trucklab* and simulation response for all four suspension struts. The *Trucklab* front and rear suspension responses are clearly opposite phased that indicates a pitch motion of the cabin. A possible cause for the difference between *Trucklab* and simulation can be the modelling of the cabin suspension dampers. For the cabin suspension no clear improvement is observed as a result of the implemented model adjustments.

8.1.3 Lateral accelerations

In Figure 8.6 the lateral chassis (top) and cabin (bottom) accelerations are displayed. Looking at these lateral acceleration responses it can be seen that the acceleration of the simulation model is slightly higher than the *Trucklab* when the front and rear wheels cross the obstacle. Furthermore a weakly dampened oscillation is observed with the simulation model for $t > 20.5$ seconds, both for the chassis and cabin.

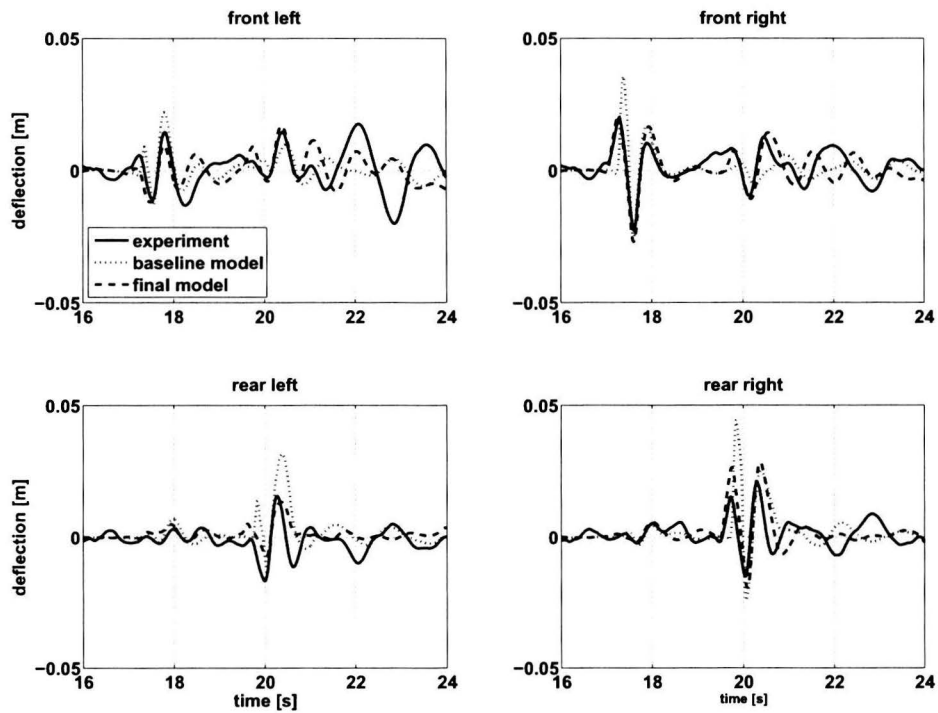


Figure 8.4: Discrete obstacle (threshold) experiment. Axle suspension deflection, *Trucklab* (solid), *baseline model* (dotted) and *final model* (dashed). Positive deflection corresponds to compression.

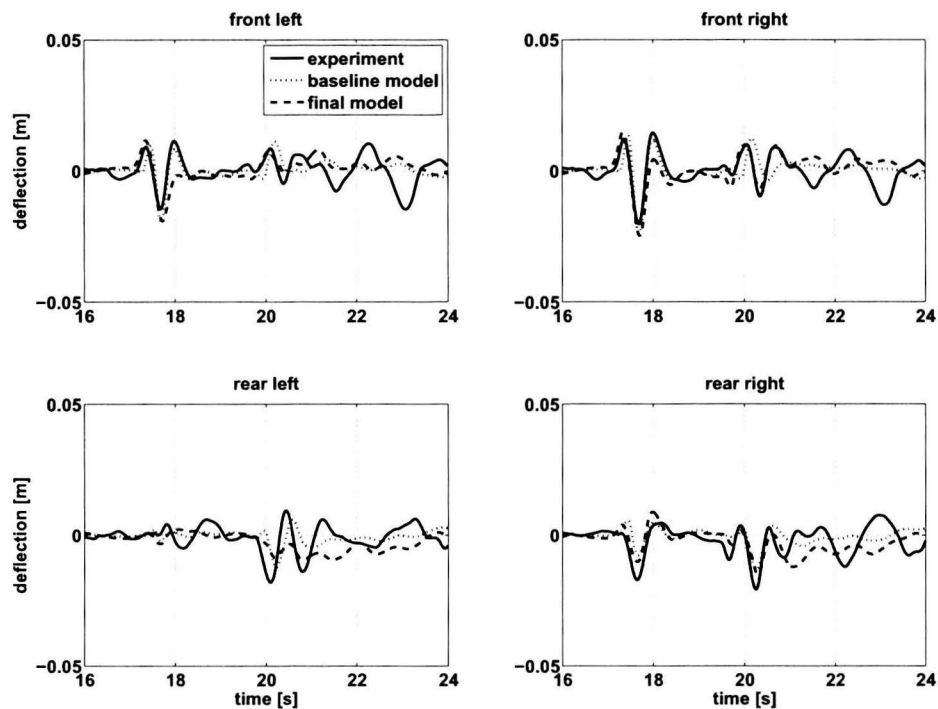


Figure 8.5: Discrete obstacle (threshold) experiment. Cabin suspension deflection, *Trucklab* (solid), *baseline model* (dotted) and *final model* (dashed). Positive deflection corresponds to compression.

8.1 Discrete obstacles

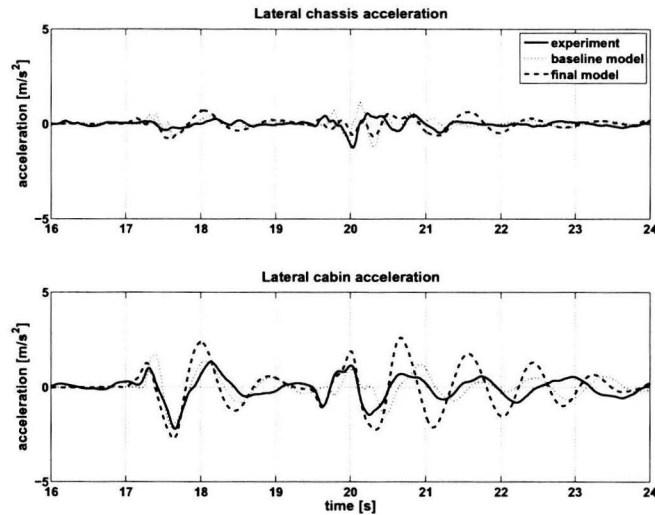


Figure 8.6: Discrete obstacle (threshold) experiment. Lateral acceleration, *Trucklab* (solid), *baseline* model (dotted) and *final* model (dashed).

The mismatch is caused by an insufficiently dampened torsional flexibility between the front and rear chassis parts of the simulation model. The simulated front axle suspension response shows an opposite phase between the left and right for $t > 20.5$ seconds, which indicates a roll motion of the front chassis part that explains the higher lateral chassis accelerations. As the cabin is mounted on the front part of the chassis, this automatically leads to an excessive roll motion of the cabin and higher lateral cabin accelerations. For the *baseline* and *final* model the damping coefficient of the chassis torsional flexibility is zero. Increasing the damping coefficient can result in more accurate lateral accelerations.

Comparing the simulation results for the *baseline* and *final* model no clear improvement can be noticed with respect to the lateral chassis accelerations when encountering discrete obstacles. Looking at the lateral cabin accelerations, a deterioration of the match between *Trucklab* and simulation model is observed.

8.1.4 Angular velocities

The angular velocities measured in the cabin and on the chassis are displayed in Figure 8.7. It can be seen that the relatively small chassis and cabin yaw velocity show a very good match over the depicted time-range. The cabin pitch velocity looks very similar when the front and rear wheels cross the obstacle; however, for $t > 20.5$ seconds a small mismatch appears. A possible cause for this can be too high damping coefficients of the cabin suspension struts. Looking at the cabin roll velocity the same phenomena can be observed as for the lateral cabin acceleration. The simulation model cabin shows a weakly dampened roll motion for $t > 20.5$ seconds. This is probably caused by the weakly dampened torsional flexibility that is discussed in section 8.1.3. For the roll velocity the implemented adjustments result in a deterioration of the match between *Trucklab* and simulation model.

8.1.5 Conclusion

Looking at the results of this section it can be concluded that the simulation model gives an accurate prediction for the appearing vertical accelerations and primary suspension deflection when riding over a discrete obstacle. The cabin suspension deflections and cabin yaw velocities are simulated quite accurately; however, there is still room for further improvement. A considerable mismatch is observed for the lateral acceleration, pitch and roll velocity of the cabin. In order to further improve the simulation model it is recommended to investigate the damping of the chassis torsional flexibility and the dampers of the cabin suspension.

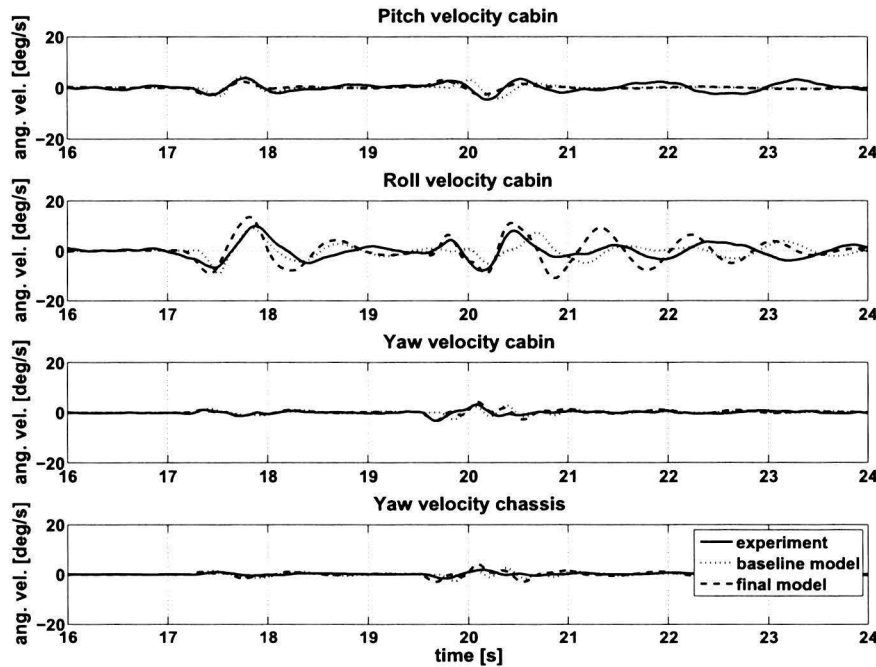


Figure 8.7: Discrete obstacle (threshold) experiment. Angular velocities, *Trucklab* (solid), *baseline* model (dotted) and *final* model (dashed).

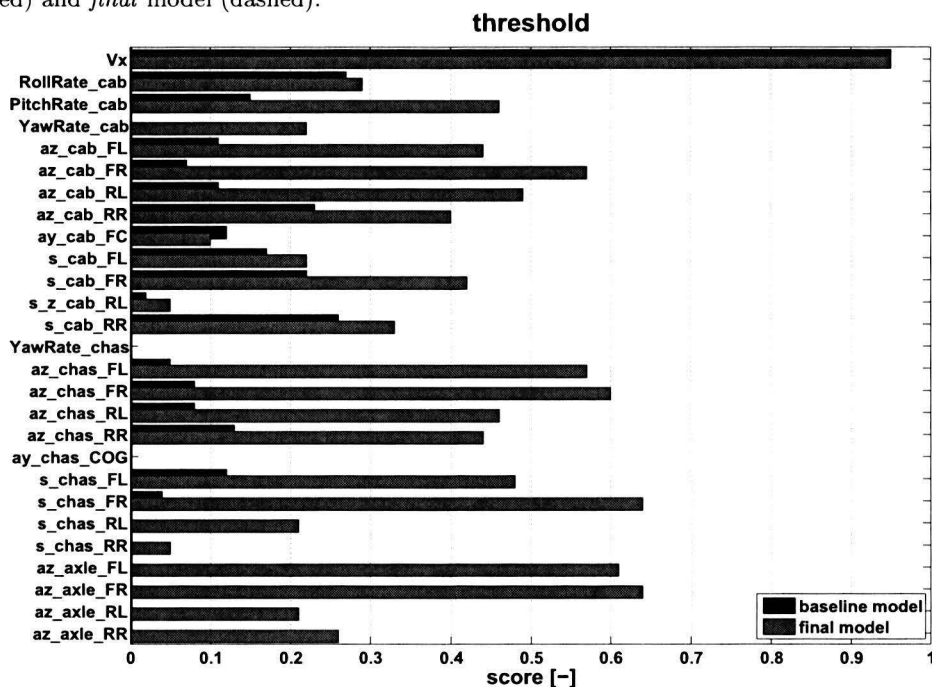


Figure 8.8: Discrete obstacle experiment (threshold). Evaluation scores, *baseline* model (black) and *final* model (gray).

Judging by the evaluation results in Figure 8.8 and the results displayed in this section it can be concluded that the model adjustments included in the *final* model show a clear improvement with respect to the *baseline* model for the majority of the observed signals. However, the improvement of the *final* model with respect to the *reference* model is less clear (Figure 8.9). Some signals are improved, others show a slight deterioration in computed scores (cabin and rear axle suspension deflections). For this type of experiment, the model adjustments discussed in chapter 6 (parameter update and tyre model) make the largest contribution to improving the model. Finally, it can be concluded that

8.2 Acceleration

the evaluation scores do not always provide an accurate reflection of the match between *Trucklab* and simulation. *Trucklab* signals with a relatively high noise level automatically result in low evaluation scores, for example the vertical acceleration signals.

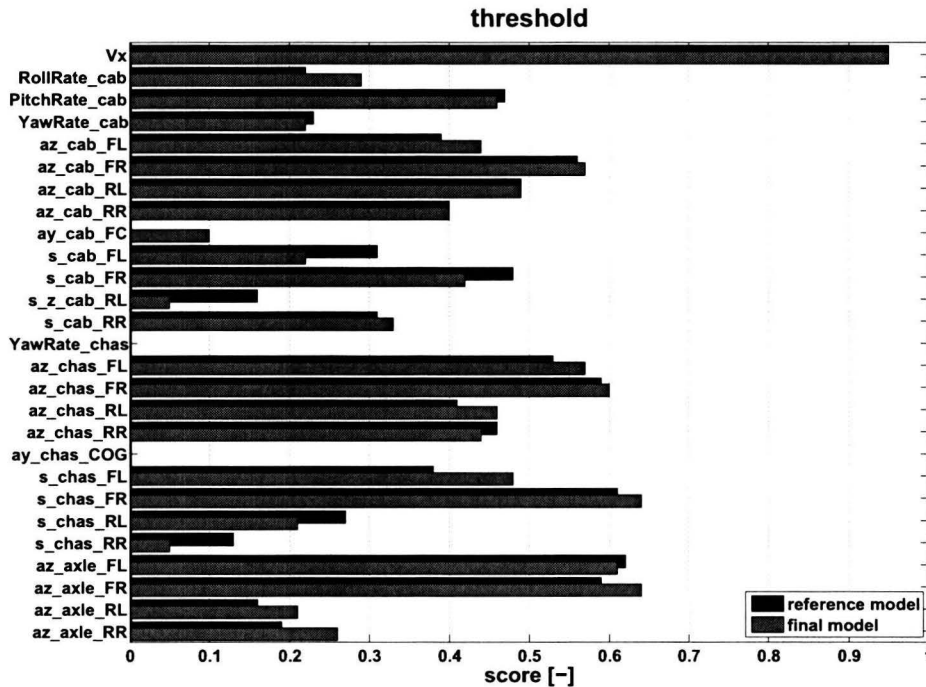


Figure 8.9: Discrete obstacle experiment (threshold). Evaluation scores, *reference* model (black) and *final* model (gray).

8.2 Acceleration

For the acceleration test the vehicle accelerates from a standstill to approximately 9 km/h in first gear. When the maximum velocity is reached the clutch pedal is pressed. This experiment is performed on a level road surface.

8.2.1 Suspension deflections

Figure 8.10 displays the axle suspension deflection for an acceleration test. It can be seen that the suspension deflection is predicted accurately both for the front and rear axle. Clearly visible is the difference in suspension deflection between the front left and right suspension struts as result of a twisting chassis due to the engine torque. Comparing the *baseline* and *final* simulation results, it is clear that the *final* model gives a far more accurate prediction of the suspension deflection than the *baseline* model. This improvement is the result of the corrected fifth wheel coupling height, discussed in section 6.3.1 and the adapted rear axle suspension of section 7.1.

The suspension deflection of the cabin (Figure 8.11) shows that there is a mismatch in cabin suspension response. The *final* model shows a larger deflection than the *Trucklab* cabin suspension. However, it is unlikely that this is caused by a mismatch of the spring stiffness, as these are originating from *Trucklab* cabin suspension measurements. It is more likely that the *Trucklab* cabin was slightly pitched backwards creating less negative travel for the front and less positive travel for the rear struts. This is supported by the conclusion with regard to the cabin suspension deflection when braking (section 8.3). Looking at the difference between the results of the *baseline* and *final* model, it can be seen that no clear improvement is achieved with regard to the cabin suspension between simulation model and the *Trucklab*.

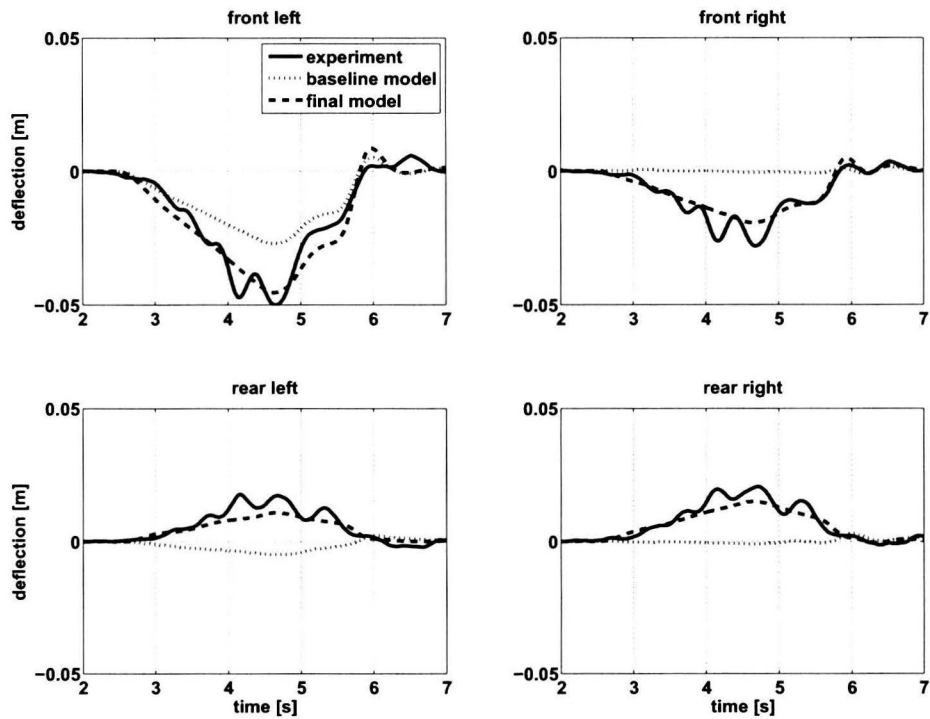


Figure 8.10: Acceleration experiment. Axle suspension deflection, *Trucklab* (solid), *baseline* model (dotted) and *final* model (dashed). Positive deflection corresponds to compression.

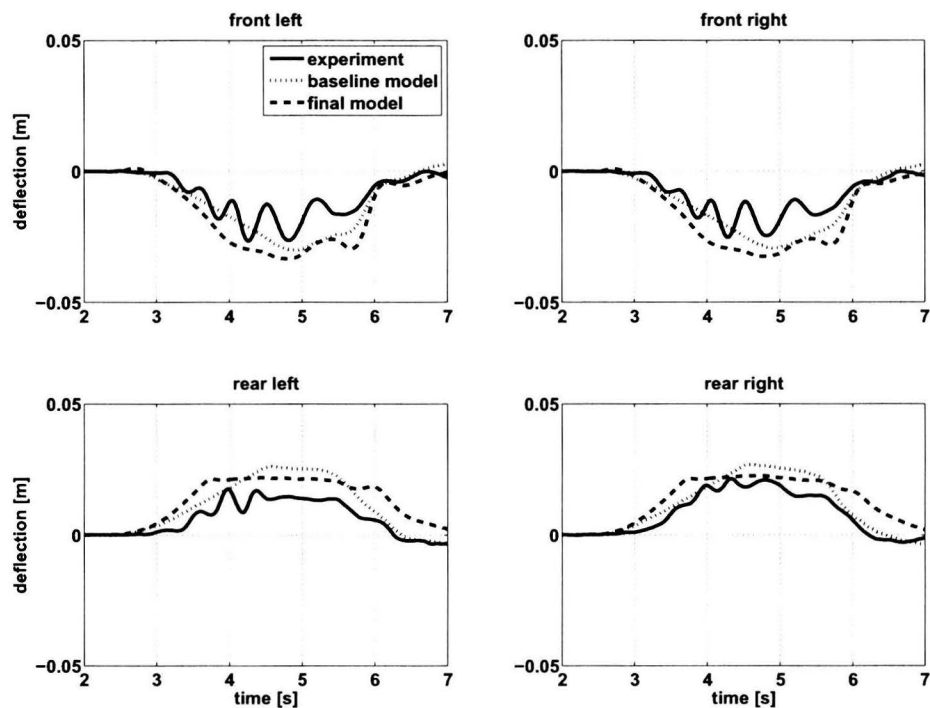


Figure 8.11: Acceleration experiment. Cabin suspension deflection, *Trucklab* (solid), *baseline* model (dotted) and *final* model (dashed). Positive deflection corresponds to compression.

8.2 Acceleration

8.2.2 Longitudinal accelerations

The longitudinal acceleration for the chassis and cabin are shown in Figure 8.12. Clearly, the *Trucklab* and simulated longitudinal accelerations are very similar both for the chassis and the cabin. Looking at the longitudinal cabin acceleration it can be seen that the results of the *final* model show a better match with the *Trucklab* than the *baseline* model. For the longitudinal chassis acceleration no clear difference between the two models is observed.

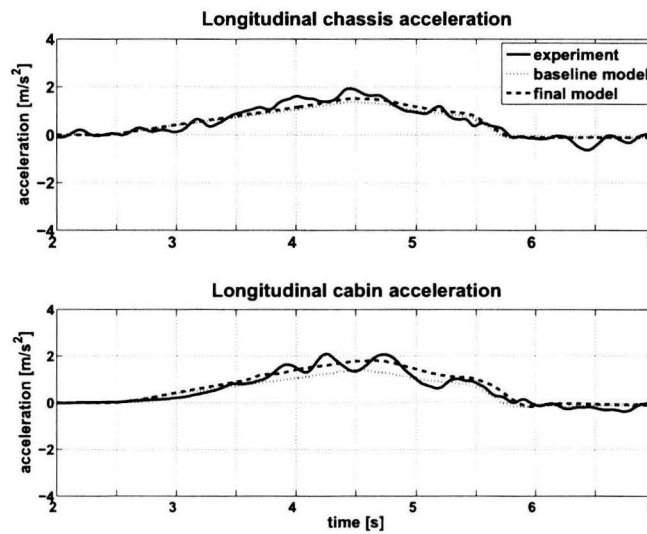


Figure 8.12: Acceleration experiment. Longitudinal chassis (top) and cabin (bottom) acceleration, *Trucklab* (solid), *baseline* model (dotted) and *final* model (dashed).

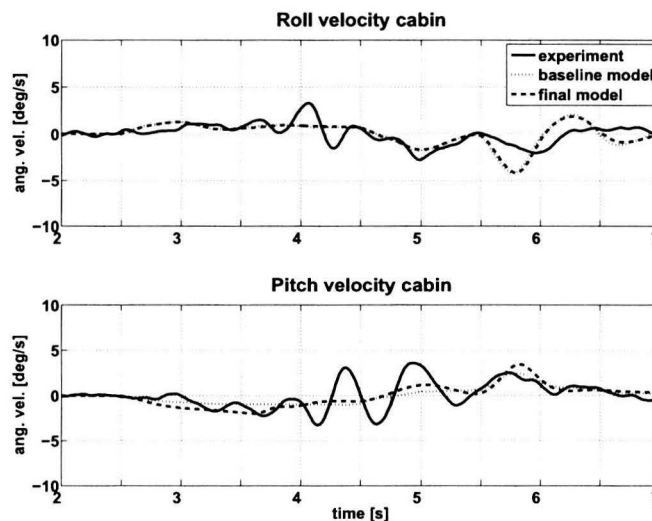


Figure 8.13: Acceleration experiment. Cabin roll (top) and pitch (bottom) velocity, *Trucklab* (solid), *baseline* model (dotted) and *final* model (dashed).

8.2.3 Angular velocities

The cabin roll and pitch velocities for the acceleration test are shown in Figure 8.13. Note that the cabin roll velocity is not included for the evaluation of the acceleration experiment (Figure 8.14) as it was initially considered to be irrelevant. However, after studying the cabin movements it appeared that the cabin makes a clear roll motion when accelerating induced by the twisting of tractor chassis

due to the engine torque. Because of that, the cabin roll velocity is included in the validation of the acceleration test. The pitch motion of the cabin is the result of the longitudinal acceleration of the vehicle.

Looking at Figure 8.13 it can be seen that main trend in pitch and roll velocities are the same for the *Trucklab* and *final* model. However, in the measured *Trucklab* pitch and roll velocities there are also a number of additional oscillations. The difference between simulated and measured cabin roll and pitch velocities are probably caused by a higher cabin damping for the *final* model. When comparing the *baseline* and *final* model it can be seen that the difference between both models is small.

8.2.4 Conclusion

Looking at the various signals observed in this section it can be concluded that the *final* simulation model gives an accurate prediction for the appearing axle suspension deflections and longitudinal chassis and cabin accelerations when accelerating from a standstill to the maximum velocity in first gear. Additional attention must be given to the cabin suspension, especially the damping of the cabin, in order to improve the match between *Trucklab* and simulation model. Performing additional *Trucklab* acceleration experiments are required for the investigation of the cabin suspension and to find out whether the original *Trucklab* measurements are correct. Examining the results displayed in this section and the evaluation scores in Figure 8.14 it can also be concluded that the model adjustments included in the *final* model result in a large improvement with respect to the *baseline* model for the axle suspension deflections.

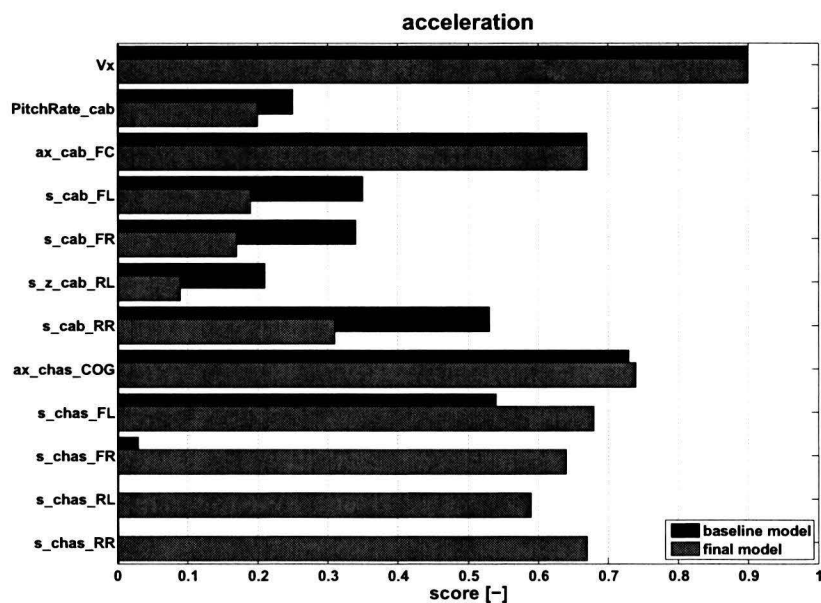


Figure 8.14: Acceleration experiment. Evaluation scores, *baseline* model (black) and *final* model (gray).

Comparing the evaluation results of Figure 8.14 and Figure 8.15, it can be seen that a large score improvement for the front axle suspension deflection is achieved with respect to the *baseline* model. Moreover, the score improvement with respect to the *reference* model is very small. This means that the largest improvement is achieved by the model adjustment discussed in section 6.3.1, the corrected fifth wheel coupling height. For the rear axle suspension deflection the score improvement with respect to the *reference* model is far larger than the improvement with respect to the *baseline* model. This means that the adapted rear axle suspension of chapter 7 makes the largest contribution to improving the primary suspension deflection when accelerating.

8.3 Braking

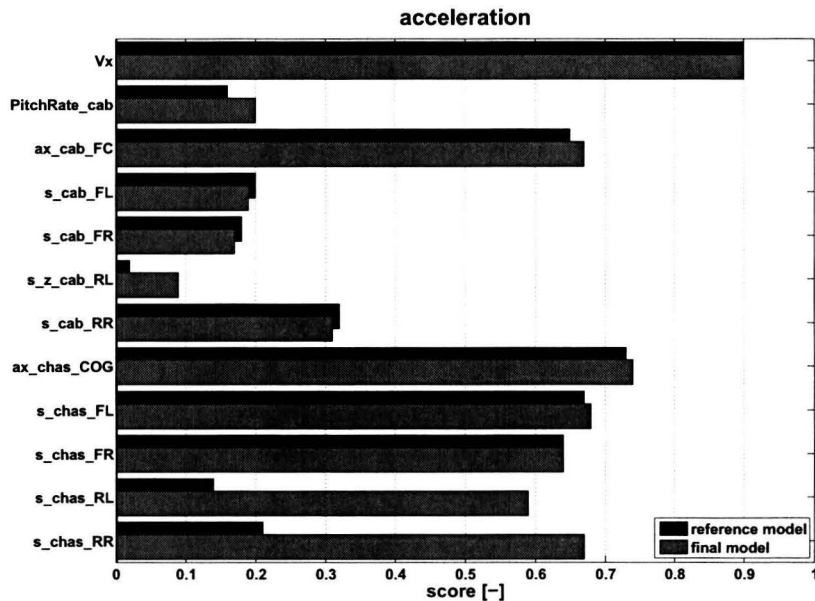


Figure 8.15: Acceleration experiment. Evaluation scores, *reference* model (black) and *final* model (gray).

8.3 Braking

The braking experiments consists of two types of braking tests: normal and heavy braking. These braking experiments are performed on a straight level road with an initial vehicle speed of 60 km/h. The difference between these two types of braking tests is the severity of braking. As heavy braking has the most severe impact on the vehicle, the braking validation is based on this test.

8.3.1 Suspension deflections

The axle suspension deflections for the front and rear tractor axle are given in Figure 8.16. The axle suspension deflection can be very accurately predicted both for the front and rear axle. However, for $t > 18$ seconds a mismatch appears between the simulation model and *Trucklab*. At the front axle this mismatch is larger than at the rear axle. This difference in front axle suspension response is caused by a phenomenon called axle wind-up. This is not included for the simulation model as this requires a leaf spring model for the front axle suspension. Moreover, a simplified friction model for the brakes and tyre deformation also contributes to this mismatch in suspension response. For the rear axle suspension response, only the simplified friction model for the brakes and the tyre deformation contribute to the mismatch.

Comparing the *baseline* and *final* model results it can be seen that a large improvement is realised with respect to the rear axle suspension deflection. The main contributors to this improvement are the corrected height of the fifth wheel coupling; the implemented rear axle suspension geometry and the adapted brake force distribution.

Figure 8.17 displays the response of the cabin suspension when braking and shows that there is a clear difference in deflection between *Trucklab* and simulation model for $t < 18$ seconds. This holds for the front and rear cabin suspension struts. A possible cause for this difference is that the *Trucklab* cabin was slightly pitched backwards creating more positive travel for the front and more negative travel for the rear struts. This agrees with the conclusion with regard to the cabin suspension deflection when accelerating (section 8.2). It is unlikely that the difference is caused by a mismatch of the spring stiffness, as these are originating from *Trucklab* cabin suspension measurements. Looking at the dif-

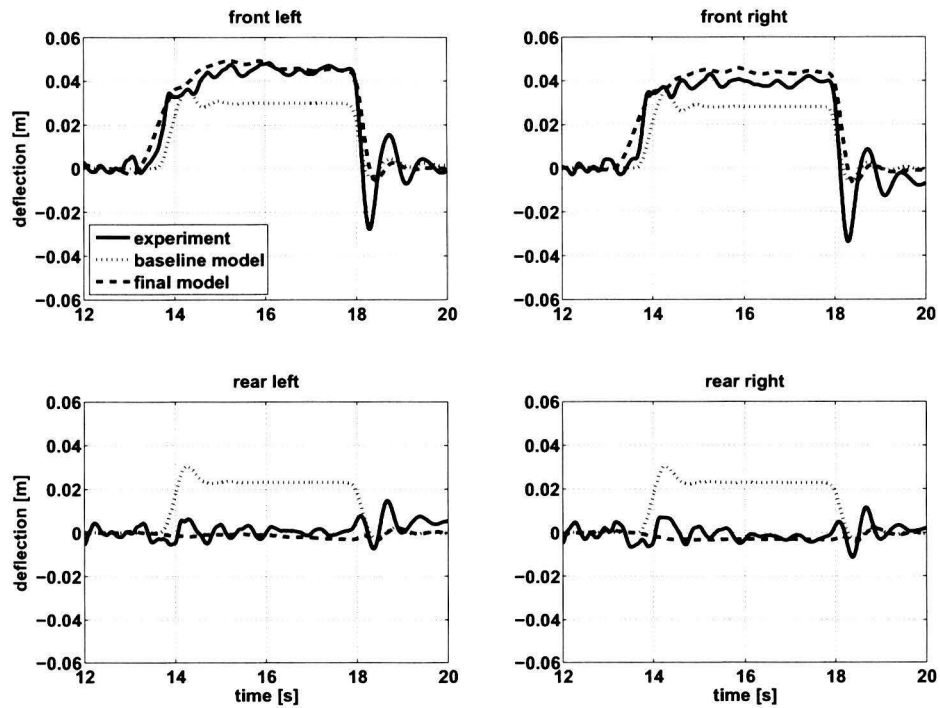


Figure 8.16: Braking experiment. Axle suspension deflection, *Trucklab* (solid), *baseline* model (dotted) and *final* model (dashed). Positive deflection corresponds to compression.

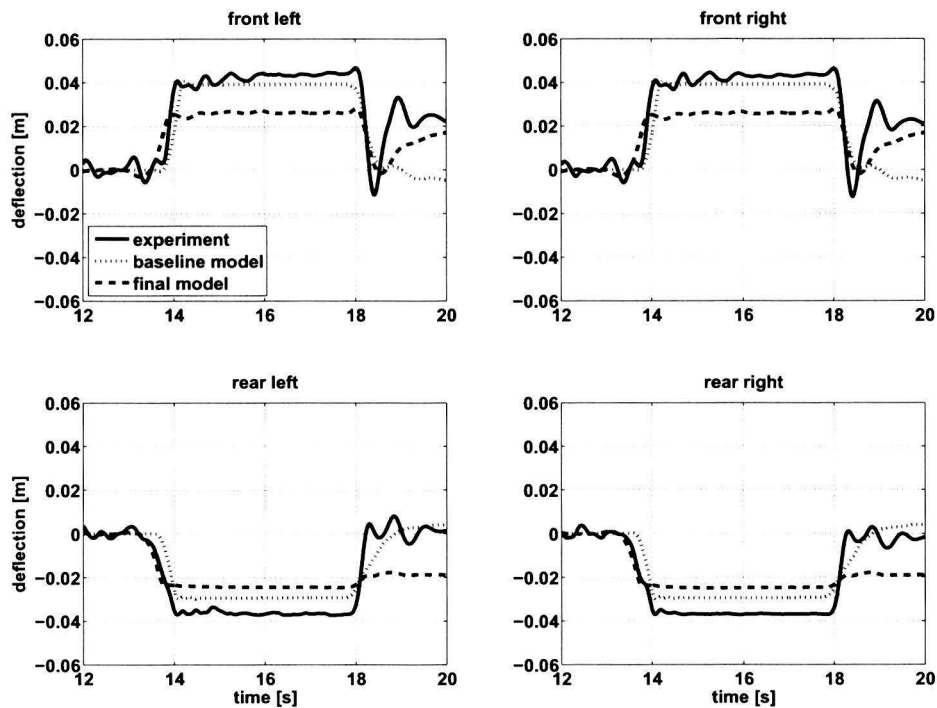


Figure 8.17: Braking experiment. Cabin suspension deflection, *Trucklab* (solid), *baseline* model (dotted) and *final* model (dashed). Positive deflection corresponds to compression.

8.3 Braking

ference between *baseline* and *final* model for $t < 18$ seconds, it can be seen that the *final* model shows a deterioration of the cabin suspension deflections. This is the result of the implemented measured spring characteristics (Figure 7.28).

For $t > 18$ seconds there is a profound difference in deflection at the rear side of the cabin. What causes this difference is still unclear. A detailed investigation of the *Trucklab* cabin suspension is necessary, as the cabin suspension response of the *final* model is as expected. For $t > 18$ seconds the *final* model front cabin suspension shows a clear improvement and the rear a deterioration with respect to the *baseline* model. This is the result of switching off the cabin suspension levelling controller and the implementation of drag force acting on the cabin.

8.3.2 Longitudinal accelerations

When comparing the *Trucklab* and simulated longitudinal accelerations at the chassis and the cabin (Figure 8.18), it can be seen that these are very similar. However, a considerable mismatch occurs at $t = 18.2$ seconds. The *Trucklab* shows relatively large acceleration spikes when the vehicle comes to a standstill. This is also the result of the phenomenon with regard to the front and rear axles when braking. This causes a small motion of the chassis in longitudinal direction.

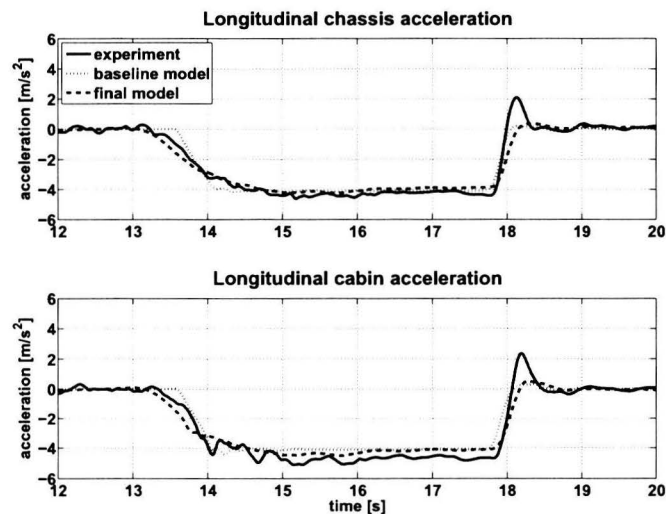


Figure 8.18: Braking experiment. Longitudinal chassis (top) and cabin (bottom) acceleration, *Trucklab* (solid), *baseline* model (dotted) and *final* model (dashed).

8.3.3 Angular velocities

The cabin pitch velocity is displayed in Figure 8.19. The pitch velocity peak at $t = 13.8$ seconds is the result of applying the brakes and the peak at $t = 18.2$ seconds is the result of coming to a standstill. For the first peak there is a small mismatch in peak values and a short time difference. The latter is the result of a small delay in the operation of the brakes between the *Trucklab* and simulation model. For the second peak the mismatch is substantially larger. This is expected given the mismatch of the longitudinal cabin acceleration at $t = 18.2$ seconds (Figure 8.18) as a result of the phenomenon with regard to the front and rear axles when braking. Looking at the difference between the two models, it can be seen that a small improvement of timing of the first peak, as a result of the adapted driver model, and a small improvement with respect to the amplitude of the second peak are achieved.

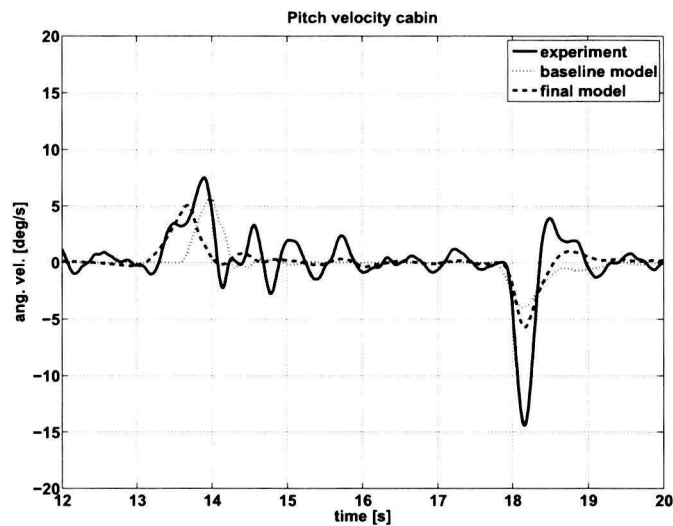


Figure 8.19: Braking experiment. Cabin pitch velocity, *Trucklab* (solid), *baseline* model (dotted) and *final* model (dashed).

8.3.4 Conclusion

Examining the results displayed in this section, it can be concluded that the *final* model is able to accurately predict the front and rear axle suspension deflections and the longitudinal chassis and cabin accelerations. A large improvement with respect to rear axle suspension deflection is achieved as a result of the adjusted rear axle suspension. However, there remains a mismatch in suspension response as soon as the vehicle comes to a standstill. In order to improve the cabin suspension deflections, additional *Trucklab* braking experiments are required for the investigation of the cabin suspension and to find out whether the original *Trucklab* measurements are correct.

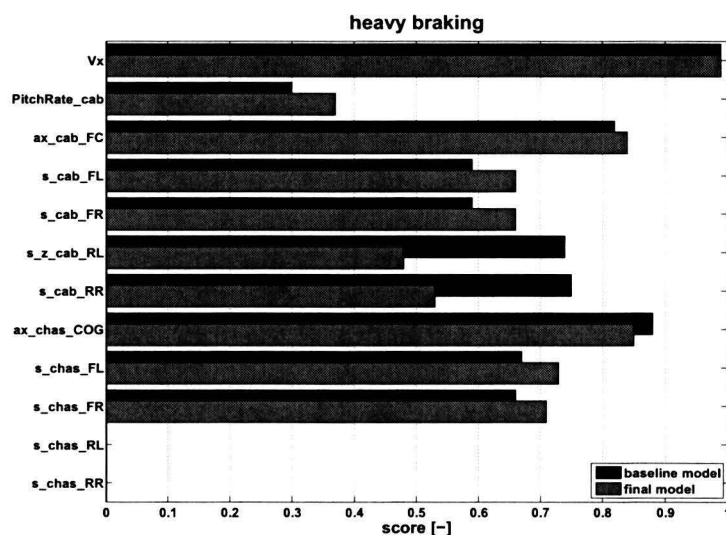


Figure 8.20: Heavy braking experiment. Evaluation scores, *baseline* model (black) and *final* model (gray).

The evaluation scores for heavy braking (figures 8.20 and 8.21) and normal braking appendices C.2 and C.3 show none or little improvement of the rear axle suspension deflections in contrast to the results of section 8.3.1. This is the result of a small oscillation of the *Trucklab* rear axle suspension that affects the evaluation score calculation badly. For the rear axle suspension deflection, the computed *weighted root mean squared error* is larger than the computed *weighted root mean square* of the *Trucklab*

8.4 Steering

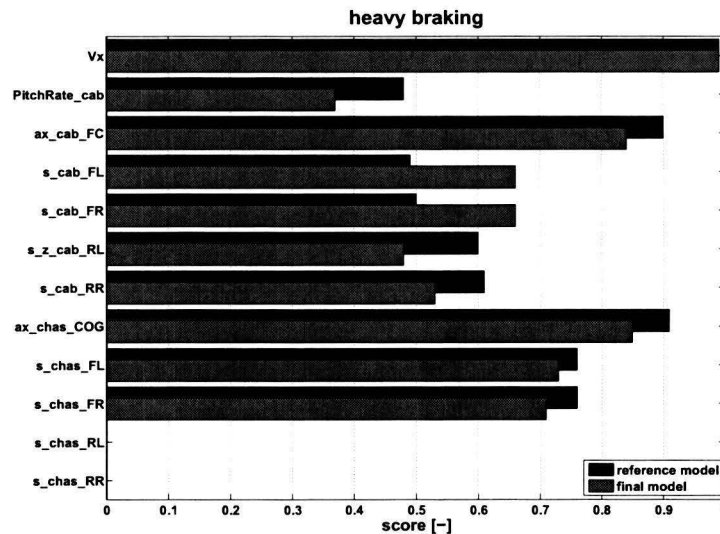


Figure 8.21: Heavy braking experiment. Evaluation scores, *reference* model (black) and *final* model (gray).

signal. This results in a computed evaluation score of 0. For this situation the adopted evaluation method is insufficient. With the exception of the rear axle suspension, the evaluation scores give an accurate representation of the match between *Trucklab* and simulation model.

8.4 Steering

The steering experiments consist of three types of steering manoeuvres: the circle test; the step steer test; and the double lane change test. As the double lane change is one of the standard tests for vehicle handling, this type of steering manoeuvre is used for the validation of the steering experiments. The double lane change test implies severe steering at which the vehicle steers to a parallel lane and subsequently back to its initial lane. This test is performed on a straight and level road.

8.4.1 Suspension deflections

As a result of the lateral accelerations when performing the double lane change test, the vehicle will roll. This roll motion of the vehicle is clearly visible in the front and rear axle suspension deflection. Figure 8.22 displays the front and rear axle suspension deflection. It can be seen that the model gives an accurate representation of the *Trucklab* suspension deflection both for the front and rear axle. Comparing the *baseline* and *final* model, a large improvement is achieved with respect to the rear axle suspension deflection. The main contributors to this improvement are the implemented rear axle suspension geometry and the updated model parameters.

In Figure 8.23 the cabin suspension deflection is given. The front side suspension struts show a relatively small deflection with respect to the rear side struts. This is the result of a stiff anti-roll bar mounted at the front side of the cabin. The main trend of the front suspension deflection accurately matches *Trucklab* and simulation model. However, the rear suspension struts show a relatively large mismatch. The rear cabin suspension shows there is more relative movement of the cabin with respect to the chassis for the *Trucklab* than for the simulation model. A possible cause for this is the torsional flexibility of the chassis. Improving the match between *Trucklab* and simulation model can be achieved by developing a flexible tractor chassis. Clearly, two rigid chassis parts interconnected by a torsional spring is not sufficient. Comparing the *baseline* and *final* model, it can be seen that the *baseline* model gives a better result, though there is a relatively large mismatch.

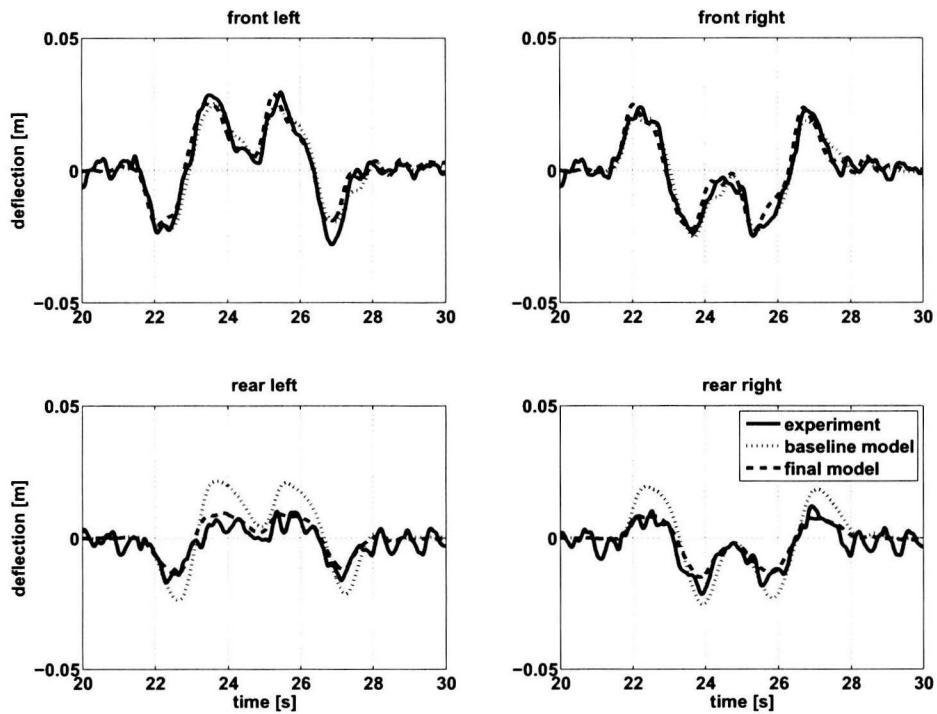


Figure 8.22: Double lane change experiment. Axle suspension deflection, *Trucklab* (solid), *baseline* model (dotted) and *final* model (dashed). Positive deflection corresponds to compression.

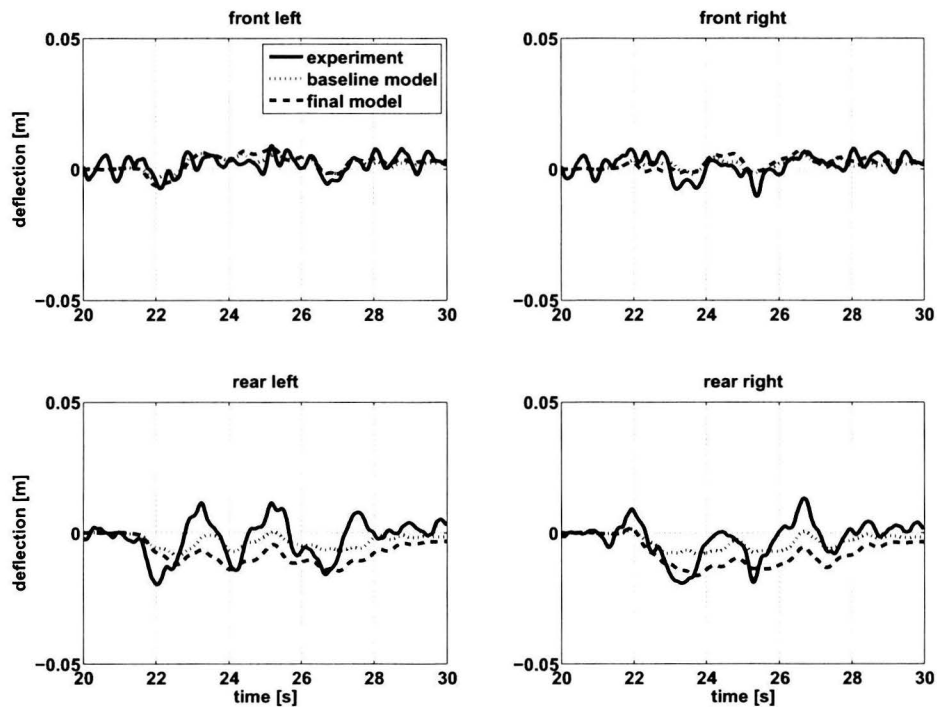


Figure 8.23: Double lane change experiment. Cabin suspension deflection, *Trucklab* (solid), *baseline* model (dotted) and *final* model (dashed). Positive deflection corresponds to compression.

8.4.2 Lateral accelerations

The execution of the double lane change manoeuvre results in high lateral accelerations. The lateral chassis (top) and cabin (bottom) accelerations are given in Figure 8.24. Clearly, the lateral accelerations of the *final* model show an accurate match with the *Trucklab* both for chassis and cabin. Comparing the results of both simulation models shows that the *final* model is more accurate. The main contributor to the achieved improvement is the combination of steering arm, steering rod, pitman arm, steering box and bump steer compensation rods.

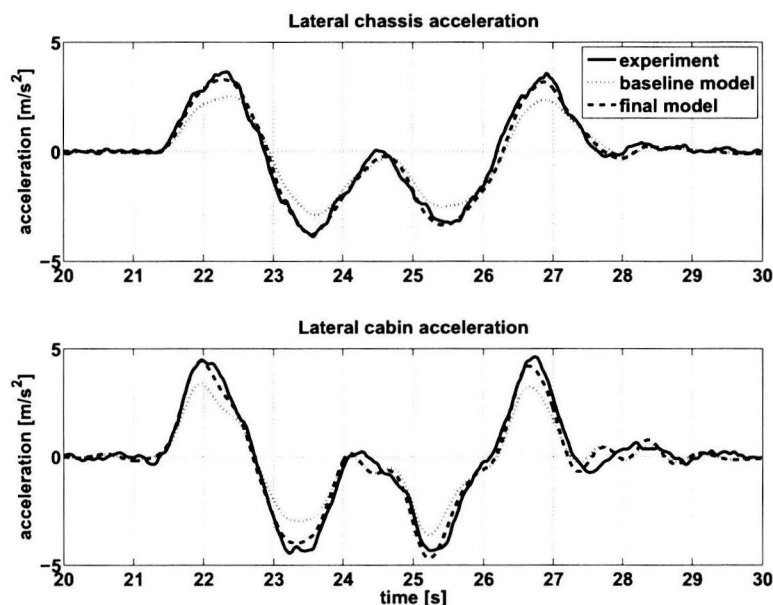


Figure 8.24: Double lane change experiment. Longitudinal chassis (top) and cabin (bottom) acceleration, *Trucklab* (solid), *baseline* model (dotted) and *final* model (dashed).

8.4.3 Angular velocities

As stated before, the vehicle will roll as a result of the lateral accelerations. The cabin roll velocity is displayed in the top graph of Figure 8.25. The match between *Trucklab* and *final* model is accurate; however, there remain small differences in peak values. A possible cause for these small differences is a relatively high cabin roll damping for the *final* model. The improvement of the *final* model with respect to the *baseline* model is small.

The centre and bottom graph of Figure 8.25 display the cabin and chassis yaw velocities respectively. As can be seen, the simulation model gives a very accurate representation of the *Trucklab* for the cabin and chassis yaw velocities. Like the cabin roll velocity, there is no clear difference between the two simulation models.

8.4.4 Conclusion

As a result of the double lane change validation it can be concluded that the *final* model gives an accurate representation of the *Trucklab* with respect to the front and rear axle suspension deflections; the lateral cabin and chassis accelerations; and angular velocities of cabin and chassis. Improvements are achieved with respect to rear axle suspension deflection and lateral cabin and chassis accelerations according to the results displayed in this section as well as the evaluation results in Figure 8.26. Comparing the evaluation scores of figures 8.26 and 8.27 for the rear axle suspension deflections, it shows that the improvement is mostly the result of the model adjustments discussed in chapter 6 (updating model parameters). Further study of the cabin suspension is required with respect to the deflection

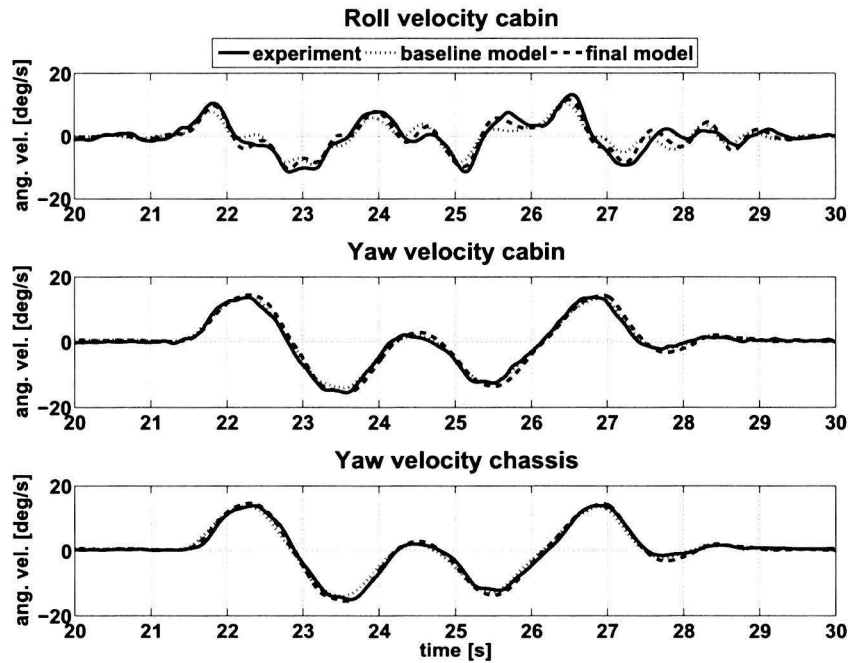


Figure 8.25: Double lane change experiment. Cabin roll (top), cabin yaw (mid) and chassis yaw (bottom) velocities, *Trucklab* (solid), *baseline model* (dotted) and *final model* (dashed).

at the rear side of the cabin. Developing a flexible tractor chassis for the simulation model may result in a better match. Comparing the results of this section with the computed evaluation scores, it can be concluded that the scores give an accurate representation of the match between *Trucklab* and simulation model.

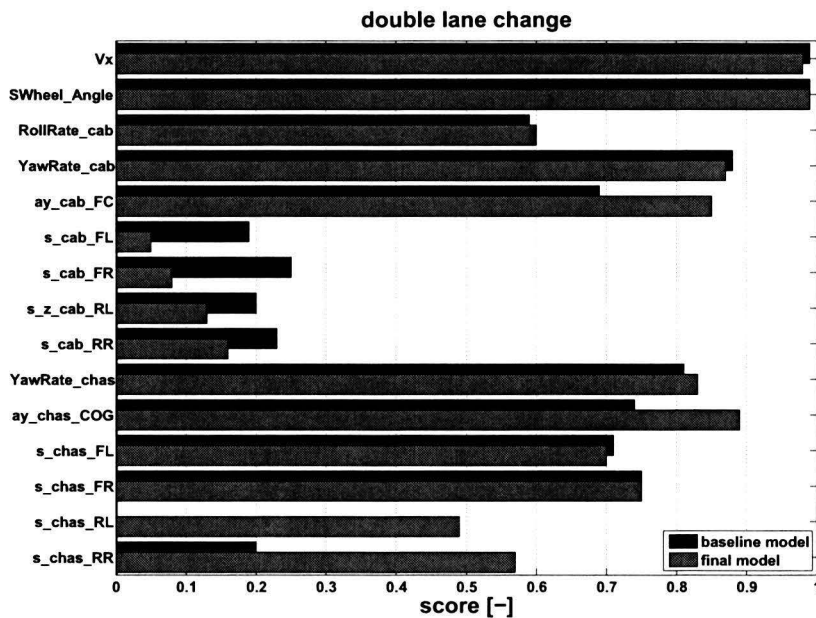


Figure 8.26: Double lane change experiment. Evaluation scores, *baseline model* (black) and *final model* (gray).

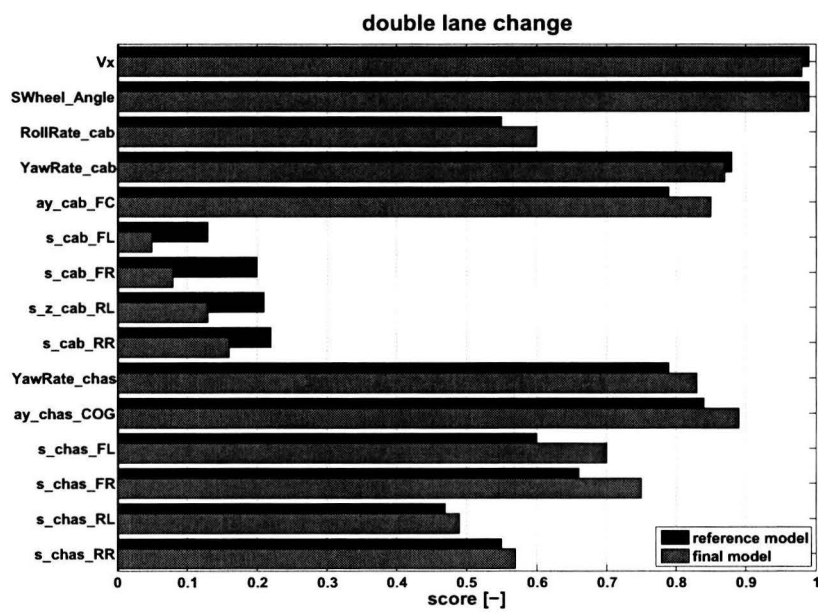


Figure 8.27: Double lane change experiment. Evaluation scores, *reference model* (black) and *final model* (gray).

Chapter 9

Conclusions and recommendations

Prior to this master's thesis, *TNO Automotive* in association with the *Eindhoven University of Technology* and *DAF Trucks* initiated a project for the development of a three-dimensional tractor semi-trailer multibody simulation model. In July 2006 the first version of this tractor semi-trailer multibody simulation model has been completed. Next, a wide variety of experiments are performed using a specially prepared tractor semi-trailer test vehicle. These experiments have been performed on a proving ground and consist of acceleration, braking and different steering tests. Furthermore, riding over different road surfaces and obstacles are also part of the performed experiments. Having a large amount of test vehicle data and simulation model which has not been validated, the main problem of this master's thesis can be defined as:

"The validation and improvement of a three-dimensional tractor semi-trailer simulation model that is capable of accurately predicting dynamic vehicle behaviour."

Within the problem statement of this master's thesis, the following main objectives are formulated:

- Evaluation of the *baseline* model using test truck data;
- Analysis of the simulation results and improving the model;
- Validation of the modified model.

Moreover, the following sub-objectives are defined:

- Development of a model evaluation methodology;
- Formulation of a model evaluation algorithm.

This chapter presents the main conclusions with regard to this master's thesis. In addition, some recommendations with regard to future work are formulated.

9.1 Conclusions

The conclusions are split into four parts. The first part comprehends the implemented adjustments to improve the model. The second part encompasses the validation of the *final* simulation model. The third part deals with the adopted model evaluation methodology and the fourth and last part is the main conclusion.

9.1.1 Model adjustments

After close examination of the evaluation results and additional time-domain graphs for the *baseline* model, it is concluded that the *baseline* model can be improved on certain aspects in order to obtain an accurate match with the *Trucklab* when subjected to the different types experiments. The first adjustments consists of updating the model parameters, eliminating modelling errors and implementation of the *MF-Swift* tyre model. Moreover, the standard *SimMechanics* acceleration sensor for measuring longitudinal and lateral accelerations is modified and the driver model is adjusted. After evaluating the adapted simulation model it can be concluded that this model gives a more accurate match with respect to the vertical axle, chassis and cabin accelerations. In addition, the primary and cabin suspension deflections show also some improvement. Still, a considerable mismatches between *Trucklab* and simulation model are observed for the rear axle suspension deflections and cabin suspension deflections. For further improvement the following adjustments are made:

- *Rear axle suspension*

The *Trucklab* rear axle suspension is measured and implemented in the simulation model. With this suspension geometry an *anti-rise* effect when braking and an *anti-squab* effect when accelerating are introduced for the rear axle suspension. Moreover, it also introduces a small amount of roll steer when cornering. This adjustment clearly improves the rear axle suspension deflection when braking and accelerating.

- *Brake system*

A brake system with variable brake force distribution is implemented. This system is based on the differential slip between the various axles where each wheel generates equal wheel slip. With this brake system the simulation model meets the legal requirements with regard to commercial vehicle braking. The system can be used for different loading conditions and vehicle configurations. This adjusted brake system affect the weight transfer and therefore the suspension deflection. This brake system result in a better match with the *Trucklab* regarding the primary suspension deflection when braking.

- *Steering system*

The *Trucklab* steering geometry is measured and implemented. With this adjustment the "Ackerman" geometry is closely approximated. The implemented geometry introduces a small amount of front axle roll steer when cornering and eliminates the bump steer effect. However, it also affects the front axle suspension deflection because of the bump steer compensation rods. This adjusted steering system results in more accurate wheel steer angles and in a better match with regard to the lateral chassis acceleration and yaw velocity for a steering manoeuvre. This is the result of a more accurate steer ratio.

- *Cabin suspension*

The adjustments with respect to the cabin suspension are: the implementation of the measured spring-damper characteristics; the addition of the anti-roll bar geometry; the introduction of the aero dynamic drag force acting on the cabin; and switching off the cabin levelling control as soon as the cabin is levelled.

The two adjustments mentioned last, improve the front side cabin suspension deflection after the vehicle has come to a standstill. The effect on the deflections at the rear of the cabin remain unclear as it is most likely that the *Trucklab* rear cabin suspension has a defect when braking. During the braking manoeuvre itself no clear suspension deflection improvement is observed. A mismatch between *Trucklab* and simulation remains, which is most likely to be caused by an incorrectly levelled *Trucklab* cabin. The combination of the aerodynamic drag force with the switched off cabin levelling control results in an improved cabin suspension deflection when braking. The implementation of the anti-roll bar geometry and measured spring/damper characteristics show no large improvement with respect to the suspension response. There remains a considerable mismatch between simulation model and *Trucklab*.

9.1 Conclusions

9.1.2 Validation of the final simulation model

The following conclusions are drawn with regard to the validation of the *final* model.

Discrete obstacles

The final model gives an accurate prediction for the appearing vertical accelerations and primary suspension deflection when riding over a discrete obstacle. The cabin suspension deflections and cabin yaw velocity are simulated quite accurately; however, the match between *Trucklab* and simulation can still be improved. A considerable mismatch remains for the lateral acceleration, pitch and roll velocities of the cabin. Comparing the *baseline* and *final* model it can also be concluded that considerable improvements are achieved for the vertical accelerations and primary suspension deflections.

Acceleration

It can be concluded for the acceleration experiment that the *final* model gives an accurate prediction for the appearing axle suspension deflections and longitudinal chassis and cabin accelerations. A large improvement with respect to the primary suspension deflection is achieved. The cabin suspension deflection, roll and pitch velocities are not sufficiently accurate, therefore further research with regard to the cabin suspension is required.

Braking

When performing a braking manoeuvre it can be concluded that the *final* model is able to predict the front and rear axle suspension deflections and the longitudinal chassis and cabin accelerations very accurately. A large improvement with respect to the rear axle suspension deflection is achieved as a result of the adjusted rear axle suspension. However, there remains a mismatch between the *Trucklab* and simulated cabin suspension response. The cabin suspension deflection and pitch velocity are not sufficiently accurate, therefore further research with regard to the cabin suspension and axle suspension (axle wind-up) is required.

Steering

The results of the steering experiments show that the *final* model gives an accurate representation of the *Trucklab* with respect to the front and rear axle suspension deflection; the lateral cabin and chassis accelerations; and angular velocities of cabin and chassis. Clear improvements are achieved with respect to rear axle suspension deflection and lateral cabin and chassis accelerations. However, the rear cabin suspension deflections are still not very accurate for the *final* model. Improving the rear cabin suspension deflections can be achieved by developing a flexible tractor chassis.

9.1.3 Evaluation methodology

Concerning the model evaluation methodology it is concluded that for the majority of the evaluated signals, the calculated evaluation scores give an accurate representation of the match between *Trucklab* and simulation model. However, for a few evaluated signals the computed score is not accurate (rear axle suspension deflection when braking). For this situation the computed *weighted root mean squared error* value and *weighted root mean square* value of the measured signal have approximately the same magnitude; furthermore, when these values are also very small, this can result in evaluation scores which do not give a good indication of the match.

9.1.4 Main conclusion

Considering the problem statement of this master's thesis, it is concluded that the *final* model represents the dynamic vehicle behaviour fairly accurately for the considered tractor semi-trailer combination. Considerable improvements are achieved concerning the primary suspension deflections; the vertical accelerations; and the lateral cabin and chassis accelerations with regard to the *baseline* model. However, there is still room for further improvement of the cabin suspension. Considering the objectives of this master's thesis, it is concluded that not every objective is completely achieved, as the

simulation model has not been validated for riding over different types of road surfaces in order to restrict the amount of work.

9.2 Recommendations

In this section the recommendations are presented with respect to future work and further improvement of the simulation model. In addition, some recommendations concerning the execution of future validation experiments with the *Trucklab* are presented.

Simulation model

Concerning the simulation model it is recommended to:

- Adjust the cabin levelling controller of the *final* model by switching it off as soon as the brakes are applied. By doing so, the cabin levelling control is only switched off for braking experiments and prevents peculiar cabin suspension response for other experiments.
- Consider the implementation of a flexible tractor chassis. Clearly, two rigid chassis bodies interconnected by a torsional spring is not sufficient for achieving accurately matched cabin suspension deflections at the rear when steering.
- Perform additional *Trucklab* braking and acceleration experiments to determine whether the *Trucklab* cabin suspension at the rear has a defect. Furthermore, these experiments can also be used to determine whether the cabin is levelled correctly before braking and accelerating.
- Consider modelling a leaf spring for the front axle suspension. This contributes to achieve a more accurate suspension response after the vehicle comes to a standstill when performing a braking manoeuvre. Adding a leaf spring to the front axle also results in a more accurate way for compensating the bump steer effect than the bump steer compensation rods in combination with vertical springs.
- Improve the brakes by using a more accurate friction model (LuGre). This also contributes to achieve a more accurate suspension response after the vehicle comes to a standstill.
- Validate the simulation model for riding on different road surfaces and determine the accuracy of the model.
- Include a detailed drive line model for more realistic acceleration experiments.

Performing validation experiments with the *Trucklab*

For future experiments, it is also recommended to:

- Perform the braking and the acceleration experiments with and without the fully loaded and empty semi-trailer. This provides more information on the effect of a fully loaded and empty semi-trailer on the dynamic vehicle behaviour of the tractor.
- Make sure that the *Trucklab* cabin is levelled correctly before performing an experiment. Determine the height between chassis and cabin at the front and rear when the cabin is levelled correctly; furthermore, measure the length of the *Trucklab* spring-damper elements when the cabin is levelled and the length when these elements touch the bump stops. This yields the maximum positive and negative deflection from the levelled position before touching the bump stops.
- Do not reset the cabin suspension deflection signals, as this results in losing useful information of the cabin position.

9.2 Recommendations

- Include a considerable amount of idle-time in the measurements before performing an experiment. This time is required for the simulation model to initiate when measured inputs are used.
- Add the throttle position and the brake pressure inside the brakes to the measurements. This gives valuable information on the exact time of applying the brakes or throttle.

Evaluation method

Concerning the adopted evaluation method it is recommended to revise the score computation (5.8) for the suspension deflections by replacing the \bar{g}_{rms} with the maximum suspension deflection of the concerning suspension strut. This may result in a better indication of the match between *Trucklab* and simulated signals.

General recommendations

As this Master's thesis proves that fairly accurate dynamic vehicle behaviour is achieved with a multi-body simulation model, it is recommended to investigate the applicability of multibody simulation models for simulating dynamic behaviour of passenger cars, busses and heavy industrial vehicles.

For *The MathWorks* company it is recommended to improve the standard *SimMechanics* visualisation environment, as a proper visualisation environment is a practical tool in preventing and detecting modelling errors.

Bibliography

- [1] D.S. Bae and E.J. Haug. "A Recursive Formulation for Real-Time Dynamic Simulation". Proceedings of the 1988 ASME Design Automation Conference, 1988. p. 499 - 508.
- [2] O. Balci. "Validation, Verification, and Testing Techniques Throughout the Life Cycle of a Simulation Study", volume 53. Annals of Operations Research, 1994. p. 121 - 173.
- [3] O. Balci. "Principles and techniques of simulation validation, verification, and testing". Proceedings of the 1995 Winter Simulation Conference, 1995. p. 147 - 154.
- [4] J.S. Bendat and A.G. Piersol. "RANDOM DATA: Analysis and measurement procedures". John Wiley & Sons, Inc., 1971. ISBN: 0-471-06470-X.
- [5] I.J.M. Besselink. "Advanced Vehicle Dynamics lecture notes". Eindhoven University of Technology, 2005.
- [6] I.J.M. Besselink. "Third exercise Advanced Vehicle Dynamics: Tractor semi-trailer optimal brake force distribution". Eindhoven University of Technology, 2006.
- [7] I.J.M. Besselink. "Vehicle dynamics analysis using SimMechanics and TNO Delft-Tyre". MATLAB IAC Conference, 2006.
- [8] B. Breurer and K.H. Bill. "Bremsenhandbuch, Grundlagen, Komponenten, Systeme, Fahrdynamik". Friedr. Vieweg & Sohn Verlag/GWV Fachverlage GmbH, 2003. ISBN: 3-528-13952-8.
- [9] J.S. Carson. "Model verification and validation". Proceedings of the 2002 Winter Simulation Conference, 2002. p. 52 - 58.
- [10] P.B. Checkland. "Systems Thinking, Systems Practice". J. Wiley, 1981. ISBN: 9780471279112.
- [11] J.P. Chrstos. "A Simplified Method for the Measurement of Composite Suspension Parameters". Number 910232. Society of Automotive Engineers (SAE) Technical Papers, 1991.
- [12] J.C. Dixon. "Tyres, suspension and handling". Cambridge University Press, 1991. ISBN: 0 521 40194 1.
- [13] Schlesinger et al. "Terminology for Model credibility", volume 32. Simulation, March 1979. p. 103 - 104.
- [14] T.D. Gillespie. "Fundamentals of vehicle dynamics". Society of Automotive Engineers, Inc., 1992. ISBN: 1-56091-199-9.
- [15] E.J. Haug. "High Speed Multibody Dynamic Simulations and its Impact on Man-Machine Systems". Advanced Multibody System Dynamics, 1993. p. 1 - 18.
- [16] E.J. Haug and R. Deyo. "Real-Time Intergration Methods for Mechanical System Simulation", volume F69. NATO ASI Series, 1990.
- [17] H. Heisler. "Advanced Vehicle Technology". Edward Arnold, 1989. ISBN: 0 7131 3660 X.

- [18] R. Limpert. *"Brake Design and Safety"*. Society of Automotive Engineers, Inc., 1999. ISBN: 1-56091-915-9.
- [19] W.F. Milliken and D.L. Milliken. *"Chassis Design, Principles and Analysis"*. Professional Engineering Publishing Limited, 2002. ISBN: 1 86058 389 X.
- [20] United Nations. *"Uniform provisions concerning the approval of vehicles of categories M, N and O with regard to braking"*. 2004.
- [21] DAF Trucks N.V. <http://www.daf.nl>, 2007.
- [22] H.B. Pacejka. *"Tyre and vehicle dynamics"*. Butterworth-Heinemann, 2002. ISBN: 0 7506 5141 5.
- [23] J. Reimpell. *"Fahrwerktechnik: Lenkung"*. Vogel-Buchverslag, 1984. ISBN: 3-8023-0739-9.
- [24] S. Robinson. *"Simulation model verification and validation: Increasing the users' confidence"*. Proceedings of the 1997 Winter Simulation Conference, 1997. p. 53 - 59.
- [25] R.G. Sargent. *"An assessment procedure and a set of criteria for use in the evaluation of computerized models and computer-based modeling tools"*. 1981. p. 104 - 114.
- [26] R.G. Sargent. *"A Tutorial on validation and verification of simulation models"*. Proceedings of the 1988 Winter Simulation Conference, 1988. p. 33 - 39.
- [27] R.G. Sargent. *"Verification and validation of simulation models"*. Proceedings of the 2005 Winter Simulation Conference, 2005. p. 130 - 143.
- [28] B.A. Suresh and B.J. Gilmore. *"Vehicle model Complexity How Much is Too Much"*. Number 940656. Society of Automotive Engineers (SAE) Technical Papers, 1994.
- [29] Centraal Bureau voor de Statistiek. <http://www.cbs.nl>, 2007.

Appendix A

Trucklab and simulation model sensors and signals

A.1 *Trucklab* sensor position

Table A.1 contains the measured *Trucklab* sensor positions. The positions are defined with respect to the coordinate system of Figure A.1.

Table A.1: Sensor positions

Sensor definition	sensor signals	position*
Angular velocity cabin	(Roll/Pitch/Yaw)Rate_cab)	[5.35 0.00 1.89]
Acceleration cabin	(ax/ay/az)_cab_FC	[5.35 0.00 1.89]
Vertical acceleration cabin	az_cab_FL	[5.82 0.59 1.37]
	az_cab_FR	[5.82 -0.59 1.37]
	az_cab_RL	[3.81 0.65 1.33]
	az_cab_RR	[3.81 -0.65 1.33]
Cabin suspension deflection	s_cab_FL	[5.76 0.67 1.06]
	s_cab_FR	[5.80 -0.77 1.02]
	s_z_cab_RL	[3.77 0.43 1.14]
	s_cab_RR	[3.77 -0.43 1.14]
Horizontal cabin deflection	s_y_cab_RL	[3.77 0.43 1.30]
Vertical acceleration chassis	az_chas_FL	[5.44 0.47 0.81]
	az_chas_FR	[5.44 -0.47 0.77]
	az_chas_RL	[3.81 0.43 0.97]
	az_chas_RR	[3.81 -0.43 0.97]
Angular velocity chassis	YawRate_chas	[2.51 -0.15 0.95]
Acceleration chassis	(ax/ay/az)_chas_COG	[2.69 0.00 0.95]
Axle suspension deflection	s_chas_FL	[4.89 0.47 0.73]
	s_chas_FR	[4.89 -0.47 0.73]
	s_chas_RL	[0.53 0.40 0.93]
	s_chas_RR	[0.53 -0.40 0.93]
Vertical acceleration axle	az_axle_FL	[4.64 0.51 0.40]
	az_axle_FR	[4.64 -0.51 0.40]
	az_axle_RL	[0.84 0.52 0.68]
	az_axle_RR	[0.84 -0.52 0.68]

* the sensor positions are defined with respect to the coordinate system of Figure A.1.

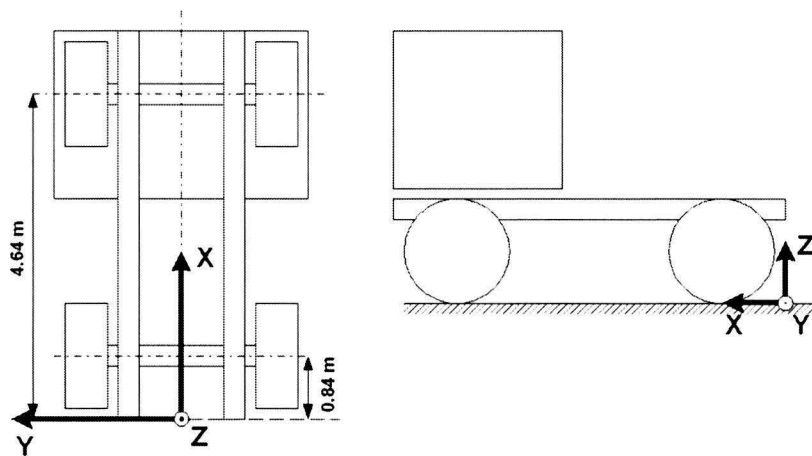


Figure A.1: Axis system for measuring *Trucklab* sensors.

A.2 Experimental test filename definition

Table A.2 contains the first two characters of a experimental *Trucklab* data file with its corresponding experimental test name.

Table A.2: Experimental test filenames.

first characters of filename	experimental test
1A	undulating asphalt
1B	concrete slabs
1C	brick road
1D	cobblestones
1E	smooth asphalt
2A	pyramid
2B	step down
2C	threshold
3A	acceleration level
3B	acceleration slope
3C	normal braking
3D	heavy braking
4A	circle
4B	double lane change
4C	step steer

A.3 Sensor signal names for *Trucklab* and simulation model

A.3 Sensor signal names for *Trucklab* and simulation model

Tabel A.3 contains the definitions of the *Trucklab* sensor signals and their corresponding simulation model counterparts.

Table A.3: Sensor signal names for *Trucklab* and simulation model.

signal definition	Trucklab signal	simulation signal
time	t	s.time
forward velocity	Vx	s.Vx
roll velocity cabin	RollRate_cab	s.cabin.angvel(:,1)
pitch velocity cabin	PitchRate_cab	s.cabin.angvel(:,2)
yaw velocity cabin	YawRate_cab	s.cabin.angvel(:,3)
yaw velocity chassis	YawRate_cab	s.chassis.yawvel(:,1)
susp. defl. axle front left	s_chas_FL	s.axle.damper.displ(:,1)
susp. defl. axle front right	s_chas_FR	s.axle.damper.displ(:,2)
susp. defl. axle rear left	s_chas_RL	s.axle.damper.displ(:,3)
susp. defl. axle rear right	s_chas_RR	s.axle.damper.displ(:,4)
susp. defl. cabin front left	s_cab_FL	s.cabin.defl(:,1)
susp. defl. cabin front right	s_cab_FR	s.cabin.defl(:,2)
susp. defl. cabin rear left	s_z_cab_RL	s.cabin.defl(:,3)
susp. defl. cabin rear right	s_chas_RR	s.cabin.defl(:,4)
vertical acc. axle front left	az_axle_FL	s.frontaxle.acc(:,3)
vertical acc. axle front right	az_axle_FR	s.frontaxle.acc(:,6)
vertical acc. axle rear left	az_axle_RL	s.rearaxle.acc(:,3)
vertical acc. axle rear right	az_axle_RR	s.rearaxle.acc(:,6)
vertical acc. chassis front left	az_chas_FL	s.cabin.chassis.acc(:,3)
vertical acc. chassis front right	az_chas_FR	s.cabin.chassis.acc(:,6)
vertical acc. chassis rear left	az_chas_RL	s.cabin.chassis.acc(:,9)
vertical acc. chassis rear right	az_chas_RR	s.cabin.chassis.acc(:,12)
longitudinal acc. chassis (C.O.G)	ax_chas_COG	s.chassis.acc(:,1)
lateral acc. chassis (C.O.G)	ay_chas_COG	s.chassis.acc(:,2)
vertical acc. chassis (C.O.G.)	az_chas_COG	s.chassis.acc(:,3)
vertical acc. cabin front left	az_cab_FL	s.cabin.corner.acc(:,3)
vertical acc. cabin front right	az_cab_FR	s.cabin.corner.acc(:,6)
vertical acc. cabin rear left	az_cab_RL	s.cabin.corner.acc(:,9)
vertical acc. cabin rear right	az_cab_RR	s.cabin.corner.acc(:,12)
longitudinal acc. cabin front centre	ax_cab_FC	s.cabin.acc(:,1)
lateral acc. cabin front centre	ay_cab_FC	s.cabin.acc(:,2)
vertical acc. cabin front centre	az_cab_FC	s.cabin.acc(:,3)

Appendix B

Evaluation data

B.1 Dominant vehicle modes

Table B.1 contains the dominant symmetric and anti-symmetric vehicle modes for a solo 4×2 tractor configuration according to [5].

Table B.1: Dominant vehicle modes. [5]

Dominant vehicle modes		
mode definition	frequency [Hz]	
Symmetric	Cabin pitch	0.9
	Cabin + chassis bounce	1.0
	Chassis and trailer bounce	1.3
	Trailer bounce	1.5
	Cabin - chassis bounce	2.5
	Engine pitch	7.5
	Front axle bounce	10
	Rear axle bounce	11
	Engine bounce	10
Anti-symmetric	Vehicle roll	1.0
	1 st chassis + trailer torsion	1.8
	Cabin yaw	4.5
	Lateral frame bending	8
	Front axle roll	10
	Engine yaw	12
	Rear axle roll	13

B.2 Evaluation signals

In Table B.2 the evaluated signals for the different experiments are given. For each type of experiment solely the relevant signals are evaluated.

Table B.2: Signals used for evaluation.

signal	pyramid step down threshold	acceleration normal braking heavy braking	circle double lane change step steer
t	•	•	•
Vx	•	•	•
SWheel_Angle			•
RollRate_cab	•		•
PitchRate_cab	•	•	
YawRate_cab	•		•
az_cab_FL	•		
az_cab_FR	•		
az_cab_RL	•		
az_cab_RR	•		
ax_cab_FC		•	
ay_cab_FC	•		•
s_cab_FL	•	•	•
s_cab_FR	•	•	•
s_z_cab_RL	•	•	•
s_cab_RR	•	•	•
YawRate_chas	•		•
az_chas_FL	•		
az_chas_FR	•		
az_chas_RL	•		
az_chas_RR	•		
ax_chas_COG		•	
ay_chas_COG	•		•
s_chas_FL	•	•	•
s_chas_FR	•	•	•
s_chas_RL	•	•	•
s_chas_RR	•	•	•
az_axle_FL	•		
az_axle_FR	•		
az_axle_RL	•		
az_axle_RR	•		

B.3 RMS value *Trucklab* sensor noise

In table B.3 the noise *RMS* values for the *Trucklab* signals is given. The *RMS* values of the sensor noise are determined with sensor data originating from an experiment where the *Trucklab* is in standstill with the engine running.

Table B.3: RMS value *Trucklab* sensor noise.

Signal	<i>RMS</i> value noise
az_axle_FL	0.1066 [m/s ²]
az_axle_FR	0.0927 [m/s ²]
az_axle_RL	0.0977 [m/s ²]
az_axle_RR	0.0952 [m/s ²]
az_chas_FL	0.0359 [m/s ²]
az_chas_FR	0.0427 [m/s ²]
az_chas_RL	0.0404 [m/s ²]
az_chas_RR	0.0665 [m/s ²]
az_cab_FL	0.0771 [m/s ²]
az_cab_FR	0.0835 [m/s ²]
az_cab_RL	0.0811 [m/s ²]
az_cab_RR	0.0827 [m/s ²]
PitchRate_cab	0.0025 [rad/s]
RollRate_cab	0.0023 [rad/s]
YawRate_cab	0.0016 [rad/s]
ax_cab_FC	0.0247 [m/s ²]
ay_cab_FC	0.0186 [m/s ²]
az_cab_FC	0.0434 [m/s ²]
ax_chas_COG	0.0428 [m/s ²]
ay_chas_COG	0.0432 [m/s ²]
az_chas_COG	0.1181 [m/s ²]
s_cab_FL	0.000088 [m]
s_cab_FR	0.000066 [m]
s_z_cab_RL	0.000045 [m]
s_cab_RR	0.000060 [m]
s_chas_FL	0.000158 [m]
s_chas_FR	0.000089 [m]
s_chas_RL	0.000066 [m]
s_chas_RR	0.000102 [m]

B.4 Time-shift signals

In Table B.4 the time-shift signals for the different types of experiments are given. These signals are used to synchronise the measured and simulated data.

Table B.4: Time-shift signals.

Test	Time shift signal
discrete obstacle pyramid	az_axle_FR
discrete obstacle step down	az_axle_FR
discrete obstacle threshold	az_axle_FR
acceleration	ax_chas_COG
normal braking	Vx
heavy braking	Vx
circle	Vx
double lane change	SWheel_Angle
step steer	SWheel_Angle

Appendix C

Evaluation scores

C.1 *baseline* model vs. *reference* model evaluation scores

This section contains the evaluation scores for each type of experiment. These evaluation scores are computed using the evaluation method discussed in chapter 5. A comparison is made between the *baseline* and *reference* model. The *baseline* model is defined as the first version of the model dated Juli 2006. The *reference* model is defined as an updated version of the *baseline* model which includes the model adjustments discussed in chapter 6.

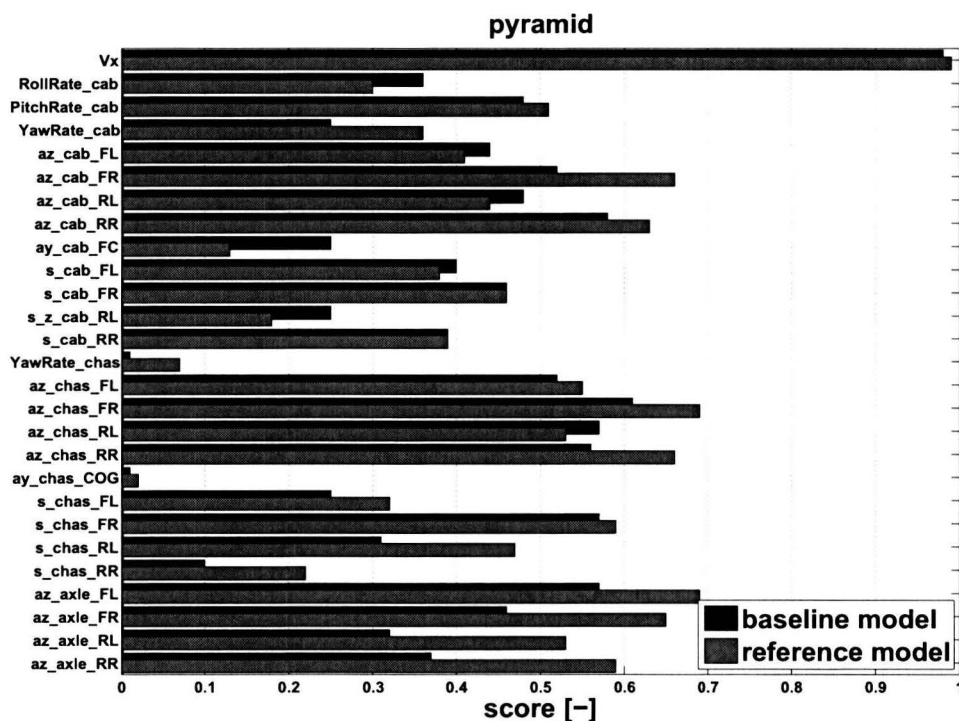


Figure C.1: Discrete obstacle experiment (pyramid). Evaluation scores, *baseline* model (black) and *reference* model (gray).

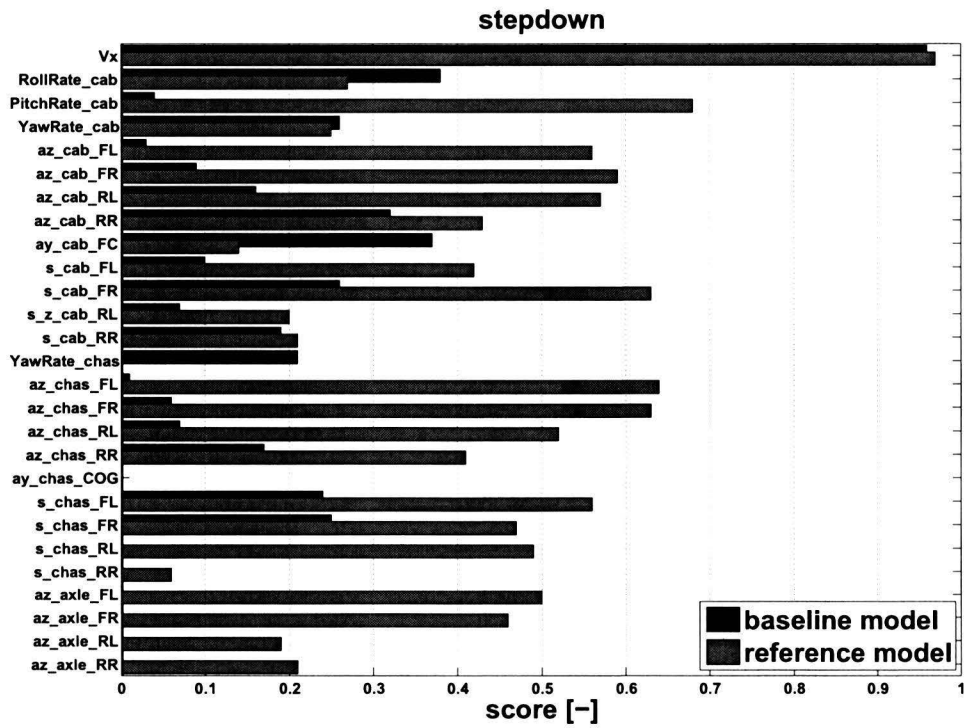


Figure C.2: Discrete obstacle experiment (stepdown). Evaluation scores, *baseline* model (black) and *reference* model (gray).

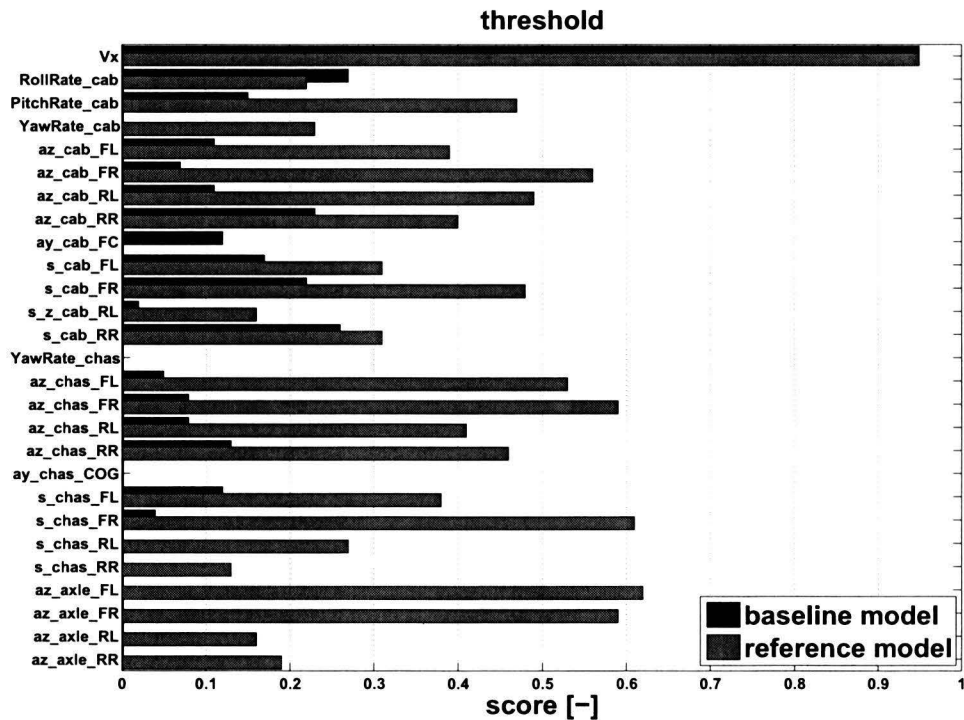


Figure C.3: Discrete obstacle experiment (threshold). Evaluation scores, *baseline* model (black) and *reference* model (gray).

C.1 baseline model vs. reference model evaluation scores

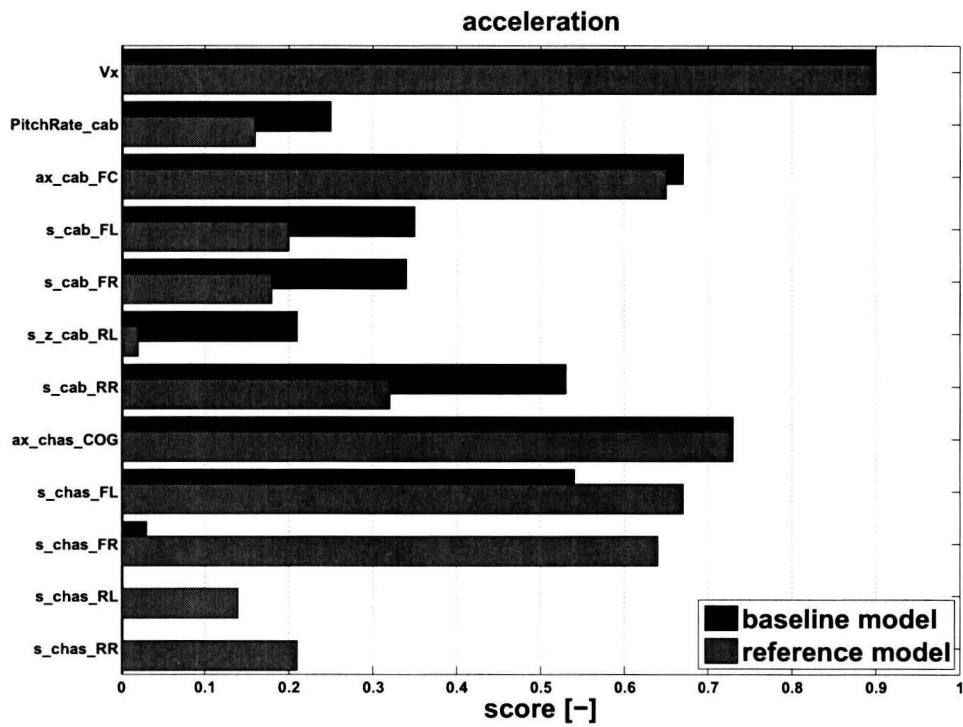


Figure C.4: Acceleration experiment. Evaluation scores, *baseline model* (black) and *reference model* (gray).

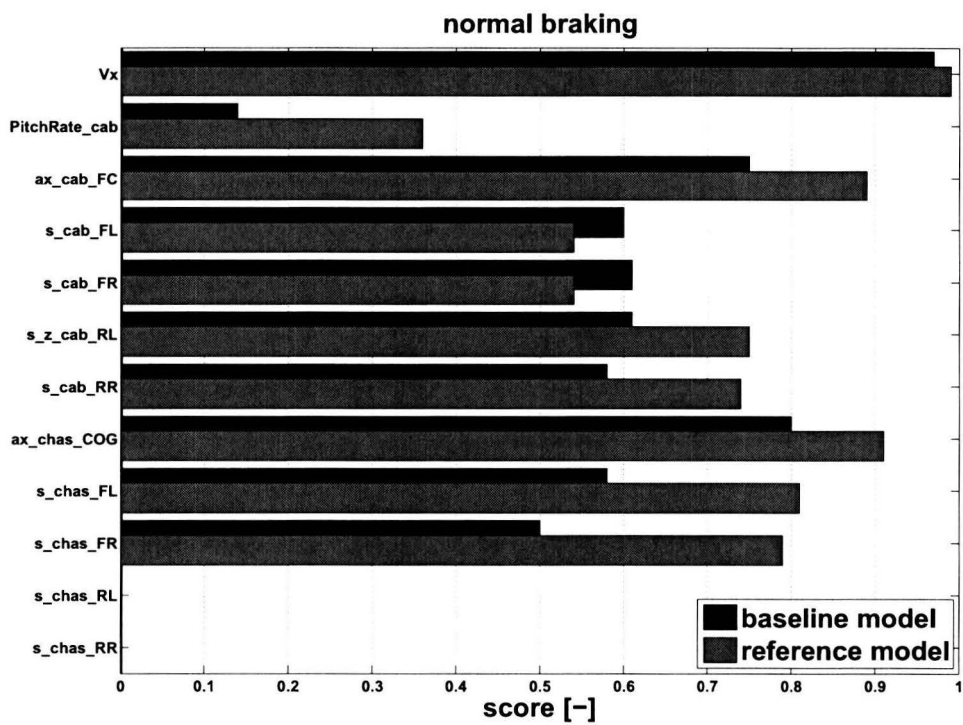


Figure C.5: Normal braking experiment. Evaluation scores, *baseline model* (black) and *reference model* (gray).

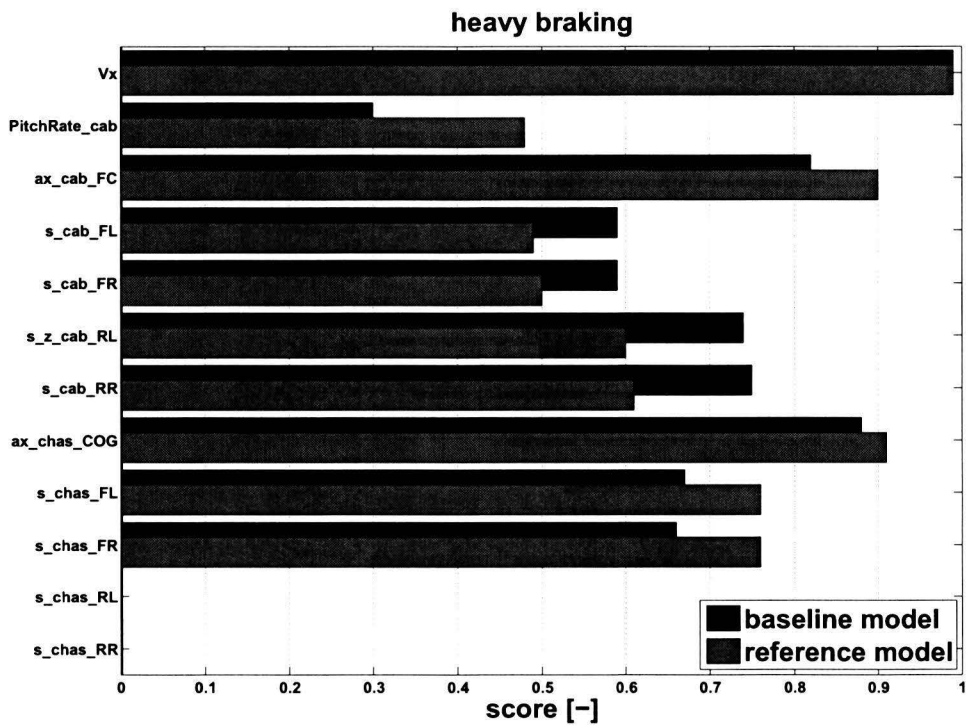


Figure C.6: Heavy braking experiment. Evaluation scores, *baseline* model (black) and *reference* model (gray).

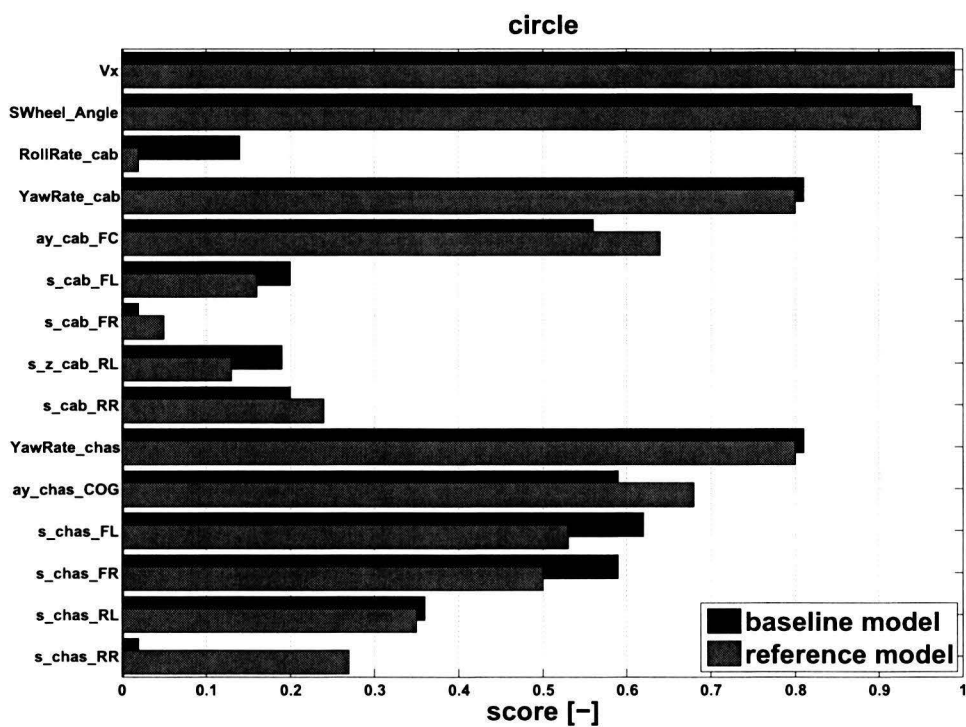


Figure C.7: Circle experiment. Evaluation scores, *baseline* model (black) and *reference* model (gray).

C.1 *baseline* model vs. *reference* model evaluation scores

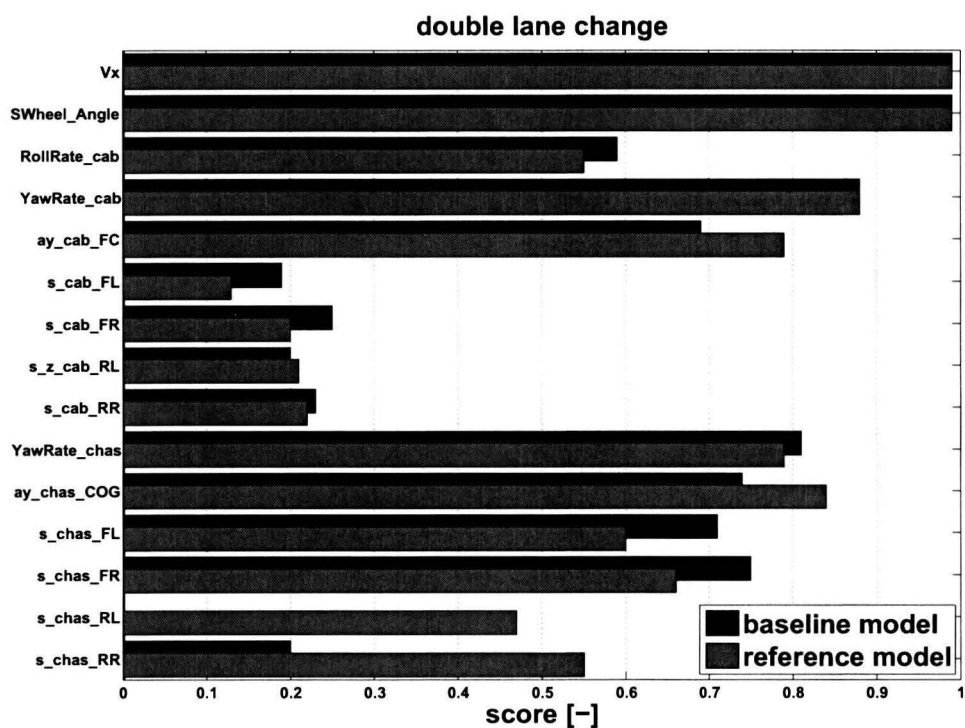


Figure C.8: Double lane change experiment. Evaluation scores, *baseline* model (black) and *reference* model (gray).

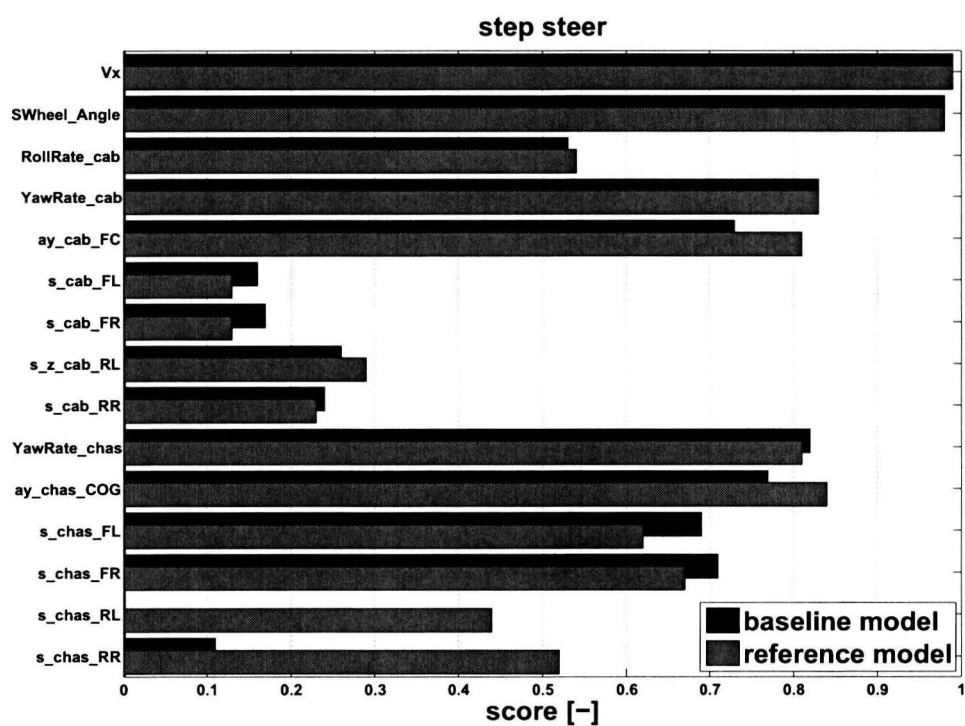


Figure C.9: Step steer experiment. Evaluation scores, *baseline* model (black) and *reference* model (gray).

C.2 *baseline* model vs. *final* model evaluation scores

This section contains the evaluation scores for each type of experiment. These evaluation scores are computed using the evaluation method discussed in chapter 5. A comparison is made between the *baseline* and *final* model. The *baseline* model is defined as the first version of the model dated Juli 2006. The *final* model includes the model adjustments discussed in chapter 6 and 7.

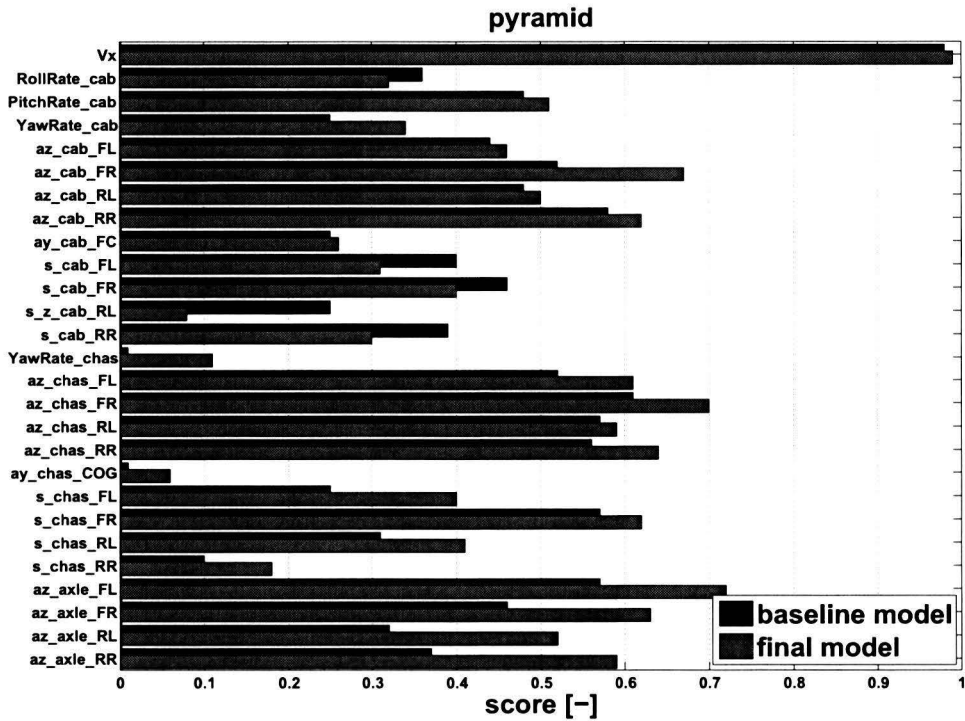


Figure C.10: Discrete obstacle experiment (pyramid). Evaluation scores, *baseline* model (black) and *final* model (gray).

C.2 *baseline* model vs. *final* model evaluation scores

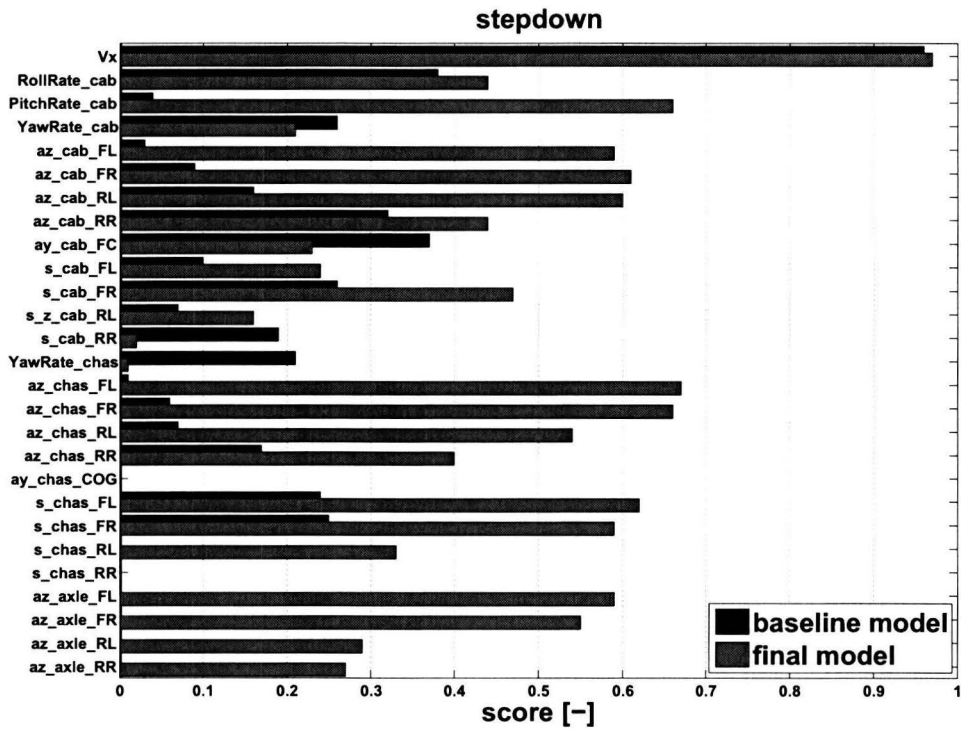


Figure C.11: Discrete obstacle experiment (stepdown). Evaluation scores, *baseline* model (black) and *final* model (gray).

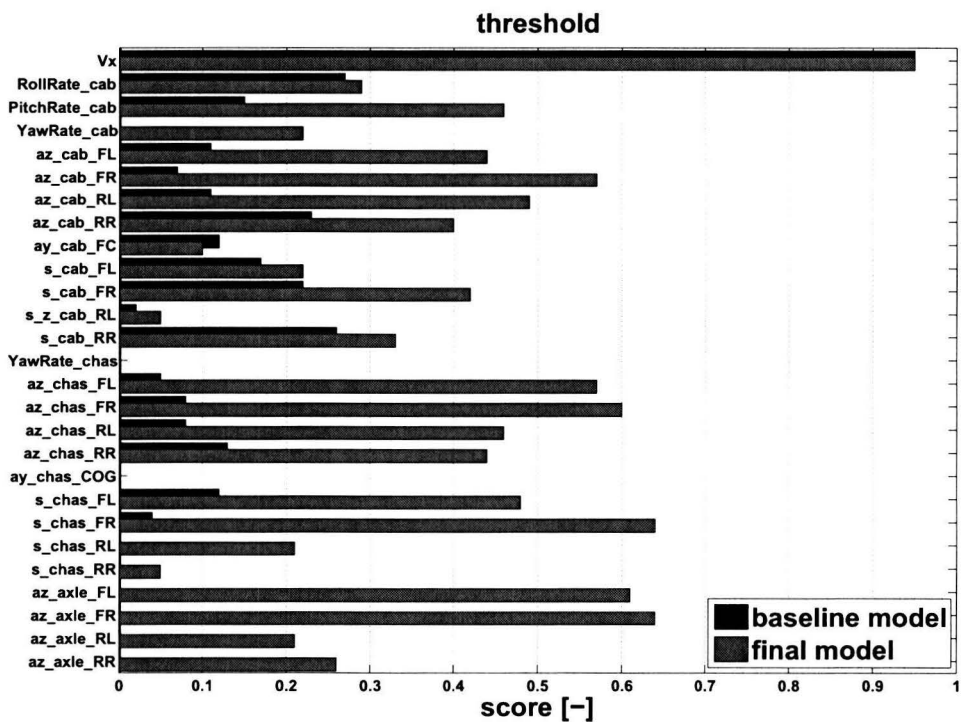


Figure C.12: Discrete obstacle experiment (threshold). Evaluation scores, *baseline* model (black) and *final* model (gray).

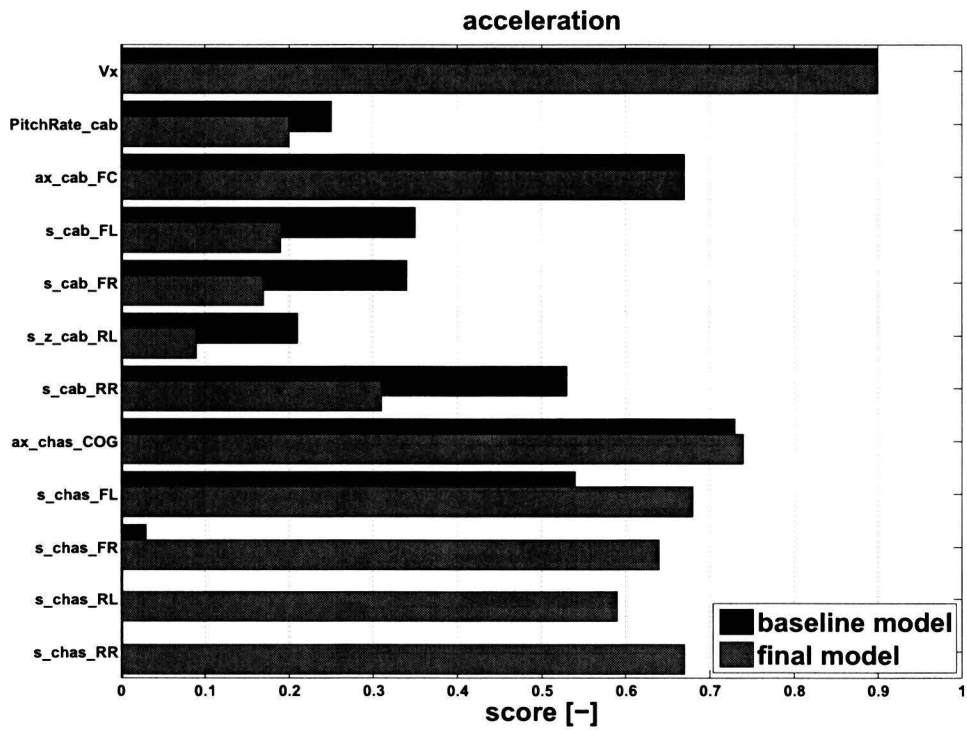


Figure C.13: Acceleration experiment. Evaluation scores, *baseline* model (black) and *final* model (gray).

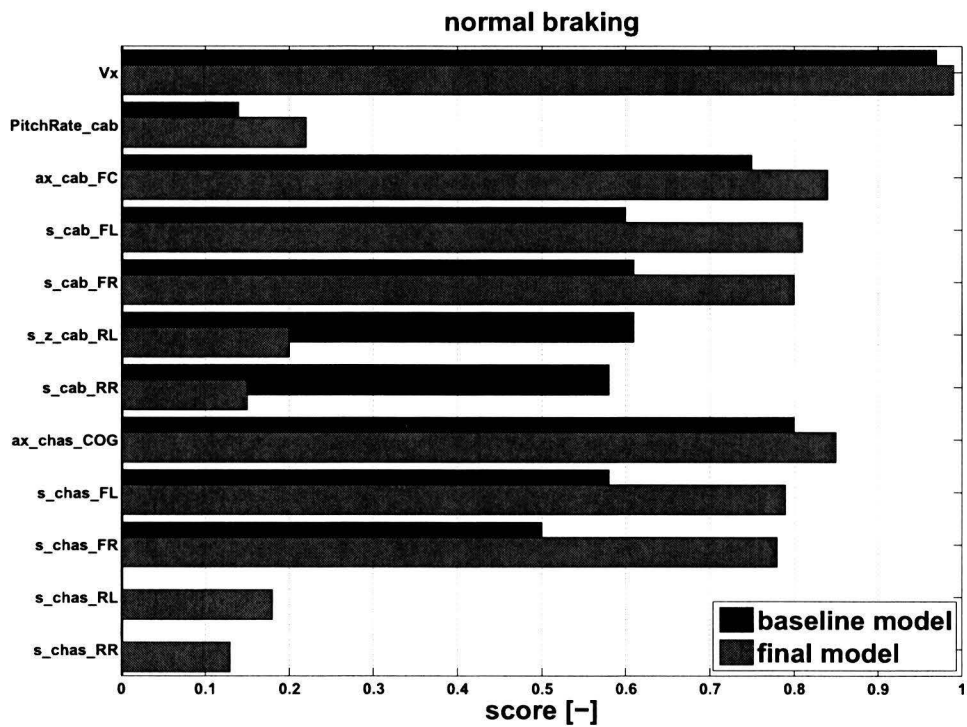


Figure C.14: Normal braking experiment. Evaluation scores, *baseline* model (black) and *final* model (gray).

C.2 *baseline* model vs. *final* model evaluation scores

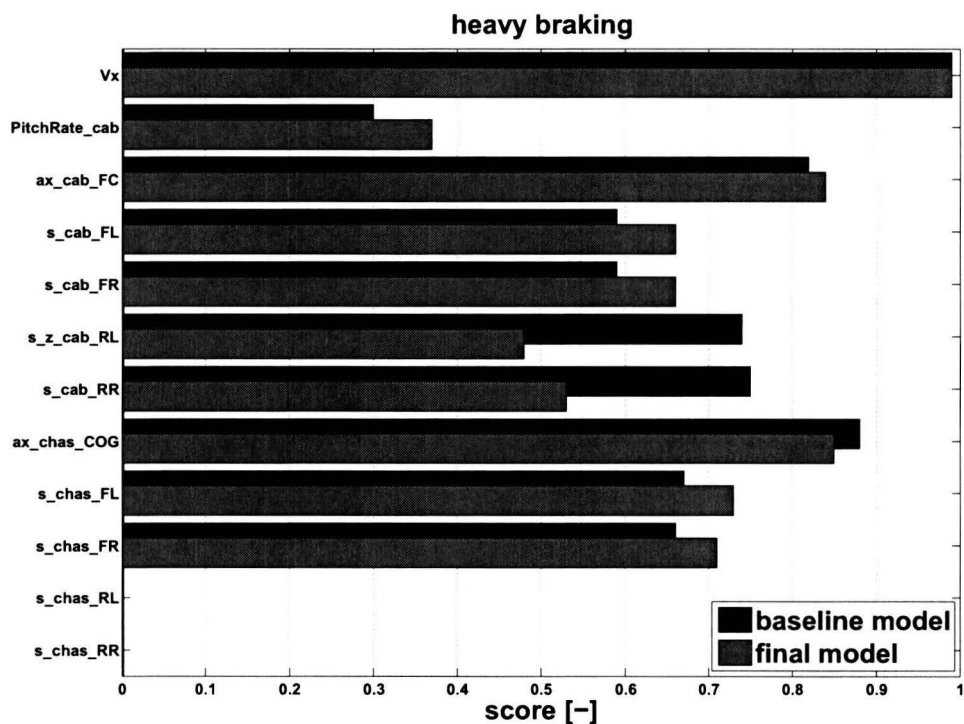


Figure C.15: Heavy braking experiment. Evaluation scores, *baseline* model (black) and *final* model (gray).

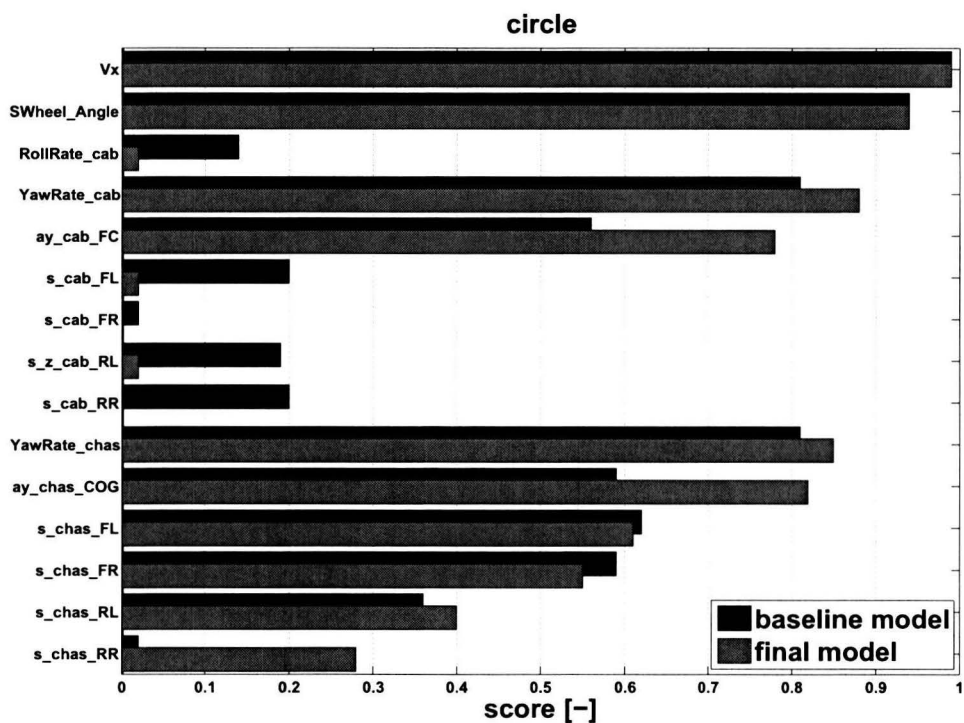


Figure C.16: Circle experiment. Evaluation scores, *baseline* model (black) and *final* model (gray).

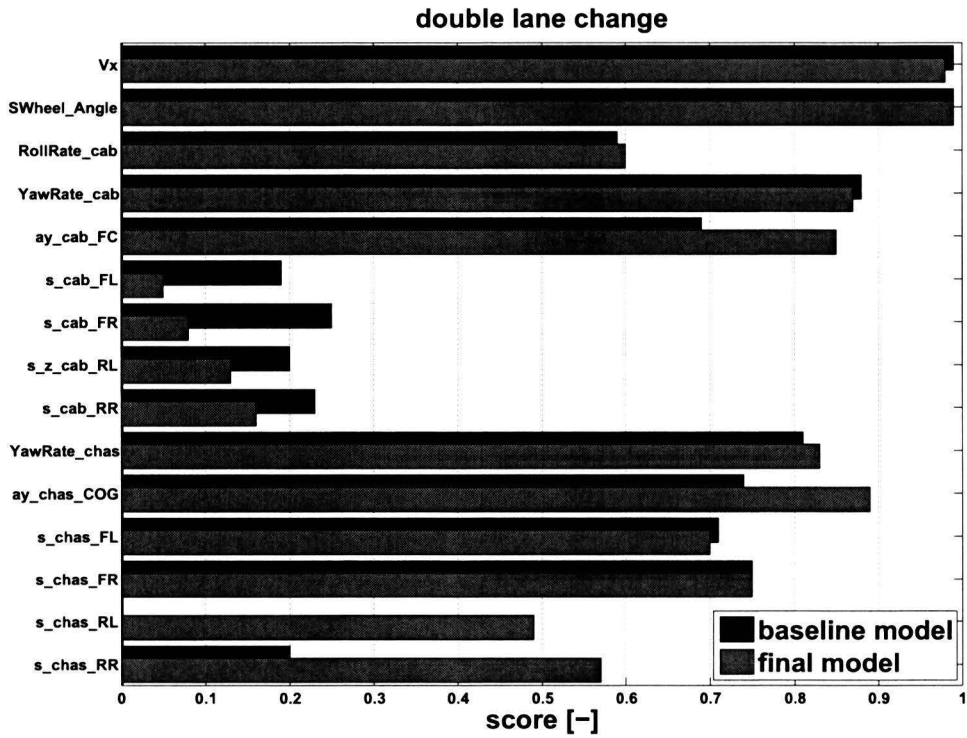


Figure C.17: Double lane change experiment. Evaluation scores, *baseline* model (black) and *final* model (gray).

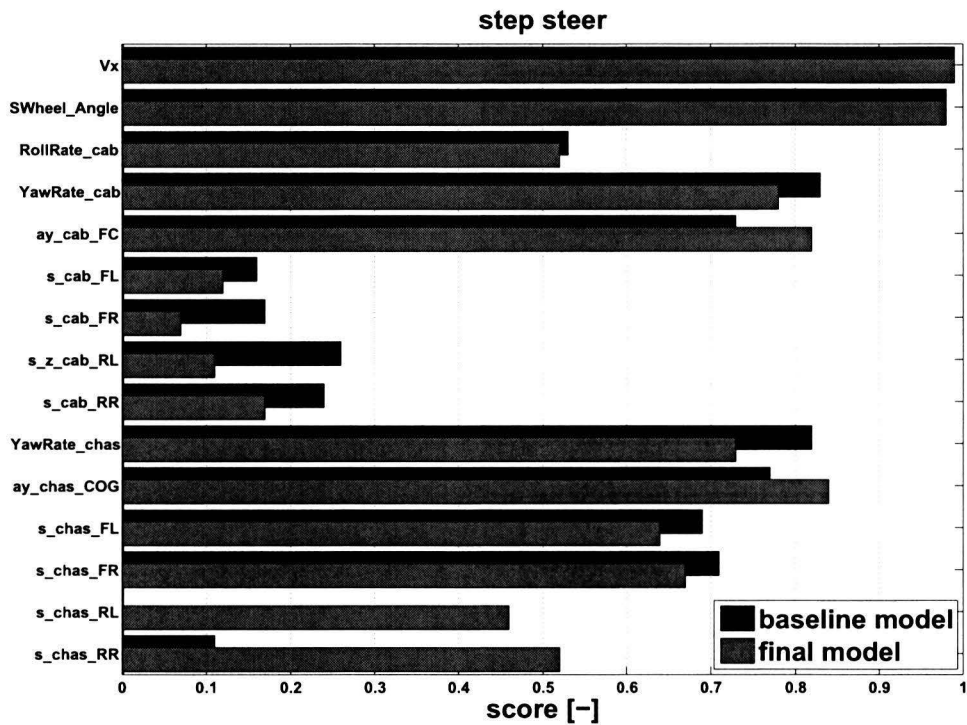


Figure C.18: Step down experiment. Evaluation scores, *baseline* model (black) and *final* model (gray).

C.3 reference model vs. final model evaluation scores

This section contains the evaluation scores for each type of experiment. These evaluation scores are computed using the evaluation method discussed in chapter 5. A comparison is made between the *reference* and *final* model. The *reference* model is defined as an updated version of the *baseline* model which includes the model adjustments discussed in chapter 6. The *final* model includes the model adjustments discussed in chapter 6 and 7.

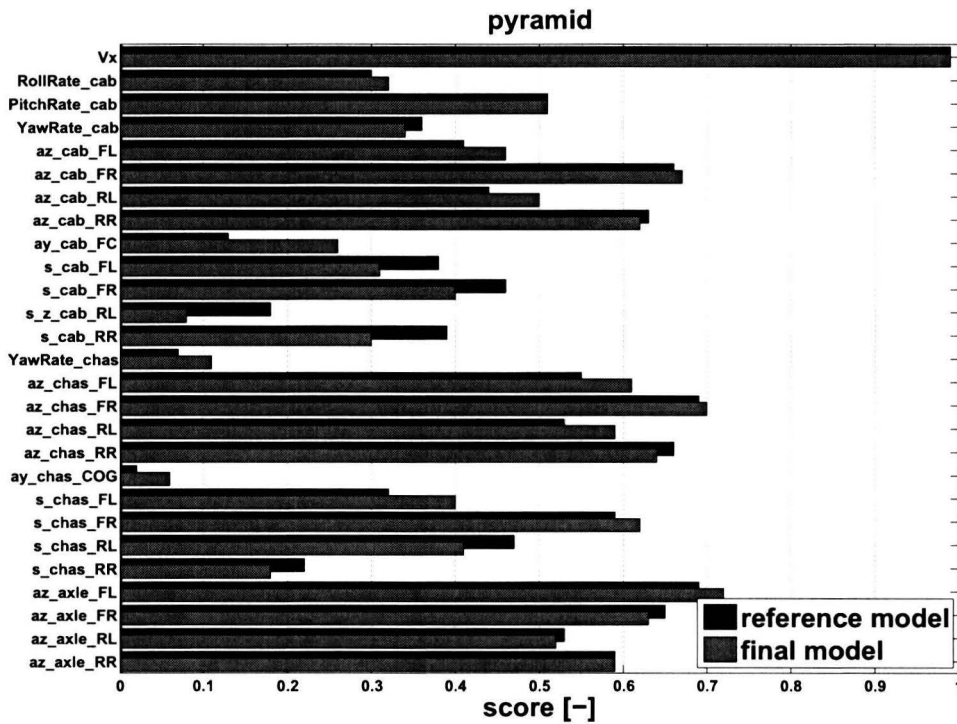


Figure C.19: Discrete obstacle experiment (pyramid). Evaluation scores, *reference* model (black) and *final* model (gray).

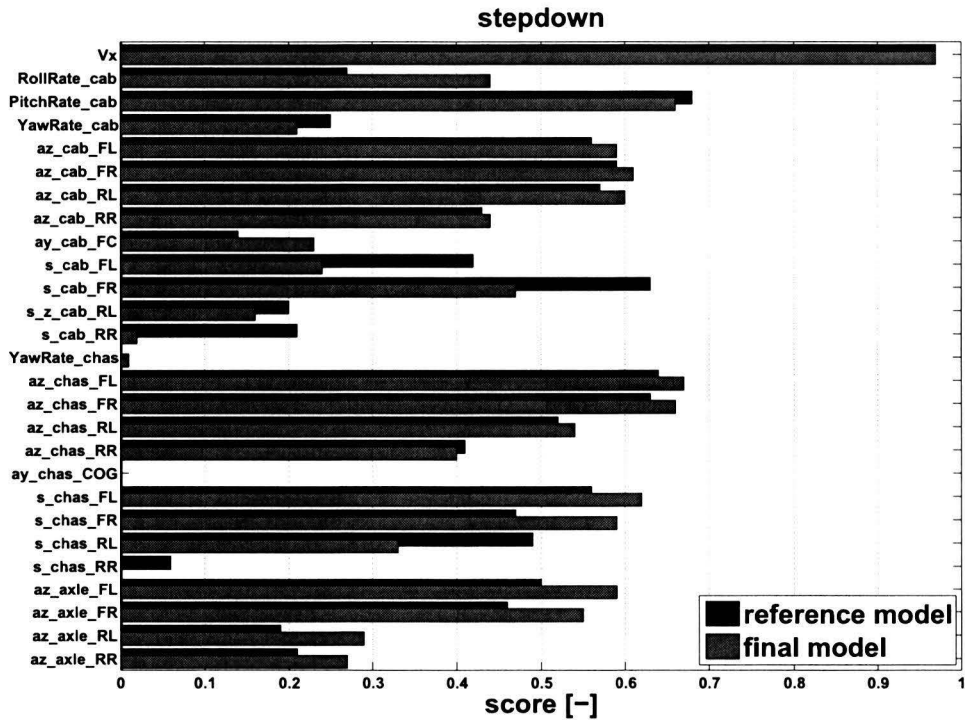


Figure C.20: Discrete obstacle experiment (stepdown). Evaluation scores, *reference* model (black) and *final* model (gray).

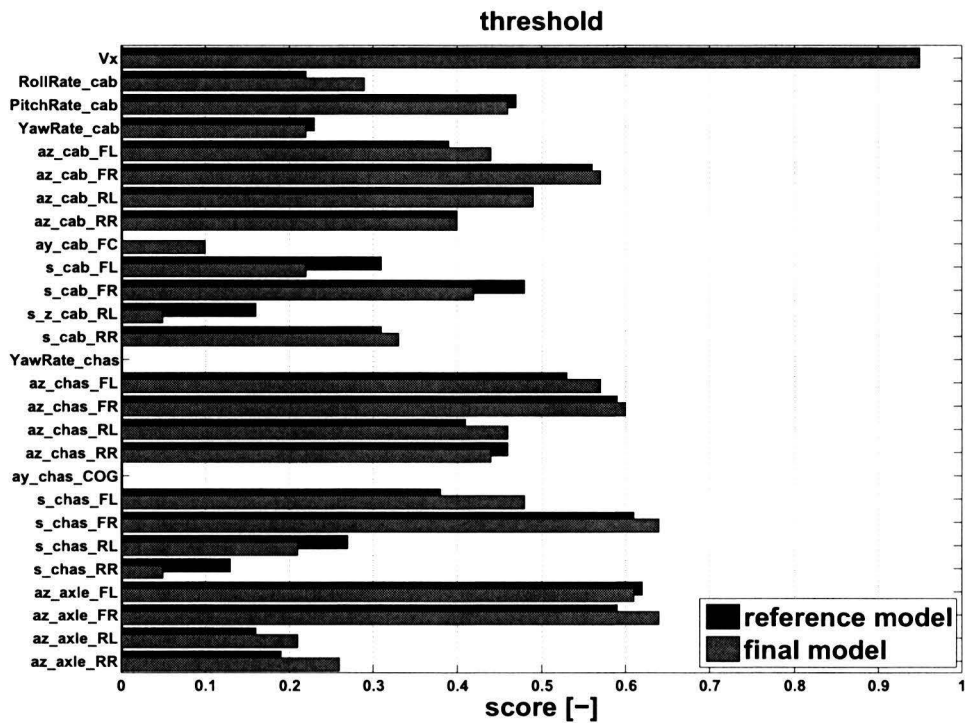


Figure C.21: Discrete obstacle experiment (threshold). Evaluation scores, *reference* model (black) and *final* model (gray).

C.3 reference model vs. final model evaluation scores

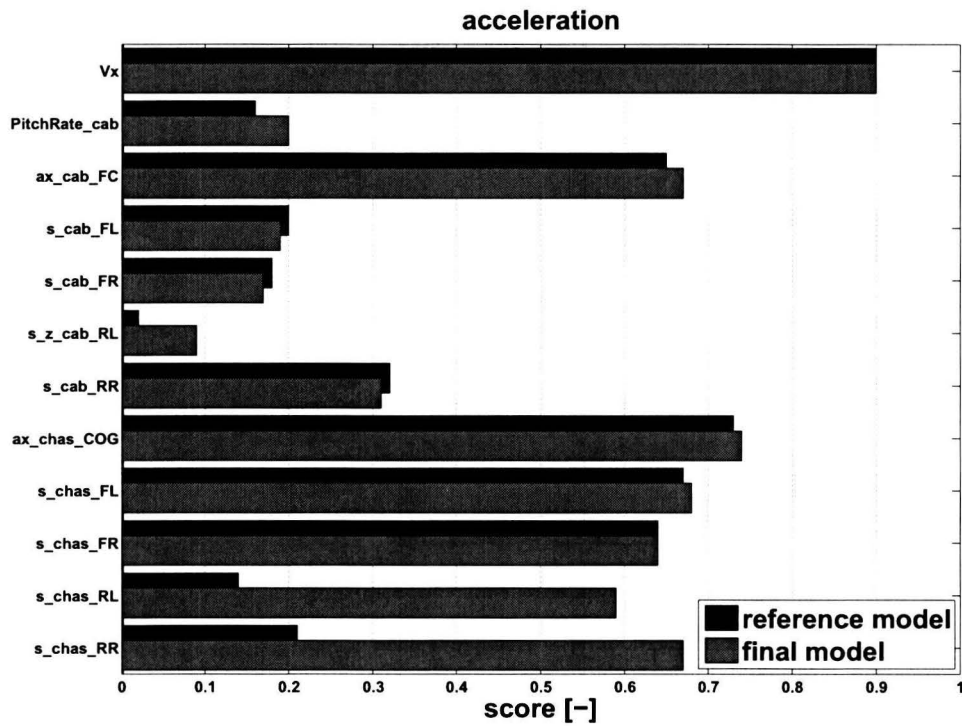


Figure C.22: Acceleration experiment. Evaluation scores, *reference* model (black) and *final* model (gray).

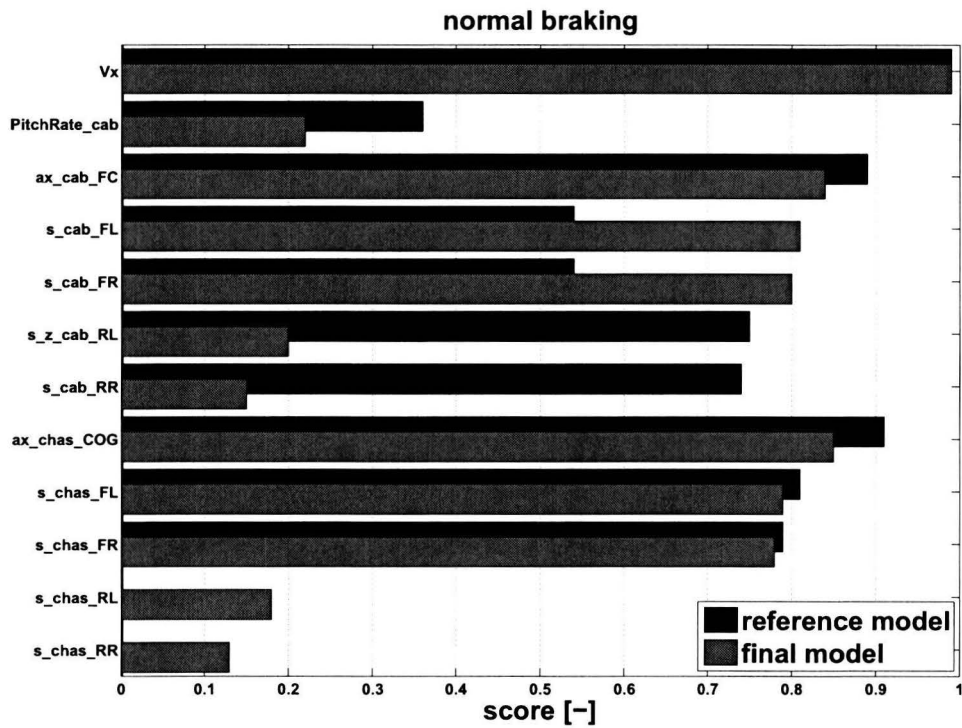


Figure C.23: Normal braking experiment. Evaluation scores, *reference* model (black) and *final* model (gray).

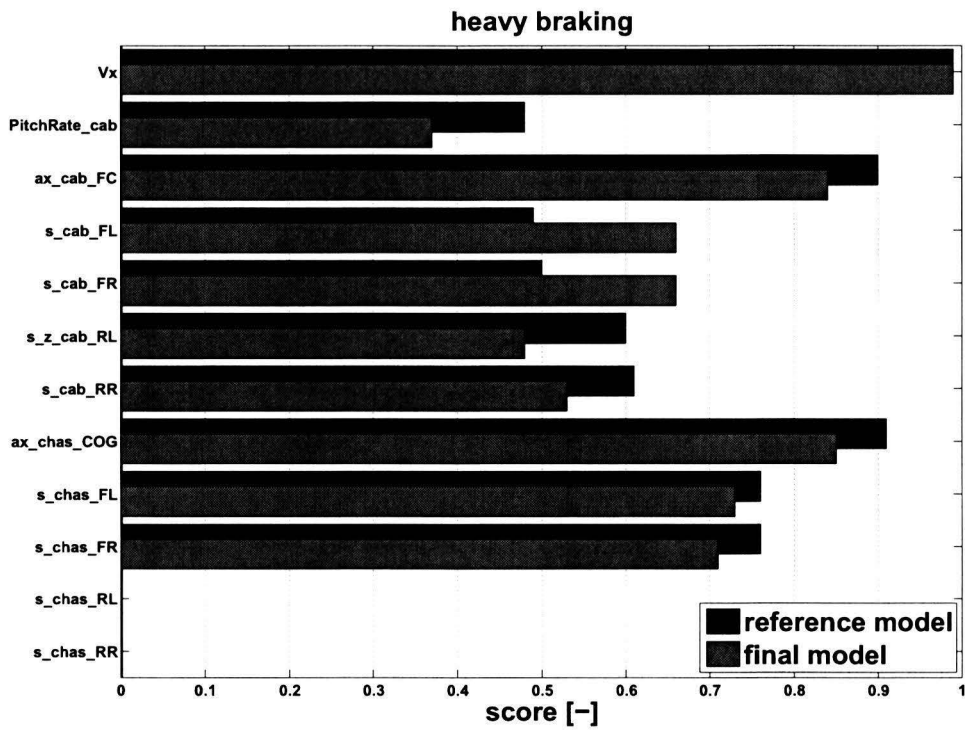


Figure C.24: Heavy braking experiment. Evaluation scores, *reference model* (black) and *final model* (gray).

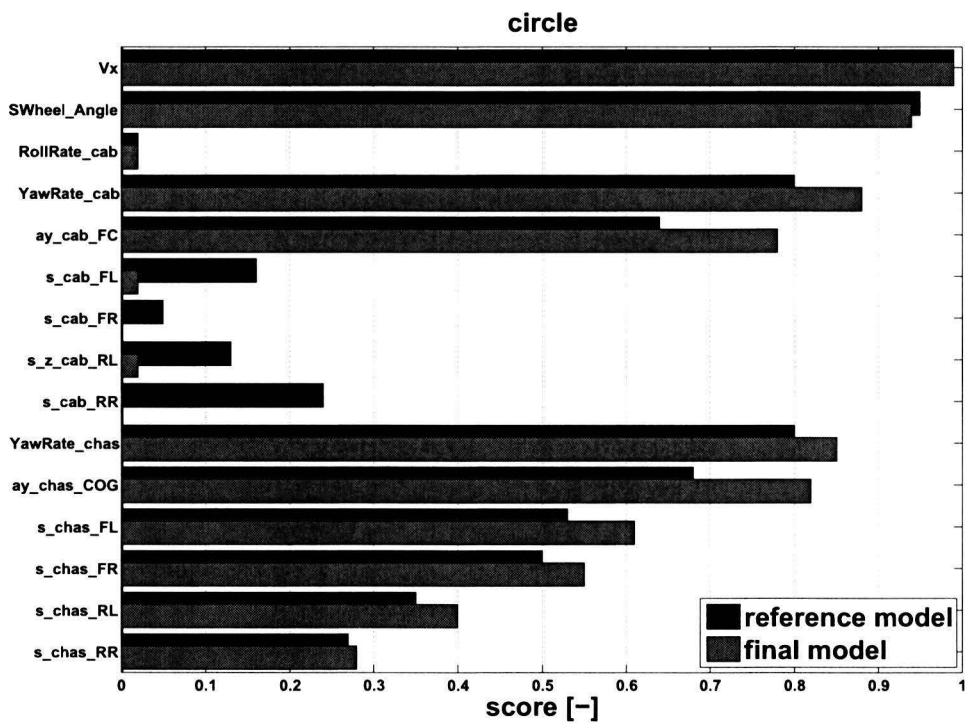


Figure C.25: Circle experiment. Evaluation scores, *reference model* (black) and *final model* (gray).

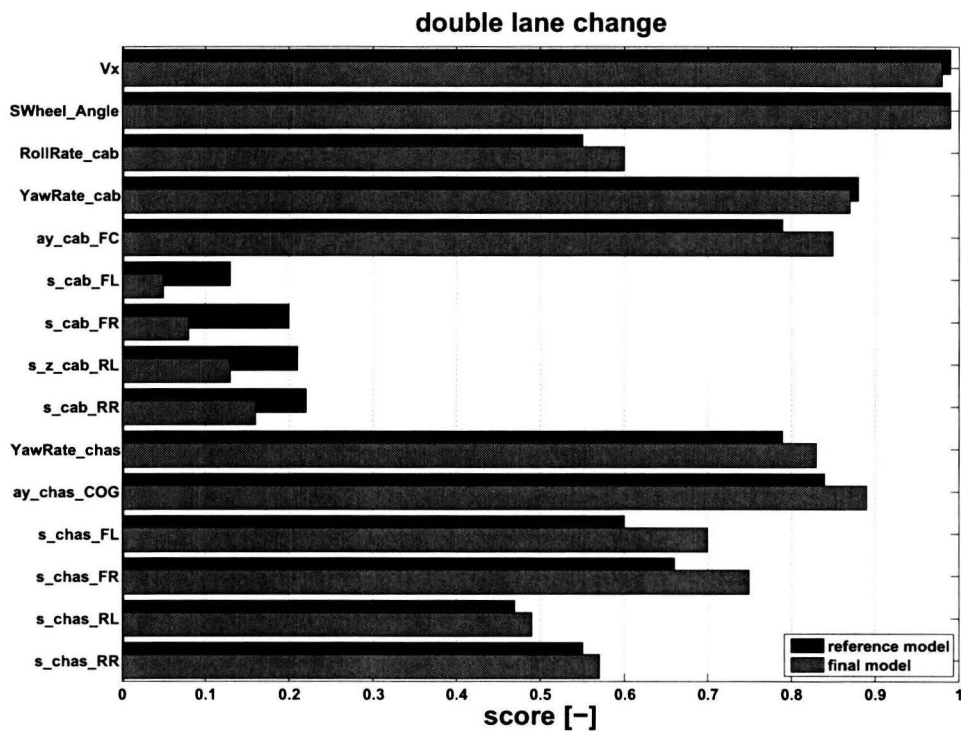


Figure C.26: Double lane change experiment. Evaluation scores, *reference* model (black) and *final* model (gray).

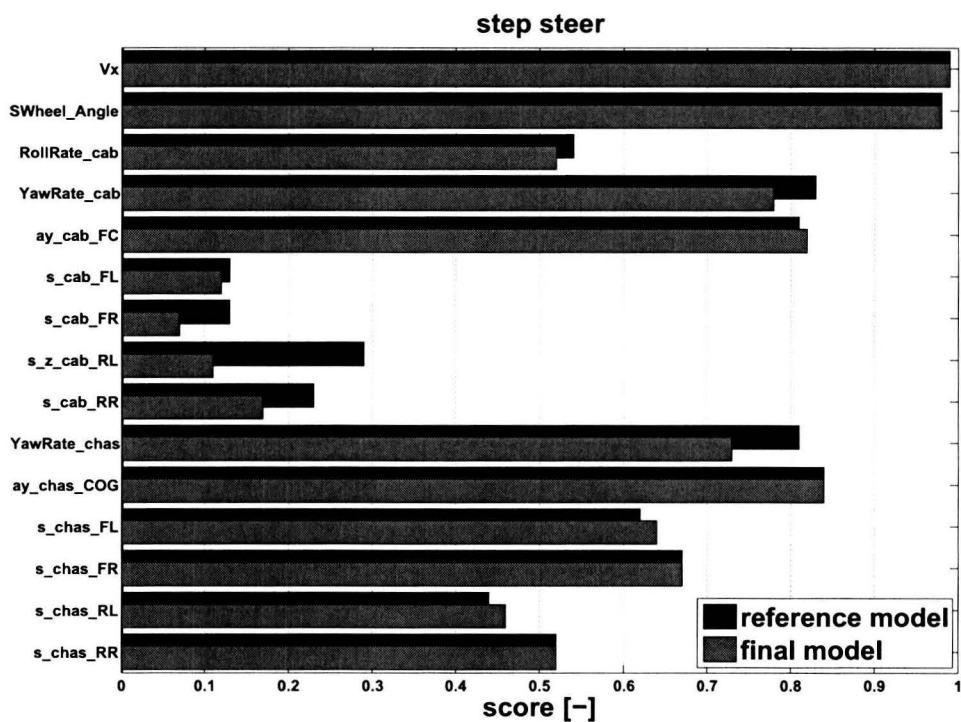


Figure C.27: Step down experiment. Evaluation scores, *reference* model (black) and *final* model (gray).